Technische Universität München
TUM School of Life Sciences

Cachexia in patients with gastrointestinal tumor diseases – an interplay of tissues and molecular mechanisms

Simone Eva-Maria Heisz

Vollständiger Abdruck der von der TUM School of Life Sciences der Technischen Universität München zur Erlangung einer

Doktorin der Naturwissenschaften (Dr. rer. nat.)

genehmigten Dissertation.

Vorsitz: Prof. Dr. rer. nat. Martin Klingenspor

Prüfer*innen der Dissertation:

1. Prof. Dr. med. Johann J. Hauner
2. apl. Prof. Dr. rer. nat. Klaus-Peter Janssen

Die Dissertation wurde am 15.02.2023 bei der Technischen Universität München eingereicht und durch die TUM School of Life Sciences am 22.05.2023 angenommen.

Table of contents

I. Abbreviations

Abbreviation	Meaning
18S	18S ribosomal RNA
ABCC2	ATP binding cassette subfamily C member 2
AEG	Adenocarcinoma of the esophagogastric junction
AP	Serous cystadenoma of the pancreas
ARID5B	AT-rich interaction domain 5B
ASA	American society of anesthesiologists (score)
ATP	Adenosine triphosphate
CA19-9	Cancer antigen 19-9
cAMP	Cyclic adenosine monophosphate
CEA	Carcinoembryonic antigen
C/EBP	CCAAT/enhancer-binding protein
COPD	Chronic obstructive pulmonary disease
CP	Chronic pancreatitis
CRC	Colorectal cancer
CRP	C-reactive protein
Ct	Cycle threshold
DC	Duodenal carcinoma
EtOH	Ethanol
FASN	Fatty acid synthase
FFA	Free fatty acid
FTO	Fat mass and obesity-associated
GAPDH	Glycerinaldehyd-3-phosphat-dehydrogenase
GGT	Gamma glutamyl transferase
GLUT4	Glucose transporter type 4
GOT	Glutamate oxaloacetate transaminase
GPDH	Glycerol-3-phosphate dehydrogenase
GPS	Glasgow prognostic score
GPT	Glutamate pyruvate transaminase
H	Hour
HDL	High density lipoprotein
HIV	Human immunodeficiency virus
IL-1	Interleukin-1
IL-4	Interleukin-4
IL-6	Interleukin-6
IL-6R	Interleukin-6 receptor
IPO8	Importin 8
IRX3	Iroquois homeobox 3
IRX5	Iroquois homeobox 5
IPMN	Intraductal papillary mucinous neoplasm
KLF	Krüppel-like factor
LA	Liver adenoma
LDH	Lactate dehydrogenase
LDL	Low density lipoprotein
Max	Maximum

Abbreviation	Meaning
MCAC	Mucinous cystadenocarcinomas of the pancreas
Min	Minimum
Min	Minutes
MT-CO2	Mitochondrially encoded cytochrome C oxidase II
mU	Milli-Unit (10-3 Unit)
MURF1	Muscle RING finger 1
NEC	Neuroendocrine carcinoma
OD	Optical density
Om	Omental
PAC	Preadipocyte
PDAC	Pancreatic ductal adenocarcinoma
pg	Picogram
PPARγ	Nuclear receptor peroxisome proliferator-activated receptor γ
PRDM16	PR/SET domain 16
PTHrP	Parathyroid hormone-related protein
Rpm	Revolutions per minute
RPS20	Ribosomal protein S20
RQ	Relative quantification
RT	Room temperature
S	Second
Sc	Subcutaneous
SCC	Squamous cell carcinoma
SEM	Standard error of the mean
sIL-6R	Soluble Interleukin-6 receptor
SREBP1	Sterol regulatory element binding protein-1
TG	Triacylglycerol/triacylglycerides
TNFα	Tumor necrosis factor alpha
UCP 1	Uncoupling protein 1
UPS	Ubiquitin proteasome system
Vc	Visceral
vs.	Versus
WT	Wild type
ZAG	Zinc-alpha-2-glycoprotein

II. List of Tables

III. List of Figures

IV. Abstract

Cachexia is a multifactorial and multi-organ wasting syndrome which is characterized by an uncontrolled loss of muscle mass and an optional loss of adipose tissue mass, a condition which is difficult to manage by nutritional support and requires better treatment due to its potentially fatal consequences. Cancer-associated cachexia is highly prevalent in gastrointestinal tumor diseases and can negatively influence the patient's treatment as well as the general outcome. Some circulating cytokines were proposed to be biomarker candidates for early detection of cachexia.

In this study, we built up a biobank containing blood, liver, muscle, subcutaneous as well as omental adipose tissue from patients with either benign or malign diseases of the gastrointestinal tract. Plasma levels of Interleukin-6 were measured and correlated with clinical as well as survival data. Additionally, gene expression analysis was used to investigate the effect of cachexia and sarcopenia on browning, lipolysis, lipogenesis and adipogenic differentiation within the sampled tissues and preadipocytes in a separate cell culture approach.

Direct markers of browning, lipolysis and lipogenesis were not involved in cachexia. However, preadipocytes of cachectic patients revealed a slightly decreased AT-rich interaction domain 5B and an increased iroquois homeobox 3 and iroquois homeobox 5 expression, connecting cachexia to fat mass and obesity-associated specific genes, but not to its genotype. The differentiation capacity of adipocytes was altered, since CCAAT/enhancer-binding protein alpha expression in subcutaneous preadipocytes was decreased in cancer patients compared to cancer-free controls. Interestingly, enzymatic glycerol-3-phosphate dehydrogenase activity was elevated in preadipocytes derived from individuals with cachexia. The gene expression of the muscle-growth inhibitor myostatin was significantly downregulated in muscle tissue of cachectic patients versus controls. As possible explanations posttranscriptional mechanisms as well as negative feedback loops should be taken into account. Plasma interleukin-6 was proven to be a promising prognostic marker. It not only predicted survival of individuals with gastrointestinal tumors in general and pancreatic ductal adenocarcinoma in particular, but also correlated with C-reactive protein and albumin building a bridge to cachexia diagnosis via the Glasgow Prognostic Score.

Summarizing, the present thesis provides a comprehensive overview of the possible molecular mechanisms of cachexia and sarcopenia in a variety of target tissues from patients with gastrointestinal tumor diseases and can be used as basis for future cachexia research.

V. Zusammenfassung

Kachexie ist ein multifaktorielles und organübergreifendes Syndrom, das durch einen unkontrollierten Verlust an Muskelmasse und einen fakultativen Verlust an Fettgewebsmasse gekennzeichnet ist. Dies ist ein Umstand, der sich durch gezielte Ernährungsintervention allein kaum verbessern lässt. Die krebsbedingte Kachexie, die vor allem bei gastrointestinalen Tumorerkrankungen auftritt, kann sich sowohl negativ auf die Behandlung des Patienten, als auch den allgemeinen Gesundheitszustand auswirken. Einige zirkulierende Zytokine stehen bereits als Kandidaten zur Früherkennung von Kachexie im Fokus.

Im Rahmen dieser Studie bauten wir eine Biobank, bestehend aus Plasma, Leber- und Muskelgewebe, subkutanem und omentalem Fettgewebe von Patienten mit benignen oder malignen Erkrankungen des Gastrointestinaltrakts, auf. Plasmamessungen von Interleukin-6 wurden mit klinischen und Daten zum Überlebensstatus korreliert. Zusätzlich wurden Genexpressionsanalysen durchgeführt, um die Auswirkungen von Kachexie und Sarkopenie auf Browning, Lipolyse, Lipogenese sowie adipogene Differenzierung zu untersuchen. Hierfür analysierten wir sowohl die gesammelten Gewebetypen, als auch Präadipozyten mittels eines Zellkulturversuchs.

Eine direkte Beteiligung von Browning, Lipolyse und Lipogenese konnte nicht gezeigt werden, obwohl Präadipozyten von Patienten mit Kachexie eine tendenziell verringerte Expression von *AT-rich interaction domain 5B* sowie eine leicht erhöhte Expression von *iroquois homeobox 3* und *iroquois homeobox 5* aufwiesen. Dies stellte zwar eine Verbindung zwischen Kachexie und dem *fat mass and obesity*-assoziierten Genlokus, jedoch nicht zu den *fto*-Genotypen selbst her. Die Differenzierungskapazität von Adipozyten zeigte sich dahingehend verändert, dass die Expression von *CCAAT/enhancer-binding protein alpha* in subkutanen Präadipozyten von Krebspatienten im Vergleich zu krebsfreien Individuen vermindert war. Interessanterweise zeigte sich die enzymatische *glycerol-3-phosphate dehydrogenase* Aktivität in Präadipozyten unter Kachexie erhöht. Die Genexpression des Muskelwachstumshemmers Myostatin war im Muskelgewebe von Kachexie-Patienten im Vergleich zu Kontrollen signifikant herabreguliert. Mögliche Erklärungen hierfür sind posttranskriptionelle Mechanismen und negative Rückkopplungsschleifen. Plasma Interleukin-6 erwies sich als ein vielversprechender prognostischer Marker. Es sagte nicht nur das Überleben von Personen mit gastrointestinalen Tumoren im Allgemeinen und beim duktalen Adenokarzinom des Pankreas im Besonderen voraus, sondern korrelierte auch signifikant mit dem C-reaktiven Protein und Albumin, was eine Brücke zur Diagnose von Kachexie über den Glasgow Prognostic Score schlug.

Zusammenfassend bietet die vorliegende Arbeit einen umfassenden Überblick über die möglichen molekularen Mechanismen von Kachexie und Sarkopenie in einer Vielzahl von

beeinflussten Gewebetypen bei Patienten mit gastrointestinalen Tumorerkrankungen und kann daher als Basis für zukünftige Kachexieforschung genutzt werden.

1 Introduction

1.1 Tumor burden around the world

Together with cardiovascular diseases, cancer is the globally leading cause of death for altogether 127 countries in the world in 2021 (Bray et al., 2021). The Global Cancer statistics 2020, which are based on the GLOBOCAN estimates pointed out that, besides Asia, Europe shows not only the highest incidence of cancer with a proportion of 22.8 % of all cancer cases worldwide, but also the highest cancer-related mortality (19.6 %), although Europe only constitutes 9.7 % of the world's total population (Sung et al., 2021). Furthermore, the GLOBOCAN database 2018 revealed that the distribution of gastrointestinal tumor diseases accounts for 35 % of all cancer-related deaths worldwide and, additionally, shows geographic variations with the highest prevalence of esophageal, gastric and liver cancer in Asia, but the highest occurrence of colorectal and pancreatic cancer in Europe and North America (Arnold et al., 2020). Underlying causes of high colorectal and pancreatic cancer case numbers in developed countries can be attributed to the genetic background, decreased physical activity, unhealthy diet, alcohol consumption, smoking and related lifestyle-associated diseases such as obesity or type 2 diabetes (Center et al., 2009; Ferrari et al., 2007; Ilic & Ilic, 2016).

1.2 Cachexia and sarcopenia as cancer comorbidities

Since cancer diseases do not only affect the direct location of the tumor, but the whole body and its organs, for example through increased energy expenditure due to hypermetabolism, they often come along with a variety of comorbidities such as cancer cachexia and sarcopenia (Argilés et al., 2014; Muscaritoli et al., 2015). Both complications are not exclusively related to cancer, but, in the case of cachexia, can for example also be linked to infections with the human immunodeficiency virus, chronic obstructive pulmonary disease, sepsis, heart failure or severe burn injuries (Roenn et al., 1992; J. Song et al., 2021). Cachexia is a multifactorial and multi-organ wasting syndrome, which is characterized by an uncontrolled loss of muscle mass and an optional loss of adipose tissue mass due to a negative protein and energy balance which is impossible to be rescued by nutritional support alone (K. Fearon et al., 2011). Cachexia appears in most cancer types with the highest percentage occurrence in liver and pancreatic cancer (Anker et al., 2019). Although different opinions exist whether cachexia directly or indirectly causes mortality by driving the inflammatory state of the cancerous disease, it indispensably leads to decreased quality of life due to functional impairment and for that reason, patients end up in a vicious circle (Davidson et al., 2004; Kalantar-Zadeh et al., 2013). Besides physiological and psychological worsening, cachexia furthermore negatively influences the efficacy of chemotherapy by causing additional side effects which lead to less

completed cycles of treatment depending on the chemotherapeutic scheme (Suzuki et al., 2013).

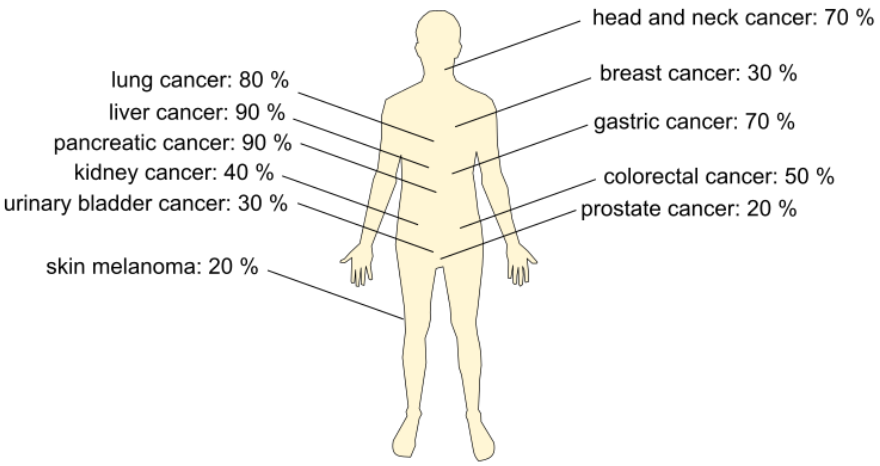

Figure 1: Cancer cachexia and its prevalence in Europe.
Data according to *Anker* and coworkers (Anker et al., 2019).

Sarcopenia is a state of progressive skeletal muscle loss that can, on the one hand, be a sign for age-related physical decline and, on the other hand, be a characteristic comorbidity of severe general illness such as cancer (Cruz-Jentoft et al., 2019). Since symptoms and diagnostic criteria of sarcopenia and cachexia overlap, it is still discussed whether disease-related sarcopenia is an early form of cachexia or one of its symptoms (Bauer et al., 2019). As already mentioned in the context of cachexia, especially female sarcopenic patients may suffer from increased side effects during chemotherapy due to a direct linkage between low lean body mass and toxicity of the used chemotherapeutic agents (Prado et al., 2007).

1.3 Definitions and limitations of cachexia and sarcopenia research

Since the underlying mechanisms and metabolic changes during cachexia as well as sarcopenia remain largely unknown, proper definitions have to be found to support not only research but also physicians in daily clinical practice. Because cachexia as a disease reveals overlapping symptoms with sarcopenia and anorexia, such as physical impairment by changing body composition, loss of appetite and malnutrition, cachexia research is still limited and faces a variety of different scientific challenges. One of the most influential publications in the last decade that discusses and structures the topic of cachexia is the international consensus on cancer cachexia published by *Fearon et al.* in 2011. Besides the different stages of cachexia - named pre-cachexia, cachexia and refractory cachexia - relevant key features as well as catabolic drivers and a detailed possible definition of cancer cachexia were provided. According to the experts' opinion, a patient suffers from cachexia if he or she experiences a weight loss of at least 5 % over the past 6 months or a weight loss of 2 % in the mentioned

time frame if accompanied by a BMI of less than 20 kg/m^2 or measurable sarcopenia (K. Fearon et al., 2011). Driven by the need to improve staging and diagnosis of cachexia, a special scoring system was developed by *Argilés et al.* in 2011 named the CASCO score. Here, the combination of body composition data, selected blood values evaluating an inflammatory state or metabolic disturbances and a questionnaire to be answered by the patient regarding physical performance, anorexia and quality of life provides a score that classifies into subgroups with either mild, moderate, severe or terminal cachexia, shown in Table 1. (Argiles et al., 2011)

Table 1: CASCO score and its parameters.

Scoring parameter	Range of points
Body weight loss and composition	0 - 40
Inflammation, metabolic disturbances and immunosuppression	0 - 20
Physical performance	0 - 15
Anorexia	0 - 15
Quality of life	0 - 10

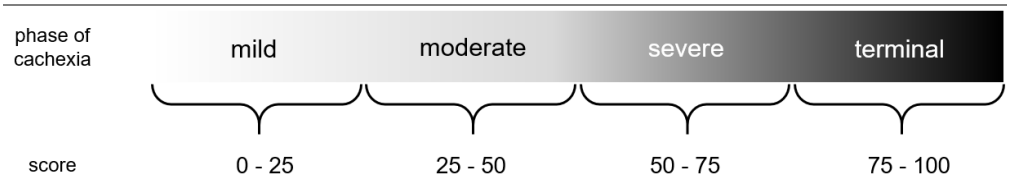

Modified according to *Argiles* and coworkers (Argiles et al., 2011).

Since the determination of body composition or the usage of special questionnaires may be too laborious for clinical practice, some studies exclusively concentrated on making statements of a possible cachectic status via routinely measured laboratory blood parameters, such as C-reactive protein (CRP). This is the basis of the often-used Glasgow Prognostic Score (GPS), which was first described in 2003 in non-small-cell lung cancer by *Forrest et al.* A modified version now uses thresholds of serum albumin and CRP and their proportion to one another to score patients from 0 to 2 (Douglas & McMillan, 2014; Forrest et al., 2003). Zero either describes a non-cachectic or undernourished state, whereas a score of one stands for pre-cachexia and the maximum score of two for refractory cachexia shown in Table 2 (Douglas & McMillan, 2014). It has been shown that this scoring system successfully predicts survival not only in pancreatic adenocarcinomas but also among cancerous diseases of the colon and rectum (Kurahara et al., 2015; McMillan et al., 2007). Furthermore, other studies modified the just mentioned cachexia definitions and classifications or decided upon a combination of publications to individually match the needs of the performed study.

Table 2: GPS and its parameters.

CRP [mg/l]	Albumin [g/l]	GPS	Interpretation
< 10	> 35	0	no cachexia
< 10	< 35	0	undernourished
> 10	> 35	1	pre-cachexia
> 10	< 35	2	refractory cachexia

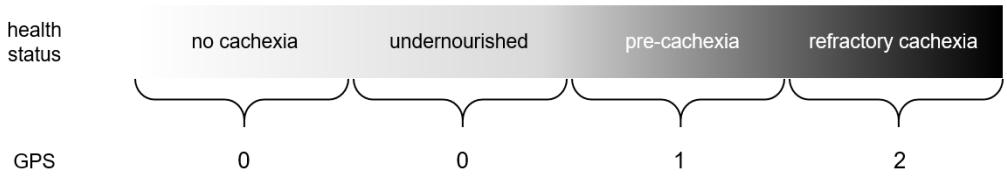

Modified according to Douglas et al. (Douglas & McMillan, 2014).

At first glance, the definition of sarcopenia seems more straightforward in comparison to cachexia due to the involvement of mere muscle tissue instead of muscle and fat tissue. Definitions of sarcopenia, however, overlap not only with cachexia but also with conditions like frailty and, therefore, led to several consensus meetings of experts in this field. The first report of the European Working Group on Sarcopenia in Older People (EWGSOP) took place in 2010 and was complemented by a second consensus meeting in 2018. The contributors defined sarcopenia as a combination of low muscle strength, low muscle quantity and quality as well as low physical performance. They stated that, among a clinical setting, the investigation of muscle strength and physical performance was in focus which included measurement of hand grip strength and the accomplishment of, for example, the gait speed test or the chair stand test. For most of the named tests and methods cut-off points were provided (Cruz-Jentoft et al., 2010; Cruz-Jentoft et al., 2019). Muscle quantity and quality in terms of sarcopenia were frequently used in research-based publications. A commonly used technique to investigate muscle tissue loss is the direct measurement and extrapolation of whole-body muscle mass via CT scans at the third lumbar vertebral body (L3). In 2008, *Prado et al.* demonstrated sarcopenia to be determined in obese patients with respiratory or gastrointestinal cancer by calculating the skeletal muscle area index (SMAI) out of cross-sectional areas at L3. Given cut-offs according to sex (52.4 cm^2/m^2 for men and 38.5 cm^2/m^2 for women) provide a helpful tool to define a sarcopenic status and, therefore, to predict the patients' future functional status, survival and possibly even chemotherapy toxicity. (Prado et al., 2008)

Summarizing, recent research delivered numerous possible approaches to define and classify cachexia as well as sarcopenia, but the often-unjustifiable expense in clinical practice in addition to the huge heterogeneity of patients regarding their diseases and stages of tumors is still a challenge.

1.4 Cachexia as a multi-organ syndrome

Muscle tissue is mainly affected by cachexia due to its close linkage to sarcopenia and the fact that muscle loss appears to be the central symptom of both cancer comorbidities. But research revealed cachexia to be a multi-organ syndrome in which organs such as different types of adipose tissues, heart, brain, gut and especially liver additionally contribute to the manifestation of the described metabolic state by direct interaction and cross-talk signaling (Argilés et al., 2018).

1.5 Muscle tissue loss and its connection to cachexia

Muscle tissue loss in patients suffering from cachexia can have various reasons, reaching from a negative energy balance through loss of appetite and brain triggered anorexia towards metabolic alterations in skeletal muscle and connected tissues (Argilés et al., 2018). Muscle atrophy in healthy muscle tissue, which describes the decrease of myocyte cell size through the loss of proteins, cell organelles and cytoplasm, is induced by two main degradation systems: the ubiquitin proteasome system (UPS) and the autophagy lysosome system (Argilés et al., 2018). UPS is one of the main processes to degrade misfolded or damaged proteins through enzyme-assisted binding of ubiquitin to a protein which is hence marked and can be dismantled by the proteasome into its amino acids and is regulated by the Forkhead box O (*FoxO*) transcription factors (Sandri, 2016; Yang et al., 2020). Research revealed that murine cachexia models show increased expression of ubiquitin ligases such as *ATROGIN1* and Muscle RING Finger 1 (*MURF1*) or a transcriptional upregulation of certain proteasome subunits under cancer cachexia. Especially tumor necrosis factor alpha (*TNFα*) and its homologue TNF-related weak inducer of apoptosis successfully activated the mentioned ligase family (Dogra et al., 2007; Lecker et al., 2004; Wyke et al., 2004). One of the few human studies in this field, provided by *Sun et al.* in 2012, demonstrated that the ubiquitin ligase TRAF6 as well as the expression of *ubiquitin* itself is increased in muscle tissue of patients with gastric cancer compared to controls suggesting that TRAF6 may induce ubiquitin activity in cancer cachexia (Y.-S. Sun et al., 2012). Additionally, UPS can also be activated via the Interleukin-6/Janus kinase/Signal Transducers and Activators of Transcription (IL-6/JAK/STAT) pathway. IL-6 is a well-studied inflammatory cytokine which is produced by for example macrophages, stromal cells, epithelial cells and muscle cells. The reason why it is often brought into play as a possible cachexia or sarcopenia biomarker is the fact that it plays a crucial role in the tumor microenvironment where it is even secreted by tumor cells themselves and enhances inflammation (Vainer et al., 2018). In the context of UPS, soluble IL-6 binds to its extracellular receptor (IL-6R) and this signal is transmitted by gp130. The cascade is called the classical pathway and is restricted to cell types expressing IL-6R such

as hepatocytes, myocytes and certain epithelial cells. The so termed trans-signaling pathway, on the contrary, describes the binding of soluble IL-6 to a soluble receptor (sIL-6R) and its formation and dimerization to a complex which can directly activate gp130. This pathway is mostly relevant in the context of tumor environment and not limited to specific cell types (as the classical pathway), since gp130 is expressed in most human cells (Wolf et al., 2014). Downstream of gp130, the signal transducing chain activates JAK which phosphorylates the transcription factor STAT3, giving it the possibility to form dimers and migrate into the nucleus of the cell to stimulate certain gene expression patterns (Wang & Sun, 2014). Murine cachexia models revealed that the inhibition of JAK/STAT pathway by drug treatment leads to decreased muscle wasting, whereas a knock-in of the signal transducing chain gp130, upstream of STAT3, drives the cachectic state and promotes weight loss and the reduction of muscle and adipose tissue mass (Guo et al., 2017; Miller et al., 2017).

The autophagy lysosome system, which represents macroautophagy, describes the second main degradation system of muscle cells and cells in general. It is used to degrade macromolecules or damaged organelles. Similar to UPS, macroautophagy is activated through *FoxO* transcription factors, which induce the expression of autophagy-related genes. During the process of macroautophagy an autophagosome is formed around the material of interest which fuses with a so called lysosome containing lysis enzymes that lead to degradation of the content (Sandri, 2016). This mechanism is not only used for intracellular clean-up but also as an energy source during starvation, since amino acids derived from protein breakdown can be used for gluconeogenesis in the liver (Karsli-Uzunbas et al., 2014). The study of *Penna et al.* in 2013 demonstrated that muscle tissue degradation by the autophagy lysosome system occurs in three different murine models of cancer cachexia but, interestingly, macroautophagy is impaired in sarcopenic animals pointing out muscle atrophy in being the result of either strongly pronounced or defective autophagy (Penna et al., 2013). A human study with patients suffering from gastrointestinal cancer-associated cachexia reported specific macroautophagy-related as well as apoptosis-related proteins to be elevated in skeletal muscle tissue compared to the muscle of weight stable controls indicating that an increase in apoptosis could be a key driver of muscle wasting under cachexia (Castro et al., 2019). To note, several murine models give hint that muscle wasting under cachexia is, additionally to the already mentioned cellular degradation systems, possibly reinforced by the muscle's impaired capacity for regeneration (Bossola et al., 2016).

A growth and differentiation factor that is highly involved in the regulation of muscle tissue mass is the protein myostatin. The extracellular cytokine is a member of the TGF-β superfamily and is mainly expressed in muscle tissue where it activates Smad2/3 by binding to the type IIB activin receptor (ActRIIB) on the muscle cell's surface. This pathway initiates signaling

cascades on the one hand promoting the expression of atrogenes and on the other hand leading to decreased expression of myogenesis-related genes (Elkina et al., 2011; Sharma et al., 2015). Since myostatin is a muscle growth inhibitor, it got into focus regarding cachexia and sarcopenia research. In the context of cancer cachexia, studies in rodents revealed that cancer models show elevated myostatin protein levels whereas a blocking of myostatin or its pathway leads to prolonged survival and an increasing muscle growth (Costelli et al., 2008; Liu et al., 2008; Zhou et al., 2010). However, results among humans seem to be more heterogeneous. In the case of gastric cancer, some results indicate that *myostatin* expression is increased in cancer patients, whereas other studies demonstrate similar expression or even lower expression compared to controls (Aversa et al., 2012; Bonetto et al., 2013; D'Orlando et al., 2014). Additionally, the Smad2/3 pathway seems to be increasingly activated dependent on disease progression in PDAC, since the secretion of activin A, a second ligand of ActRIIB, was shown to be elevated in metastatic compared to stage I patients (Talar-Wojnarowska et al., 2020). But not only muscle tissue owns a role in cancer associated cachexia, also liver is involved in relevant processes.

1.6 Liver homeostasis and its role under cachexia

The liver is a central organ of the digestive system with various tasks such as lipid and cholesterol metabolism. It supports and regulates the immune system and controls the body's glucose balance. Furthermore, it controls the blood glucose levels triggered by the insulin to glucagon ratio. This ratio describes the liver's effort to promote glycolysis for adenosine triphosphate (ATP) production or storage of glucose in form of glycogen during feeding and high levels of insulin, whereas during fasting, high levels of glucagon lead to gluconeogenesis to keep blood glucose levels stable (Trefts et al., 2017). Lipid metabolism in the liver can have various appearances in regard of the dietary status. After meal consumption, when insulin levels are high, fatty acids that were not already taken up by white adipose or muscle tissue are transferred to the liver. Additionally, *de novo* lipogenesis is activated to convert glucose out of excess carbohydrates into fatty acids. These fatty acids are either directly metabolized or esterified by hepatocytes to triglycerides which can be stored as cytoplasmic lipid droplets short term. During fasting, uptake of fatty acids from plasma occurs which were beforehand released out of the depots of white adipocytes due to low insulin levels (Alves-Bezerra & Cohen, 2017). Although the liver is not seen as an immunological active organ, it highly contributes to an inflammatory immune response caused by either tissue damage, pathogens or cancer by releasing positive acute phase proteins such as CRP, serum amyloid A, fibrinogen and several complement factors into the plasma (Argilés et al., 2015; Robinson et al., 2016). Additionally, negative acute phase proteins such as albumin and transferrin are decreased during inflammation (Andersson et al., 1993). Since cancer cachexia is strongly connected to

an inflammatory state the homeostasis between albumin and CRP is used to define different status of cachexia (Douglas & McMillan, 2014). Already in 1991, *Fearon* and coworkers demonstrated that weight-losing patients with colorectal cancer undergo an increased hepatic acute phase response by means of elevated levels of circulating CRP and hypoalbuminemia additionally showing significantly increased levels of IL-6 (K. C. Fearon et al., 1991). Not only pro-inflammatory cytokines have an active role in the hepatic participation in cancer-associated inflammation. The expression of the anti-inflammatory cytokine Interleukin-4 (*IL-4*) was shown to be downregulated in the liver of patients suffering from both pancreatic cancer and cachexia (Prokopchuk et al., 2017). Immunohistochemistry stainings revealed a significantly higher amount of CD68 positive macrophages in the liver of pancreatic cancer patients compared to a weight stable control group. Additionally, a local increase of IL-6 and interleukin-1 (IL-1) immunoreactive cells occurred highlighting the liver's role during inflammation due to cachexia (Martignoni et al., 2009). Several studies in rats revealed the involvement of mitochondrial activity in the liver in energy wasting due to decreased efficiency of oxidative phosphorylation and ATP synthesis which is to some extent dependent on increased content of the mitochondrial membrane protein Cardiolipin (Dumas et al., 2011; Julienne et al., 2014). Summarizing, muscle and liver tissue behave just the opposite way under catabolic conditions such as cancer cachexia and sarcopenia. As described, muscle protein degradation leads to an amount of released amino acids which can in turn be used by the tumor itself to promote its energy-forming pathways and growth. Furthermore, the liver metabolizes these amino acids to enhance gluconeogenesis and the synthesis of acute phase proteins (Argilés et al., 2015; Hensley et al., 2013; Sirniö et al., 2019).

1.7 Adipose tissue types and their relations to cachexia

Seen as a collection of cells with the purpose of lipid storage and a mere form of connective tissue between organs in the abdominal cavity, adipose tissue was severely underestimated until the 1980s. From that moment, research began to realize that adipose tissue is a complex endocrine organ which is highly involved in energy homeostasis by either storing or supplying energy in the form of fatty acids or even controlling body temperature through thermogenesis (Rosen & Spiegelman, 2014). Furthermore, the high physiological plasticity and manifold anatomy is characterized by sophisticated vascular and neural supply to support the complex cytology of adipose tissue (Cinti, 2012). The variety of tasks to be implemented can only be managed by specialized cell and tissue types that control these metabolic pathways, speaking of white and brown, as well as beige adipose tissue. These three adipose tissue types vary not only according to their function but also to their structure, color and infiltration with non-adipose cell types (Frigolet & Gutiérrez-Aguilar, 2020). Apart from adipocytes, each type of adipose tissue consists of the so-called stromal-vascular fraction which mainly contains

adipose-derived stem cells, preadipocytes (PACs) – both progenitors of the mature adipocyte – endothelial cells, fibroblasts, smooth muscle cells and immune cells such as macrophages, lymphocytes and pericytes (Bora & Majumdar, 2017). The structure and function of white, brown and beige adipose tissue, as well as its role in cachexia will be outlined in the following sections.

1.7.1 White adipose tissue

When people talk about fat tissue, mostly white adipose tissue (WAT) is addressed which constitutes about 20 % of the body weight of human adults and is characterized by its ivory to yellow color. WAT is already predetermined *in utero* out of mesenchymal stem cells but its actual development starts after birth when the newborn is confronted with short alternating periods of feeding and fasting (Park et al., 2014). Its main and most obvious functions are the storage of fat in the form of triglycerides (according to IUPAC better named triacylglycerols (TG)), the increase of cohesion among the different organs of the abdominal cavity and also the padding of bony structures such as the heel which have to withstand constant pressure for example during walking (Frigolet & Gutiérrez-Aguilar, 2020; Rosen & Spiegelman, 2014; Saad et al., 2021). White adipocytes are the main type of parenchymal cells of WAT, they account for around 40 % of the cells but 95 % of adipose tissue's volume (Bäckdahl et al., 2021). Cells are spherical as well as unilocular and their volume is of around 90 % constituted by a single cytoplasmic lipid droplet functioning as triglyceride storage which hence forces remaining cell organelles such as the nucleus to be pressed and flattened against the cell's boundaries (Figure 3) (Cinti, 2012). According to its location, WAT is divided into two main subtypes: subcutaneous (sc) and visceral adipose tissue (vc). Sc adipose tissue is directly localized under the skin or pervades skeletal muscle tissue in the form of intramuscular fat. It represents the largest compartment of adipose tissue (Park et al., 2014; Thomas et al., 1998). Sc is further subdivided into gluteal and femoral sc as well as abdominal sc adipose tissue, which is the most prominent and well-studied depot. Vc adipose tissue surrounds the organs of the abdominal cavity and the vascular system in order to protect them from external pressure. Further, its role is to hold the organs in place. Subgrouping comprises epicardial and pericardial adipose tissue surrounding the heart, perirenal adipose tissue covering the kidneys, epididymal and parametrial adipose tissue being located around the gonads, and perivascular adipose tissue coating the vasculature. Omental adipose tissue (om) – the biggest compartment of vc adipose tissue – surrounds the intestines (Cheng et al., 2018; Frigolet & Gutiérrez-Aguilar, 2020) (Figure 2). The individual ratio of sc to vc WAT depends on various factors such as age, sex and lifestyle with women rather showing disproportionate amounts of sc WAT under overweight and obesity, whereas men tend to accumulate higher quantities of vc WAT (Power & Schulkin, 2008). Furthermore, an increased amount of vc WAT is associated

with an elevated risk of diabetes and metabolic syndrome (Gesta et al., 2007; Schoettl et al., 2018).

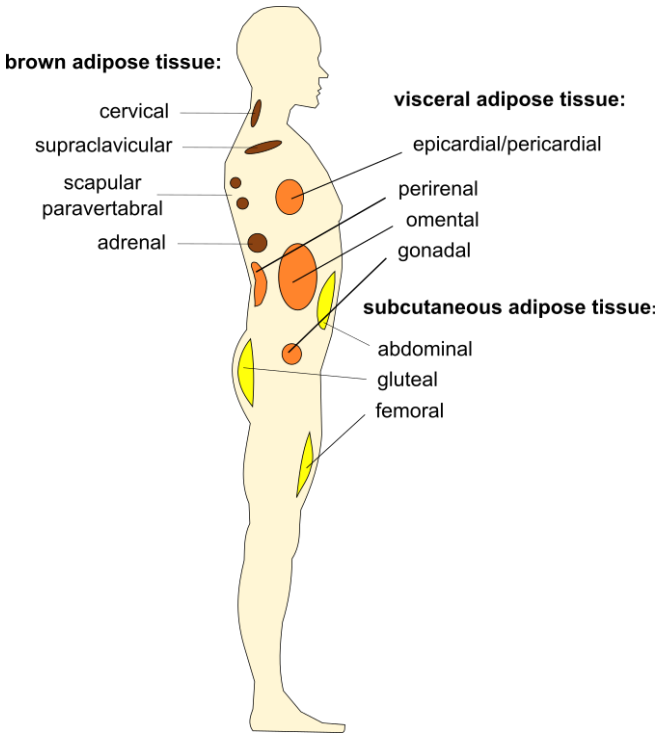

Figure 2: Designation and destination of visceral (white), subcutaneous (white) and brown adipose tissue in humans.
Modified according to Frigolet and Gutiérrez-Aguilar (Frigolet & Gutiérrez-Aguilar, 2020).

WAT controls energy homeostasis through a sophisticated interplay of lipolysis, lipid uptake and *de novo* lipogenesis. When energy demand rises either an increase of glucagon and catecholamines such as norepinephrine or a decrease of insulin triggers lipolysis, a process in which TGs are broken down into the glycerol backbone and three free fatty acids (FFA) each. The cleavage of the connective ester bonds is catalyzed by adipose triglyceride lipase, hormone sensitive lipase (HSL) and monoglycerol lipase (Duncan et al., 2007). Separated FFAs are now released into the blood stream and by the help of albumin transferred to the target tissue, where they are indirectly converted to ATP by β-oxidation (Daas et al., 2018; van der Vusse, 2009). In general, most of the body's cells are capable of *de novo* lipogenesis, since fatty acids are an essential component of all cell membranes. The highest rates of *de novo* lipogenesis are, however, observed in liver, skeletal muscle, gut, skin and WAT (Hollands & Cawthorne, 1981). White adipocyte storage and incorporation of lipids can thereby either occur through the uptake of elsewhere formed TGs or synthesized by own lipogenesis. The mentioned uptake in adipose tissue is controlled by the enzyme lipoprotein lipase (LPL) which hydrolyzes circulating TGs into fatty acids to enable fat storage, making it a homologue of monoglycerol lipase but for a different purpose (Murphy et al., 1981). In lipogenesis, glucose is taken up into the cell's cytosol by the help of insulin-stimulated transporters such as glucose

transporter type 4 (GLUT4). It is converted into pyruvate during glycolysis, carried into the mitochondria to be transformed into citrate by Acetyl-CoA. Finalization into fatty acids takes place in the cytosol via various interim steps through specialized enzymes such as fatty acid synthase (FASN). The gained fatty acids can now either be further metabolized, secreted into the bloodstream in a special transport format or esterified into TGs using a glycerol backbone and three fatty acids per molecule (Z. Song et al., 2018).

Since WAT as an endocrine organ produces several hormones and inflammatory molecules such as leptin, adiponectin, IL-6, IL-1β, TNFα, zinc-alpha-2-glycoprotein (ZAG) and many more, the research's focus on the involvement of these messenger molecules in cancer cachexia is inevitable (Daas et al., 2018). Before ZAG was discovered to be expressed in sc and vc WAT of humans by *Bing et al.* in 2004, it was just known to be a glycoprotein appearing in prostate, breast, sweat, bronchial and esophageal glands as well as in cells of pancreas, liver and kidney (Chen Bing et al., 2004; Tada et al., 1991). In *in vitro* approaches, ZAG extracted from cancer patients' plasma was shown to stimulate glycerol release in murine adipocytes and, additionally, administration of the protein to mice led to the reduction of fat mass and an increased amount of circulating fatty acids by triggering lipolysis through the activation of HSL (Hirai et al., 1998). Several studies followed, pointing out the driving force of ZAG in lipolysis in WAT by activating β3-adrenergic receptors and the cyclic adenosine monophosphate (cAMP) pathway building a bridge towards adipose tissue loss under cancer cachexia (Elattar et al., 2018; Russell et al., 2002). Additionally, it was found that exposure of leptin leads to increased lipolysis in WAT pads of rats *ex vivo* (Siegrist-Kaiser et al., 1997). Further research in the direct context of cachexia revealed cachectic patients with gastric and colorectal cancer showing increased serum levels of IL-6 and TNFα in certain stages of cachexia and, additionally, lipolysis in WAT. In experiments with cachectic mice this effect could be traced back towards IL-6 (Han et al., 2018). Concentrating on molecular mechanisms of lipolysis, increased activation of HSL is involved in WAT during cancer cachexia and in humans the inhibiting impact of insulin on lipolysis forfeits its effectiveness speaking of insulin resistance (Argilés et al., 2005; Argilés et al., 2014). In knock-out experiments, insulin resistance, an increased inflammatory response as well as lipolysis was found in adipose tissue lacking Perilipin 1, a protein which under normal conditions encircles lipid droplets and inhibits lipolysis in white adipocytes, making it a possible target for cachexia research (Sohn et al., 2018).

Besides lipolysis, cachexia seems to alter the metabolism of white adipocytes regarding lipogenesis as well as fatty acid storage with limited data available. Although some studies state lipogenesis is reduced in cachexia models suggesting TNFα as a driving force, others found that lipogenesis under cachexia may on the contrary be increased (not only in adipose

tissue but also in organs such as kidneys, liver and epididymal fat pads) using the released fatty acids as fuel for tumor growth (Fearon et al., 2012; Mulligan & Tisdale, 1991; Rohm et al., 2016; TREW & BEGG, 1959). Fatty acid storage, powered by the conditioning through LPL was investigated in several studies. It was revealed that TNFα and IL-6 do not only decrease LPL activity but also its expression, which leads to WAT wasting through absent support of its lipid accumulation (Greenberg et al., 1992; Hauner et al., 1995).

Summarizing, the fact of lipolysis in WAT in some way contributing to cancer cachexia is beyond any doubt but the involvement of its counterpart lipogenesis and a possible disturbance of this fragile homeostasis leading to adipose tissue depletion still needs to be elucidated.

1.7.2 Browning and related adipose tissues

About two decades ago, research rediscovered that adult humans not only possess adipose tissue in the form of WAT but also gain a special type of darker colored adipose tissue named brown adipose tissue (BAT) which is still metabolically active (Virtanen et al., 2009). Brown adipocytes are multilocular cells with several smaller lipid droplets and a round nucleus that contain an increased amount of mitochondria providing their characteristic color (Figure 3) (Cinti, 2012). The presence of high numbers of mitochondria defines BAT function. Unlike WAT, it is not involved in the storage of fat but contributes to energy homeostasis through thermogenesis. Here, the tissue generates heat from chemical energy, a process that is catalyzed by uncoupling protein 1 (UCP1). UCP1 uncouples oxidative phosphorylation from ATP synthesis by creating a proton leak across the inner mitochondrial membrane (Park et al., 2014; Rosen & Spiegelman, 2014). But not only the amount of mitochondria differentiates brown from white adipocytes, mitochondria in BAT are larger and own a proteome which is similar to the mitochondrial proteome of muscle cells (Lee et al., 2019). In contrast to WAT, BAT is fully developed at birth to protect the newborn child from cold by defending body temperature without shivering. This explains the fact that human babies contain significantly greater amounts of BAT compared to adults where remnants, which can be activated by stimulation with chronic cold, are only found in cervical, supraclavicular, scapular paravertebral and adrenal regions (Frigolet & Gutiérrez-Aguilar, 2020; Nedergaard et al., 2007; Park et al., 2014; Rosen & Spiegelman, 2014) (Figure 2).

Experiments in rodents revealed – after acclimatization to cold temperatures – brown colored cells beginning to appear in classical WAT regions termed as beige or brite adipocytes (Barbatelli et al., 2010). This cell type is not only found in rodents but also in humans and stands out by being not only a phenotypic but a progenitor-like linkage of brown and white adipocytes. Beige adipocytes show a multilocular appearance and a similar *UCP1* expression pattern as brown adipocytes but do not originate from the same embryonic progenitor

(Figure 3). Moreover, they are localized in WAT regions raising different hypotheses of origin. Beige adipocytes might be derived from white adipocyte precursors which develop into beige cells when exposed to certain stimuli such as cold or special hormones. Alternatively, beige adipocytes could stem from mature white adipocytes undergoing transdifferentiation, a process termed “browning” (Barbatelli et al., 2010; Frigolet & Gutiérrez-Aguilar, 2020; Klingenspor et al., 2012).

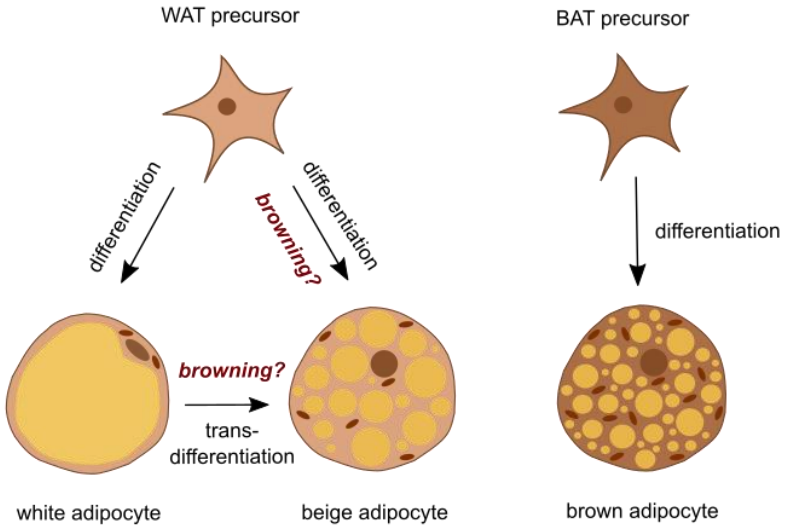

Figure 3: Schematic overview of white, beige and brown adipocytes

Several murine studies underpin the hypothesis of increased thermogenesis induced by either browning of WAT or activation of BAT elevating energy expenditure. This could worsen a cachectic state independent of thermal stimuli by the surrounding environment. *Petruzzelli* and coworkers demonstrated in 2014 that browning of sc WAT takes place in early stages of murine cachexia models. The effect is verifiably accompanied by increased expression of *UCP1* in mice as well as positive UCP1 stainings of cachectic patients compared to non-cachectic controls (Petruzzelli et al., 2014). The neutralization of parathyroid hormone-related protein (PTHrP) and the knock-out of the transcriptional coregulatory PR/SET domain 16 (*PRMD16*) in a murine cancer cachexia model led to a blockade of WAT browning and prevented loss of adipose as well as muscle tissue. Furthermore, in a human cohort of patients with non-small cell lung cancer and colorectal cancer it was shown that patients with elevated PTHrP serum levels are additionally characterized by a significantly lower lean body mass and higher resting energy expenditure. This points out the possible involvement of this tumor-derived small polypeptide in the pathways of cancer cachexia (Kir et al., 2014).The protein ZAG, which was mentioned earlier due to its participation in WAT lipolysis, is additionally involved not only in cachectic browning of WAT but also in the activity of BAT itself and functions as an extracellular stimulus under cachexia. *Elattat* and coworkers highlighted in their research with healthy mice

that ZAG stimulated the expression of peroxisome proliferator-activated receptor γ (*PPARγ*), early B cell factor 2 as well as, via its promoter *PRDM16,* which in turn enhanced browning of WAT. In BAT, ZAG elevated the expression of *PPARγ* and related genes leading to increased expression of *UCP1*, making ZAG a possible target for cachexia research due to its involvement in the regulation of thermogenesis (Elattar et al., 2018). Due to the fact that chronic inflammation is a key driver of cancer cachexia pro-inflammatory cytokines such as IL-6 came into focus early on (Fearon et al., 2012). Several studies on murine tumor models revealed blocking of soluble IL-6 as well as knock-out or blocking of IL-6 receptor to decrease browning and thereby the cachectic state by reducing UCP1 protein levels resulting in prevention of WAT atrophy (Han et al., 2018; Petruzzelli et al., 2014). Until today, it remains uncertain why a subset of patients develops cachexia or sarcopenia under cancer and why others do not. This gave rise to the question whether a patient's genetic background controls specified metabolic pathways leading to atrophic conditions. Up to date, gene polymorphisms that may contribute to low body weight and fat-free mass, such as IL-1β, IL-6 and TNFα, were investigated among cachectic chronic obstructive pulmonary disease (COPD) patients (Broekhuizen et al., 2005). But the gene that mainly attracted our attention was the fat mass and obesity-associated (*FTO*) gene first described by *Frayling et al.* in 2007 whose risk allele is known to predispose diabetes through a rising BMI (Frayling et al., 2007). Later on, *FTO* was, by the help of a genome-wide association study, successfully related to thermogenesis and browning in WAT due to the causal variant rs1421085. Here, a T-to-C single nucleotide change leads to three possible genotypes: the wild type (WT) TT, the risk type CC and the heterozygous combination CT. The risk allele (comprised in CC or CT) disturbs the functioning of AT-Rich Interaction Domain 5B (*ARID5B*) which now fails to suppress Iroquois Homeobox 3 (*IRX3*) as well as Iroquois Homeobox 5 (*IRX5*), a circumstance that leads to repressed thermogenesis and browning in WAT through – among other interactions – decreased *UCP1* expression (Claussnitzer et al., 2015). This interplay consequently results in increased lipid storage and obesity and can in theory, if an inverse action of the *FTO* gene is taken into account, possibly be linked to a thermogenesis-driven cachectic state. Studies by *Wan et al.* confirmed this hypothesis as, in patients with COPD, single nucleotide polymorphisms of the *FTO* gene might be associated to cachexia by influencing BMI and the fat-free mass index (Wan et al., 2011). Although activation of BAT and browning of WAT seem to be involved in the development and activation of cachexia and sarcopenia, further research is needed to elucidate the molecular mechanisms. To do so, various cellular models are available. One of them are mesenchymal stem cells and cells downstream of this lineage.

1.8 White adipocyte differentiation

Due to the fact that *in vivo* analyses of human adipose tissue pose a hardly resolvable challenge, research either focuses on *in vivo* experiments in rodents or on cell culture approaches performed *in vitro*. Since freshly isolated adipocytes float in medium and cannot be attached to any kind of cell culture plastics, preadipocytes are isolated instead. They can be cultivated in an adherent manner and can be differentiated into mature adipocytes using established media. The first group to successfully isolate and differentiate human preadipocytes was *Hauner* and coworkers in 1987. In this publication as well as in their following one in 1989, they demonstrated that the stromal vascular fraction of adult humans contains adipogenic precursor cells which can *in vitro* be differentiated into mature adipocytes using a stimulation cocktail of cortisol and insulin. The differentiation capacity was influenced by various factors such as the concentration of the added cortisol and the age of the human donor (Hauner et al., 1987; Hauner et al., 1989). Since other research groups were inspired by these early results, many key factors of this complex process could be discovered until today. The gained knowledge about the differentiation process of preadipocytes into mature white adipocytes is summarized and addressed in the following.

The process of adipogenesis comprises two phases, the first describing the commitment of a pluripotent mesenchymal stem cell towards the adipocyte lineage instead of the one directing to chondrocytes, myocytes or osteocytes. The pathways are controlled by a defined interplay of transcription factors which either promote or inhibit a certain lineage. During the phase of commitment certain bone morphogenic proteins (BMP2 and BMP4) induce adipogenesis via the Smad as well as the p38MAPK pathway resulting in the development of a preadipocyte (Huang et al., 2009; Tang & Lane, 2012). The second phase – often referred to as terminal differentiation – comprises the preadipocyte's acquisition of adipogenic morphology as well as the expression of adipogenic genes and describes what is under standard conditions termed "adipogenic differentiation" (Rosen & MacDougald, 2006).

Until today, multiple regulators of adipogenic differentiation – transcribed by either mRNA or miRNA – have been investigated but one transcription factor stands out: PPARγ. It is known as the master regulator of adipogenic differentiation since no factor has been discovered that is able to drive differentiation during its absence which (demonstrated by knock-out experiments) leads to a dramatic decrease of adipose tissue in rodents or even embryonic lethality (Arner & Kulyté, 2015; Barak et al., 1999; Rosen & MacDougald, 2006). Upstream of PPARγ and in a very early phase of differentiation the CCAAT/enhancer-binding protein β (C/EBPβ) is activated by Smad/p38MAPK. It receives access to the DNA resulting in the induction of *PPARγ* and *C/EBPα*. Further downstream, PPARγ enhances glycerol-3-phosphate

dehydrogenase (GPDH), a marker for late adipogenic differentiation (Patsouris et al., 2004; Tang & Lane, 2012). C/EBPα activates adipocyte specific genes and hence it is used as an adipocyte differentiation marker. Although it is unable to enhance adipogenesis in the absence of PPARγ, it was discovered that it is crucial for the acquisition of insulin sensitivity mediated by GLUT4 in mature adipocytes making it an additional key player in the differentiation process (El-Jack et al., 1999; Freytag et al., 1994; Rosen et al., 2002; Wu et al., 1999). PPARγ and C/EBPα are supported by various other proteins and transcription factors such as Krüppel-like factor 15 (KLF15). It acts as a synergistic co-player of C/EBPα by its capability to enhance GLUT4 activity or sterol regulatory element-binding proteins such as SREBP1c. Its PPARγ and C/EBPα downstream activation regulates lipid homeostasis through the expression of genes required for cholesterol and TG synthesis (Gray et al., 2002; Horton, 2002). An overview graphic of the here discussed genes is shown in Figure 4.

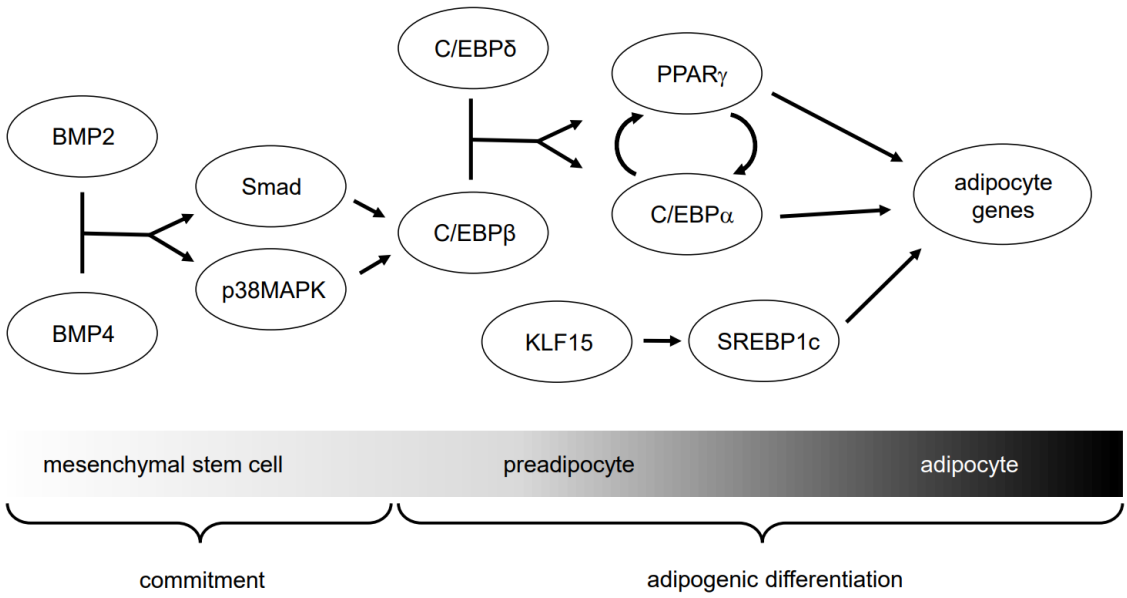

Figure 4: Key regulators during the phase of commitment and adipogenic differentiation.

Summarizing, various tissue types and diverse metabolic processes are involved in the occurrence and intensity of cachexia and sarcopenia. Therefore, research has to combine the investigation of possible alterations in early developmental phases, such as impaired cell differentiation, and changes in gene expression of mature cells. Both could shape the assembly and dismantling as well as the functioning of cachexia-related organs such as adipose tissue, skeletal muscle and liver.

2 Aims and objectives

Cachexia and sarcopenia, two challenging and often underestimated comorbidities of cancer, not only worsen the patient's quality of life, but also the outcome of the primary disease by inducing skeletal muscle as well as adipose tissue loss. Due to the fact that liver, muscle tissue and both WAT and BAT are involved in the metabolic alterations during cachexia and sarcopenia, research has to successfully combine present knowledge to uncover possible targets for effective therapy. The ongoing discussion about the best suitable definition of cachexia and the interindividual variance in reactions and symptoms underline the need for proper biomarkers to better characterize the disease and to provide personalized therapy in the future.

Although studies in rodents are indispensable in regard of fundamental research, studies in humans are vital to investigate the full range of possible cancer effects. Not only cancer types, also stagings and gradings as well as possible circulating cytokines might have an influence on the development of a patient's disease progression when burdened with cachexia or sarcopenia.

Therefore, the goal of this thesis was to build up a human cachexia biobank containing blood and different tissue types. Samples were used to elucidate possible drivers of cachexia and sarcopenia by the help of IL-6 plasma measurement of the whole cohort as well as a preadipocyte cell culture approach of selected patients to gain further insight into metabolic processes in extreme phenotypes. For this reason, associated genes such as *UCP1*, *PRDM16*, *ARID5B*, *IRX3*, *IRX5*, *C/EBP*α, *MT-CO2*, *ZAG*, *IL-6*, *Myostatin* and *PTHrP* were investigated.

3 Materials and methods

3.1 Chemicals and media

All chemicals and reagents used for the implementation of this thesis are shown in Table 3.

Table 3: Chemicals and reagents used during laboratory work.

Chemical	Company	Storage	Order number
(+)D-Biotin	Roth	4 °C	3822.1
5x MyTaq Reaction Buffer	Bioline	-20 °C	BIO-21106
10X RT Buffer, High-Capacity cDNA (Complementary deoxyribonucleic acid) Reverse Transcription Kit	Applied Biosystems	-20 °C	4368814
10X RT Random Primers, High-Capacity cDNA Reverse Transcription Kit	Applied Biosystems	-20 °C	4368814
25X dNTP (Deoxyribonucleotide triphosphate) Mix (100 mM), High-Capacity cDNA Reverse Transcription Kit	Applied Biosystems	-20 °C	4368814
Acid-phenol:chloroform 5:1	Ambion	RT	AM9720
AE buffer, Qiagen DNeasy Blood and Tissue Kit	Qiagen	4 °C	69504
alamarBlue Cell Viability Reagent	Thermo Fisher Scientific	4 °C	DAL1025
AL buffer, Qiagen DNeasy Blood & Tissue Kit	Qiagen	4 °C	69504
apo-Transferrin, human	Merck	4 °C	T2252
AW1 wash buffer, Qiagen DNeasy Blood & Tissue Kit	Qiagen	4 °C	69504
AW2 wash buffer, Qiagen DNeasy Blood & Tissue Kit	Qiagen	4 °C	69504
ß-Mercaptoethanol	Merck	RT	M3148
BCA (Bicinchoninic acid) Reagent A, Pierce Microplate BCA Protein Assay Kit	Thermo Fisher Scientific	RT	23252
BCA Reagent B, Pierce Microplate BCA Protein Assay Kit	Thermo Fisher Scientific	RT	23252
Biotinylated Goat Anti-Human IL-6 Detection Antibody	R&D Systems	4 °C	DY206
BSA (Bovine serum albumin)	Merck	4 °C	A 7906-500G
BSA for ELISA	Roth	4°C	2834.4
BSA solution 10 % in DPBS (Dulbecco's phosphate-buffered saline)	Merck	4 °C	A1595
$CaCl_2$ x 2 H_2O	Roth	RT	5239.1
Collagenase 0.2 U	Serva	4 °C	17454.01
Compatibility Reagent, Pierce Microplate BCA Protein Assay Kit	Thermo Fisher Scientific	RT	23252
Dexamethasone	Merck	4 °C	D4902
DHAP (Dihydroxyacetone phosphate)	Merck	-20 °C	D7137
DMEM/F-12 (Dulbecco's modified eagle medium/nutrient mixture F-12)	Gibco	4 °C	31330-038
DMSO (Dimethyl sulfoxide)	Merck	RT	1.02931
EDTA (Ethylenediamine tetraacetic acid)	Merck	RT	1.08417
EGF (Epidermal growth factor)	R & D Systems	-20 °C	236-EG
Elution solution, Invitrogen mirVana miRNA (Micro ribonucleic acid) and mRNA (Messenger ribonucleic acid) Isolation Kit	Thermo Fisher Scientific	any T	AM1561
EtOH (Ethanol) absolute	VWR	RT	20821.330
EtOH absolute analytical reagent grade	Thermo Fisher Scientific	RT	E/0650DF/C17
FCS (Fetal calf serum)	Merck	-20 °C	F7524
FGF (Fibroblast growth factor)	R & D Systems	-20 °C	233-FB

Chemical	Company	Storage	Order number
Gentamycin sulfate	Roth	4 °C	0233.4
Hydrocortisone	Merck	4 °C	H4001
Insulin, human	Merck	4 °C	19278
Isopropanol abs. (2-Propanol)	Thermo Fisher Scientific	RT	P/7500/PC17
IBMX (3-Isobutyl-1-methylxanthine)	SERVA	RT	26445
KCl (potassium chloride)	Roth	RT	6781.1
LightSNip rs1421085 FTO	TIB Molbiol	4 °C	Customized
Linoleic acid	Merck	-20 °C	L1376
Lysis Buffer, Invitrogen mirVana miRNA and mRNA Isolation Kit	Thermo Fisher Scientific	4 °C	AM1561
Maxima SYBR Green/ROX qPCR (Quantitative polymerase chain reaction) Master Mix (2X)	Thermo Fisher Scientific	-20 °C	K0223
$MgSO_4$ x 7 H_2O	Merck	RT	1.05886
miRNA Homogenate Additive, Invitrogen mirVana miRNA and mRNA Isolation Kit	Thermo Fisher Scientific	4 °C	AM1561
miRNA Wash Solution 1, Invitrogen mirVana miRNA and mRNA Isolation Kit	Thermo Fisher Scientific	4 °C	AM1561
miRNA Wash Solution 2/3, Invitrogen mirVana miRNA and mRNA Isolation Kit	Thermo Fisher Scientific	4 °C	AM1561
Mouse Anti-Human IL-6 Capture Antibody	R&D Systems	4 °C	DY206
MultiScribe Reverse Transcriptase (50 U/µL), High-Capacity cDNA Reverse Transcription Kit	Applied Biosystems	-20 °C	4368814
MyTaq DNA Polymerase	Bioline	-20 °C	BIO-21106
NaCl (Sodium chloride)	Merck	RT	6404
NADH (Nicotinamide adenine dinucleotide hydride)	Applichem	-20 °C	A-1393
NaH_2PO_4 x H_2O	Merck	RT	1.06346
NucBlue Live ReadyProbes Reagent Hoechst	Thermo Fisher Scientific	RT	R37605
Oleic acid	Merck	-20 °C	O1008
Pantothenate (D-Pantothenic acid hemicalcium salt)	Merck	4 °C	P5155
PBS (Phosphate-buffered saline) w/o Ca^{2+}/Mg^{2+}	Merck	RT	L182-50
PCR (Polymerase chain reaction) grade water, provided by ultrapure water system	Elga Veolia Purelab flex	RT	/
Penicillin-Streptomycin (10.000 units/10 mg/ml)	Merck	-20 °C	P0781
Proteinase K	Qiagen	RT	19131
Recombinant Human IL-6 Standard	R&D Systems	4 °C	DY206
RNAse A (17.500 U)	Qiagen	RT	19101
ROTI®Histofix 4 %	Roth	RT	P087.6
RLT buffer, RNeasy Kit	Qiagen	RT	1015762
Rosiglitazone	Merck	4 °C	R2408
Streptavidin-HRP	R&D Systems	4 °C	DY206
Substrate Solution 1x TMB	Invitrogen	4 °C	00-4201-56
Sulfuric acid (H_2SO_4)	Roth	RT	4319.1
T3 (3,3'-5-Triiodo-L-thyronin sodium salt)	Merck	-20 °C	T-6397
Triethanolamine-HCl (Hydrochloric acid)	Merck	RT	T1502
Tris-HCl	Merck	RT	T3253
Trypan Blue solution 0.4 %	Merck	RT	T8154
Trypsin/EDTA	Merck	-20 °C	T3924
Tween®20	Merck	RT	P1379

The composition as well as the preparation and storage instructions of buffers and solutions used during the laboratory process of this thesis are depicted in Table 4.

Table 4: Buffers and solutions.

Solution/buffer	Composition and preparation	C_{final}
Biotin/Pantothenate solution	400 mg Biotin 200 mg Pantothenate Dissolve in 500 ml DMEM-F12, sterile filter 0.2 µm, store at -20 °C	3.3 mM 1.7 mM
BSA solution in PBS	0.1 g BSA Dissolve in 100 ml PBS, sterile filter 0.2 µm, store at 4 °C	0.1 %
BSA solution in H_2O	20 g BSA Dissolve in 100 ml ddH_2O (double distilled water), store at 4 °C	200 mg/ml
Capture antibody solution	120 µg Mouse Anti-Human IL-6 Capture Antibody Reconstitute with 0.5 ml of PBS, shake for 15 min, produce 95 µl aliquots, store at -80 °C For usage, dilute aliquots in sufficient amount of PBS for working concentration	120 µg/0.5 ml 2 µg/ml
Collagenase solution	165 mg Collagenase Dissolve in 100 ml KRP working solution 4 %, adjust to pH 7.4, sterile filter 0.2 µm, prepare fresh	200 U/ml
Coupled FFA (free fatty acid) mix	Add 300 µl linoleic acid solution to 9.4 ml of 37 °C prewarmed BSA solution in DPBS, incubate for 30 min in 37 °C water bath, add 300 µl oleic acid solution, incubate for 30 min in 37 °C water bath, solution must be clear (if not extend incubation time), use sterile glass ware, store at 4 °C	6 mM
Detection antibody solution	3 µg Biotinylated Goat Anti-Human IL-6 Detection Antibody Reconstitute with 1 ml of reagent diluent, shake for 15 min, produce 180 µl aliquots, store at -80 °C For usage, dilute aliquots in sufficient amount of reagent diluent for working concentration	3 µg/ml 50 ng/µl
Dexamethasone solution	9.81 mg Dexamethasone Dissolve in 1 ml EtOH 95 % (stock), dilute 1:1000 in EtOH 50 % (15 µl in 14985 µl EtOH 50 %), sterile filter 0.2 µm, store at -20 °C	25 mM
DHAP buffer	3.4 mg DHAP Dissolve in 1 ml ddH_2O, prepare fresh	20 mM
EGF solution	200 µg EGF lyophilized Dissolve in 4 ml BSA solution in PBS (stock), dilute 1:10 (500 µl in 4.5 ml BSA solution in PBS), store at -20 °C	5 µg/ml
FGF solution	25 µg FGF lyophilized Dissolve in 5 ml BSA solution in PBS (stock), dilute 1:10 (500 µl in 4.5 ml BSA solution in PBS), store at -20 °C	0.5 µg/ml
Gentamycin solution	1 g Gentamycin sulfate Dissolve in 100 ml ddH_2O, sterile filter 0.2 µm, store at -20 °C	10 mg/ml
GPDH harvesting solution	788 mg Tris/HCl 29.2 mg EDTA w/o sodium 7 µl ß-Mercaptoethanol Dissolve in 80 ml ddH_2O, pH 7.4, fill up to 100 ml, store at 4 °C	0.05 M 1 mM 1 mM
Hydrocortisone solution	3.625 mg Hydrocortisone Dissolve in 1 ml EtOH abs. (stock), dilute 1:100 in EtOH 50 % (500 µl in 49.5 ml EtOH 50 %), sterile filter 0.2 µm, store at -20 °C	100 µM
IBMX solution	220 mg IBMX Dissolve in 50 ml ddH_2O plus 1 tip of a spatula Na_2CO_3, sterile filter 0.2 µm, store at 4 °C	20 mM
KRP stock solution	7.4 g NaCl 377 mg KCl 195 mg $CaCl_2$ x 2 H_2O 312 mg $MgSO_4$ x 7 H_2O Dissolve in 800 ml ddH_2O, add: 1697.3 mg NaH_2PO_4 x H_2O Adjust to pH of 7.4, add: 1 g of BSA Adjust again to pH of 7.4, fill up to 1000 ml, sterile filter 0.2 µM, store at 4 °C	126.7 mM 5.07 mM 1.36 mM 1.27 mM 12.3 mM 0.1 %

Solution/buffer	Composition and preparation	C_{final}
KRP working solution 4 %	8 g BSA Dissolve in 200 ml KRP stock solution, adjust to pH 7.4, sterile filter 0.2 µM, store at 4 °C	4 %
Linoleic acid solution	622 µl Linoleic acid Dilute in 9.378 ml EtOH abs., use sterile glass ware, store at -20 °C	200 mM
ß-Mercaptoethanol solution	7.04 ml ß-Mercaptoethanol Dissolve in 100 ml ddH_2O (stock), dilute 1:200 (25 µl in 4975 µl ddH_2O), store dark at 4 °C	5 mM
NADH buffer	8.51 mg NADH Dissolve in 1 ml TRAM buffer, prepare fresh	12 mM
Oleic acid solution	635 µl Oleic acid Dilute in 9.365 ml EtOH abs., use sterile glass ware, store at -20 °C	200 mM
Reagent diluent	2.5 g BSA for ELISA Dissolve in 250 ml PBS, sterile filter 0.2 µm, store at RT	1 %
RNA (Ribonucleic acid) harvesting solution	140 µl ß-Mercaptoethanol Dissolve in 14 ml RLT buffer, store dark at RT	1 %
Rosiglitazone solution	10 mg Rosiglitazone Dissolve in 2.797 ml DMSO (stock), dilute 1:5 (1 ml in 4 ml DMSO), sterile filter 0.2 µm, store at -20 °C	2 mM
Standard working solution IL-6	90 ng Recombinant Human IL-6 Standard Reconstitute with 0.5 ml ddH2O, use as highest standard in dilution series, store at -80 °C For standard dilutions series: create an eight-point standard curve using 2-fold serial dilutions with RD	600 pg/ml 600 pg/ml – 4.69 pg/ml
Stop solution	11.1 ml H_2SO_4 Dilute in 188.9 ml ddH_20	1 M
Streptavidin-HRP solution	N/A according to manufacturer Dilute Streptavidin-HRP with sufficient amount of reagent diluent for 40-fold dilution as working concentration, prepare fresh	40-fold dilution
T3 solution	5 mg T3 Dissolve in 7.4 ml EtOH abs. plus 2 drops 1 M NaOH, dilute 1:20 (500 µl in 9.5 ml EtOH abs.) (stock), dilute 1:25 in EtOH 50 % (500 µl in 12 ml EtOH 50 %), sterile filter 0.2 µm, store at -20 °C	2 µM
TRAM buffer	18.57 g Triethanolamine-HCl 0.931 g EDTA Dissolve in 80 ml ddH_2O, pH 7.4, fill up to 100 ml, store dark at 4 °C	1 M 1 mM
Transferrin solution	100 mg apo-Transferrin Dissolve in 100 ml ddH_2O, sterile filter 0.2 µm, store at -20 °C	1 mg/ml
Wash buffer	500 µl Tween®20 Dilute in 1000 ml of PBS, sterile filter 0.2 µm, store at RT	/

All media used during cell culture work are shown in Table 5 to Table 10.

Table 5: Components of storage medium.

	Total volume				
	100 ml	**200 ml**	**300 ml**	**500 ml**	C_{final}
DMEM/F12	94 ml	188 ml	282 ml	471 ml	
Penicillin-Streptomycin	1 ml	2 ml	3 ml	5 ml	1 %
Durability: up to 4 weeks in 4 °C storage					

Table 6: Components of isolation medium.

	Total volume				
	20 ml	**50 ml**	**100 ml**	**200 ml**	**C_{final}**
DMEM/F12	17.8 ml	44.5 ml	94 ml	188 ml	
Penicillin-Streptomycin	200 µl	500 µl	1 ml	2 ml	1 %
FCS	2 ml	5 ml	10 ml	20 ml	10 %
Durability: up to 4 weeks in 4 °C storage					

Table 7: Components of proliferation medium.

	Total volume				
	100 ml	**200 ml**	**300 ml**	**500 ml**	**C_{final}**
DMEM/F12	95.1 ml	190.2 ml	285.3 ml	475.5 ml	
Biotin/Pantothenate solution	1 ml	2 ml	3 ml	5 ml	33 µM Biotin, 17 µM Pantothenate
Penicillin-Streptomycin	1 ml	2 ml	3 ml	5 ml	1 %
FCS	2.5 ml	5 ml	7.5 ml	12.5 ml	2.5 %
Insulin	7.7 µl	15.4 µl	23.1 µl	38.5 µl	0.13 µM
EGF solution	200 µl	400 µl	600 µl	1 ml	10 ng/ml
FGF solution	200 µl	400 µl	600 µl	1 ml	1 ng/ml
Durability: up to 4 weeks in 4 °C storage					

Table 8: Components of freezing medium.

	Total volume				
	5 ml	**10 ml**	**20 ml**	**50 ml**	**C_{final}**
Proliferation medium	4.5 ml	9 ml	18 ml	45 ml	
DMSO	500 µl	1 ml	2 ml	5 ml	10 %
Durability: up to 4 weeks in 4 °C storage					

Table 9: Components of differentiation medium.

	Total volume				
	100 ml	**200 ml**	**300 ml**	**500 ml**	**C_{final}**
DMEM/F12	93.1 ml	186.3 ml	279.4 ml	465.7 ml	
Biotin/Pantothenate solution	1 ml	2 ml	3 ml	5 ml	33 µM Biotin, 17 µM Pantothenate
Penicillin-Streptomycin	1 ml	2 ml	3 ml	5 ml	1 %
Transferrin solution	1 ml	2 ml	3 ml	5 ml	0.01 %
Insulin	50 µl	100 µl	150 µl	250 µl	0.86 µM
T3 solution	50 µl	100 µl	150 µl	250 µl	0.02 mM
Hydrocortisone solution	100 µl	200 µl	300 µl	500 µl	0.1 %
FCS	2 ml	4 ml	6 ml	10 ml	2 %
Coupled FFA mix	1.67 ml	3.33 ml	5.00 ml	8.33 ml	100 µM
Durability: up to 4 weeks in 4 °C storage					

Table 10: Composition of induction medium.

	Total volume				
	25 ml	**50 ml**	**100 ml**	**200 ml**	**C_{final}**
Differentiation medium (see Table 9)	24.6 ml	49.3 ml	98.6 ml	197.2 ml	
Rosiglitazone solution	12.5 µl	25 µl	50 µl	100 µl	1 µM
Dexamethasone solution	25 µl	50 µl	100 µl	200 µl	6.25 µM
IBMX solution	312.5 µl	625 µl	1.25 ml	2.5 ml	0.25 mM
Durability: 24 h in 4 °C storage					

3.2 Cohort establishment

This thesis is part of a collaboration project between the Surgical Clinic and Policlinic of the *Klinikum rechts der Isar* and the Chair of Nutritional Medicine of the Technical University of Munich. The project's aim, in which this thesis is embedded, is to build up a biobank containing several tissues as well as blood samples of patients with any kind of gastrointestinal tumor disease and controls without tumors in order to investigate cachexia as frequent comorbidity of cancer. Exclusion criteria were an age below 18 years and infectious diseases such as hepatitis C or an infection with the human immunodeficiency virus (HIV) (Table 11). The study and all of its procedures received its ethics approval by the Ethics Committee of the Medical Faculty of the Technical University of Munich (Germany; #409/16 S) and was performed according to the Declaration of Helsinki of 2013. Furthermore, the study was registered at DRKS (Deutsches Register Klinischer Studien) under the reference number DRKS00017285.

Patients with either benign or malign gastrointestinal tumor diseases, as well as patients with any kind of non-tumorigenic disease that underwent an open surgery at the Surgical Clinic and Policlinic of the *Klinikum rechts der Isar* were considered to participate in the study. In the course of an informing meeting patients were asked for their written informed consent to take biopsies of sc fat tissue, om fat tissue, muscle (*musculus rectus abdominis*) and liver during surgery as well as blood collection before. All tissue types could be excluded separately. In case of the patient's approval clinical data, as shown in Table 12 and Table 13, was assessed and waist as well as hip circumference was measured directly using a tape.

Table 11: Inclusion and exclusion criteria.

Inclusion criteria	**Exclusion criteria**
Benign disease of the gastrointestinal tract	Age < 18 years
Malign disease of the gastrointestinal tract	Infection with hepatitis C
Open/laparoscopic surgery	Infection with HIV
Written informed consent	Pregnant women

Table 12: Weight parameters assessed during explanatory meeting and follow up.

Assessed weight parameters	
5 years before surgery [kg]	explanatory meeting
12 months before surgery [kg]	explanatory meeting
6 months before surgery [kg]	explanatory meeting
3 months before surgery [kg]	explanatory meeting
Day of surgery [kg]	explanatory meeting
3 months after surgery [kg]	follow up
6 months after surgery [kg]	follow up
12 months after surgery [kg]	follow up

Table 13: Secondary parameters assessed during explanatory meeting.

Assessed secondary parameters	
Primary diagnosis	free text
Secondary diagnosis	free text
Family anamnesis	free text
Chronic pancreatitis	yes/no
Smoker	yes/no (if yes, amount)
Alcohol	yes/no (if yes, amount)
Height	Cm
Waist circumference	Cm
Hip circumference	Cm
Icterus	yes/no
Intake of kreon	yes/no
Diabetes mellitus	yes/no (if yes, since when, medication
Karnofsky index	10 % to 100 %
ASA score	1 to 5

The collected data was supplemented by the clinical data of the *Klinikum rechts der Isar*, which was generated due to the patient's treatment. In case of permission, patients were called 3 months, 6 months and 12 months after their surgery to gain additional weight data. Additionally, BMI was calculated for all available time points. Cachexia was defined as weight loss of at least 10 % during 6 months before surgery and termed "severe cachexia", whereas for cell culture differentiation experiments also patients with a weight loss between 5 to 10 % in the mentioned time frame were considered cachectic termed "moderate cachexia". Sarcopenia was defined by measurement and calculation of SMAI from CT measurements at L3 with sex-specific cut-offs of 52.4 cm^2/m^2 for men and 38.5 cm^2/m^2 for women according to *Prado* and coworkers (Prado et al., 2008).

3.3 Sampling procedure

Depending on the written informed consent provided by each patient, sc fat, om fat, liver and muscle tissue were taken during surgery by the surgeons and blood in form of an EDTA

(S-Monovette® 9 ml, K3E EDTA, order no. 02.1066) and a serum monovette (S-Monovette® 9 ml, Serum-Gel, order no. 02.1388), both provided by Sarstedt, was drawn before surgery by the anesthesist. Both monovettes had to be inverted several times to avoid blood coagulation in case of EDTA containing blood and to distribute the gel components regarding the serum monovette.

Immediately after preoperative blood collection, the EDTA monovette was centrifuged at 4,500 x g for 10 min at RT, which led to the development of three different phases: the yellow upper phase contained blood plasma, the grey separation phase in the middle is called buffy coat, which contained for example leukocytes, monocytes and thrombocytes for later DNA isolation, and the red colored lower phase consisted of erythrocytes. Under sterile conditions plasma and buffy coat were carefully absorbed and aliquoted (cryo vials provided by Greiner; order no. E16113QQ). Before further processing, the serum monovette was incubated in an upstanding position for 30 min at RT to let the gel form its viscous condition and centrifuged at 4,500 x g for 10 min at RT. The gel separated the blood into the upper serum phase, which was still liquid, and the lower gel-like phase containing erythrocytes. Serum was removed and aliquoted. All cryo vials filled with blood components were on-site frozen on dry ice and stored at -80 °C in the laboratory in Freising.

The collected sc and om fat tissue had to be cut into pieces for different experiments and analyses. Depots were processed separately, but the procedures were identical. First, 4 pieces of fat tissue, each about the size of a pinhead, were removed with the help of scissors and tweezers, placed into 2 cryo vials filled with RNA harvesting solution and about 200 mg of silica-zirconia beads provided by Roth® (order no. 11079105) and frozen on dry ice. An additional reserve was built up by freezing 4 tissue pieces in one vial filled with isopropanol absolute. For histological analyses, 2 tissue pieces were transferred into ROTI®Histofix containing 4 % formaldehyde, stored at 4 °C for 24 to 48 h and afterwards the tissue was stored in 70 % EtOH at 4 °C. For PAC isolation, the remaining fat tissue was given into T25 or T75 flasks provided by TPP® (order no. 90026), covered with storage medium and incubated at 37 °C and 5 % carbon dioxide until cell isolation the following day. Received muscle and liver biopsies were on-site placed into 5 ml plastic tubes provided by Eppendorf® (order no. 0030122.321) without further liquid and frozen on dry ice. All cryo vials filled with tissue pieces, which were initially frozen on dry ice, were long-term stored at -80 °C.

3.4 Interleukin-6 ELISA with plasma

For evaluation of plasma IL-6 levels, a sandwich ELISA was performed using the Human IL-6 DuoSet® ELISA Development System provided by R&D Systems® (order no. DY206) in 96 well plates provided by Thermo Scientific™ (Thermo Scientific™ Immuno Clear Standard Modules, order no. 10227541; Thermo Scientific™ Frame, order no. 10524811). The ELISA was carried out according to the manufacturer's protocol. Before the measurement it was decided by pretesting that IL-6 was to be measured in human plasma without any dilution of samples and an RD containing 1 % BSA in PBS (instead of 1 % FCS). Each plate contained a standard dilution series, a blank consisting of RD, a positive control of a single individual, a positive control of three pooled individuals and the patient samples to be measured, respectively. To note, all types of samples were evaluated in duplicates and both positive controls were used for all plates measured.

Each well of the plate was coated with 100 µl of capture antibody solution in a working concentration of 2 µg/ml, sealed and incubated at RT over night while shaking at 600 rpm. The day after, the capture antibody solution was discarded and the wells were washed three times with 400 µl wash buffer each. By adding 300 µl of RD to each well and incubating it for 1 h at RT while shaking at 600 rpm, the uncoated surface of the plastic was blocked. As done earlier, all wells were washed three times before adding 100 µl of either standard, blank, one of the two positive controls, or plasma samples. According to the manufacturer's protocol, the standard dilution series represented a 2-fold serial dilution resulting in concentrations of 600 pg/ml, 300 pg/ml, 150 pg/ml, 75 pg/ml, 37.5 pg/ml, 18.8 pg/ml and 9.38 pg/ml and was processed out of the standard working solution IL-6. Since pretesting of the ELISA showed rather low concentrations of IL-6 in patient samples, an additional 8th dilution of 4.69 pg/ml was added. The plate was sealed and incubated for 2 h at RT while shaking at 600 rpm. After incubation, all wells were emptied by inverting, washed three times and 100 µl of detection antibody solution was added in a working concentration of 50 ng/ml. The plate was sealed and incubated for 2 h at RT while shaking at 600 rpm. Next, all wells were emptied and washed three times before giving 100 µl of streptavidin horseradish peroxidase solution (streptavidin-HRP solution) in a 40-fold working concentration into each well. The plate was covered and incubated for 20 min at RT in the dark while shaking at 600 rpm. Afterwards, 100 µl of substrate solution was added to the streptavidin-HRP solution and the plate was incubated for 20 min at RT in the dark while shaking at 600 rpm. The horseradish peroxidase catalyzes the substrate's oxidation resulting in a fluorescent signal, which can be detected by a photometer and which is additionally visible by eye through a blue coloring of the wells. The more intense the blue color of a well, the more IL-6 is present in a sample or the standard, respectively. During the 20 min of incubation, an increase of the standard's color intensity was observed and the

incubation period was shortened to not exceed the measurable depth of the photometer. To stop the reaction 50 µl of stop solution was added to every well, which led to a visible color change from blue to yellow. Applying the Tecan© Infinite® M200 PRO photometer (Tecan Trading AG ©; Switzerland) all wells were measured at a wavelength of 450 nm using 540 nm as reference wavelength, which was subtracted from the initially measured optical densities (OD).

For calculation of results the average of duplicate measurements was determined and the blank's OD was subtracted from all standards, controls and samples. IL-6 concentrations in ng/µl were calculated using the interpolated values originating from the standard curve using the GraphPad© Prism© software, version 5.02.

Since more than one 96 well plate had to be used to measure all plasma samples, the measured ODs had to be adjusted to exclude any external or plate-specific influences. For this reason, a plate factor was calculated, which compared the ODs of each single plate to the mean ODs of all plates, taking the values of the standard curve and both positive controls into account. For adjustment, all ODs of every plate had to be multiplied with its specific plate factor leading to the final IL-6 values.

3.5 DNA isolation with buffy coat

DNA was isolated out of buffy coat using the components of the Qiagen DNeasy Blood & Tissue Kit (order no. 69504) and performed in 1.5 ml tubes. 100 µl of buffy coat, 20 µl of Proteinase K, 4 µl of RNAse A and 100 µl of PBS were mixed, vortexed and incubated for 2 min at RT. After incubation, 200 µl of AL buffer was added and incubated for 10 min at 56 °C. For precipitation, 200 µl of EtOH absolute was added, the sample was vortexed and the suspension was transferred onto the filter of a spin column provided by the kit. After centrifugation at 8,000 x g for 1 min at RT, the flow-through was discarded and the filter containing DNA was placed into a new collection tube. To wash the filter 500 µl of AW1 buffer was added, the tube centrifuged at 8,000 x g for 1 min at RT and the flow-through was discarded. A second washing step was performed using 500 µl of AW2 buffer, the sample was centrifuged at 14,000 x g for 3 min at RT and the filter was placed into a 2 ml Eppendorf® deoxyribonucleic acid (DNA) LoBind tube (order no. 0030.108.078). To elute DNA 60 µl of to 37 °C prewarmed AE buffer was placed directly onto the filter and centrifuged at 8,000 x g for 1 min at RT. This step was repeated using 40 µl of AE buffer, obtaining 100 µl of eluted DNA in total. DNA concentrations were measured spectrophotometrically using the Tecan© Infinite® M200 PRO photometer.

3.6 FTO genotyping

To determine whether a patient had the TT (homozygous non-risk), CC (homozygous risk) or CT (heterozygous risk) *FTO* genotype, SimpleProbes provided by TIB Molbiol© were used. SimpleProbes are molecular hybridization beacons specifically designed for the gene of interest which emit fluorescence when binding to their complementary DNA which can be detected using a LightCycler®480 program (Roche Holding©; Switzerland). In this case the SimpleProbe was designed to fully match the CC mutant variant of the risk allele rs1421085 meaning that, during a melting curve, a higher temperature had to be spent to unravel SimpleProbe and complementary DNA compared to TT or CT. This resulted in a single peak at a high temperature for CC, another peak at medium temperature for CT (since one allele matches the SimpleProbe whereas the other doesn't) and one peak for TT at a lower temperature (since none of the alleles matches the SimpleProbe). The reaction was performed using a FrameStar® 384 well plate provided by 4titude (order no. 4ti-0381) and the commercially available LightSNiP assay for rs1421085 (TIB Molbiol©, Germany).

Master Mix was prepared as follows:

Table 14: Components of *FTO* genotyping master mix.

Components of master mix	Volume per DNA sample
5 x MyTaq Reaction Buffer	2 µl
Reagent Mix SimpleProbe (LightSNip rs1421085 FTO)	0.5 µl
MyTaq Polymerase	0.2 µl
PCR grade water	5.3 µl
Total volume of master mix	**8.0 µl**

Pipetting was performed on ice and 2 µl of DNA (with an approximate concentration of 25 ng/µl) was dispensed into each well of the 384 well plate and span shortly before covering the samples with 8 µl of master mix each and spinning again. For no template controls, PCR grade water was used instead of DNA. The plate was sealed with adhesive foil and put into the LightCycler®480 immediately to perform the run under following conditions:

Table 15: Program of LightCycler® 480 for *FTO* genotyping.

Program:	Denaturation	Cycling			Melting			Cooling
Parameter								
Analysis Mode	None	Quantification			Melting Curves			None
Cycles	1	45			1			1
Segment	1	1	2	3	1	2	3	1
Target [°C]	95	95	60	72	95	40	75	40
Hold [hh:mm:ss]	00:10:00	00:00:10	00:00:10	00:00:15	00:00:30	00:02:00	00:00:00	00:00:30
Ramp Rate [°C/s]	4.6	4.6	2.4	4.6	4.6	2.0	/	2.0
Acquisition Mode	None	None	Single	None	None	None	Continu.	None
Acquisition [per °C]							3	

3.7 Primary cell culture procedure

The procedure regarding the cell culture of primary PACs comprised a huge part of this thesis, since isolation of PACs and their preservation culture was an indispensable component to increase the biobank's extent. The whole cell culture procedure, meaning preservation culture as well as experimental subsets, was performed under a fume hood at sterile conditions wearing a coat and gloves at any time. Sterile and individually wrapped serological pipettes were used from Greiner Bio-One (CELLSTAR®, 5 ml, 10 ml, 25 ml, 50 ml). If not mentioned otherwise, cell culture flasks and well plates were provided by Corning Life Sciences (Corning™ Falcon™ tissue culture flask T25, T75 and Corning™ Costar™ 6 well/48 well plates flat bottom).

3.7.1 Isolation of PACs

Since the received sc and om tissue sections contained various cell types such as adipocytes, endothelial cells, blood cells and immune cells next to the required PACs, a specialized PAC isolation protocol was applied under the sterile bench to prevent contamination.

Fat tissue, which was incubated in storage medium at 37 °C and 5 % carbon dioxide overnight, was transferred into a large petri dish and single fat depots, the size in the range of about 2 mm to nearly 1 cm, were dissected by scissors and tweezers and blood vessels as well as connected tissue was discarded. To note, both depots were cut separately and a fresh dissecting set was used for each depot and patient. Dissected fat depots were transferred into a 50 ml plastic tube and minced by the scissors until it reached a pulpy consistency. The weight of the received fat tissue was determined and adequate volume of collagenase medium was added, meaning 5 ml/g fat. In case the tissue's weight appeared to be less than 1 g, 5 ml of collagenase medium was used uniformly. Plastic tubes were closed with parafilm and horizontally incubated at 37 °C in a water bath with maximum shaking intensity for 60 min.

After 30 min of incubation a 100 µl aliquot was taken from the clearly visible fat tissue layer on top of the solution under sterile conditions with pre-cut 200 µl tips to determine average adipocyte size. Remaining fat solution was further incubated at 37 °C in the water bath.

For adipocyte size measurement, the aliquot was smeared onto an object slide and microscoped with a 200 x magnification using the L20x objective of a Leica DM-IL cell culture microscope (Leica Microsystems; Germany). The size of exactly 100 adipocytes was determined with a size measurement grid embedded in the microscope's eyepiece and noted. It was carefully paid attention to measure all cells in a chosen visual field, independent of sizing to reduce interindividual differences caused by the person performing the count. Cells were excluded in case their round shape wasn't maintained anymore, which indicated a rupture of cell surface.

After incubation the solution was centrifuged at 200 x g for 10 min at RT to separate the cell types, leaving PACs in the pellet, floating adipocytes in the top layer and remaining cells, such as erythrocytes, in a middle layer. All supernatant was discarded. According to the initially engaged amount of tissue the cell pellet was resuspended in a defined amount of prewarmed isolation medium, filtered through a 70 µm cell strainer to remove left over connective tissue and seeded in either T25 flasks or 6 well plates (Table 16). For evenly distribution of PACs onto the plastic surfaces, flasks and plates were carefully shaken back and forth as well as left and right before incubating them at 37 °C and 5 % carbon dioxide. The following day, PACs were washed three times with prewarmed PBS to remove remaining erythrocytes and other non-adherent cells and incubated with proliferation medium (Table 16) which was changed twice a week.

Table 16: Seeding of preadipocytes after isolation.

Amount of tissue [g]	Plate/flask	Isolation/proliferation medium [ml]
< 0.5 – 1.0	6 well plate, 1 well	2 per well
1.0 – 1.5	6 well plate, 2 wells	2 per well
1.5 – 2.0	6 well plate, 3 wells	2 per well
2.0 – 2.5	6 well plate, 4 wells	2 per well
2.5 – 3.5	T25 flask	6
< 3.5	T25 flask * x	6 * x

3.7.2 Splitting of PACs

Due to the fact, that primary tissue pieces received during surgery are usually small to not disturb the surgery procedure or even harm the patient, splitting of cultured PACs is essential to enlarge total cell numbers to increase the output.

When cells reached a confluence state of about 95 %, medium was removed and cells were washed with PBS before adding trypsin/EDTA and incubating for 10 min at 37 °C. The trypsin/EDTA let the cells detach which could be controlled visually. After incubation the enzymatic reaction was stopped by using proliferation medium in a ratio of 1:10 and the suspension was transferred into a 50 ml tube. The suspension was gently mixed by pipetting up and down and an aliquot of 50 µl was removed and 1:1 diluted with trypan blue solution before loading each of the two chambers of a *Neubauer* chamber provided by Brand (order no. 718605) with 10 µl volume. Under a Leica DM-IL cell culture microscope, vital cells appearing white and shiny, were counted in all eight large squares on the grid. The counted cell numbers could then be used to extrapolate total cell count or cell count per ml with the following calculation:

$$cells/ml = \frac{X}{8}\ x\ 2\ x\ 10{,}000$$

$$required\ volume\ of\ cell\ suspension = \frac{Y}{cells/ml}$$

Figure 5: Cell counting via Neubauer chamber.
X = number of cells counted in eight large squares of the Neubauer Chamber. Y = required number of cells for new wells/flasks.

In order to get the desired seeding density for cell culture the cell suspension was diluted with the required volume of proliferation medium and transferred into one of the cell culture flasks or 6 well plates. For evenly distribution of PACs onto the plastic surfaces, flasks and plates were carefully shaken back and forth as well as left and right before incubating them at 37 °C and 5 % carbon dioxide. Suitable amounts of PBS for washing, trypsin/EDTA and proliferation medium are shown below:

Table 17: Reagents and volumes for splitting of PACs.

	1 well of a 6 well plate	T25 flask	T75 flask
PBS	1 ml	5 ml	10 ml
Trypsin/EDTA	500 µl	1 ml	1 ml
Proliferation medium	4.5 ml	9 ml	9 ml

3.7.3 Freezing of PACs

In order to store cultured PACs for later experiments, cells had to be frozen according to an established protocol to ensure that freezing and later thawing won't harm the cells' structure and viability.

The protocol's start was identical to the procedure of cell splitting described under 3.7.2, PACs were washed with prewarmed PBS, detached from their plastic surfaces by trypsin/EDTA and cell numbers were determined by counting PACs by the help of a *Neubauer* chamber. Since

PACs had to be frozen at a concentration of 500,000 cells/ml freezing medium, the exact amount had to be calculated and a centrifugation step of 200 x g for 10 min at RT had to be performed. After centrifugation, supernatants were removed and cells were resuspended in freshly prepared freezing medium. One ml of cell suspension was immediately distributed among each of the prepared nunc cryo vials provided by Thermo Fisher Scientific™ (order no. 3777224), transferred to a Nalgene® Mr. Frosty freezing container provided by Merck (order no. C1562-1EA) and stored at -80 °C for three days. Afterwards, cells were relocated in a liquid nitrogen tank for long-term storage.

3.8 Gene expression and differentiation experiment

3.8.1 Selection of patients

Of all patients included in the study, 20 had to be selected for a gene expression and differentiation experiment. In this experiment, 4 groups of patients consisting of 5 individuals each were needed: controls with neither cachexia nor tumor (- CAC/- ca) referred to as “healthy controls”, controls without cachexia but with tumor (- CAC/+ ca) referred to as “cancer controls”, a cachectic group with tumor and weight loss between 5 to 10 % from 6 months before surgery to the day of surgery (CAC 5-10%) referred to as group with “moderate cachexia”, and a cachectic group with tumor and weight loss over 10 % in the mentioned time frame (CAC > 10%) referred to as group with “severe cachexia”. Since the differentiation experiment acquired a certain amount of sc and om PACs, at least two cryo vials of PACs of each depot had to be available in the biobank to not run out of cells during the experiment due to unexpected incidents such as bacterial contamination or additional reasons of cell death. The same approach applied regarding the complete set of weight data from 5 years before surgery to 12 months after. Furthermore, a complete set of specimens was required, meaning that patients for whom not the whole set of muscle tissue, liver tissue, sc fat tissue, om fat tissue as well as serum and plasma was available, were excluded from the experiment. Focus was laid on patients with either pancreatic ductal adenocarcinoma (PDAC), colorectal carcinoma (CRC) or adenocarcinoma of the esophagogastric junction (AEG), since the abundance of these diseases in the biobank was high. Remaining patients were, if possible, matched according to age, BMI and sex to guarantee a similar distribution among the 4 groups. The patients chosen for the differentiation experiment are depicted in Table 18.

Table 18: Selected patients for the differentiation experiment and associated clinical data.

Group	Diagnosis	Weight loss [%]	BMI	Age [years]	Sex
Healthy controls no cachexia no tumor (- CAC/- ca)	AP	0.7	25	67	f
	CP	0	24	34	m
	Control	1.8	19	29	f
	LA	3	23	39	f
	IPMN	0	32	77	f
Cancer controls no cachexia tumor (- CAC/+ ca)	CRC	3	28	76	m
	PDAC	0	23	43	f
	PDAC	2	26	70	m
	CRC	2	32	68	m
	PDAC	1	24	56	f
Moderate cachexia cachexia (5-10 % weight loss) tumor (CAC 5-10%)	PDAC	6.5	31	55	m
	DC	7.2	22	70	m
	PDAC	8.3	20	55	f
	CRC	7.6	29	75	f
	PDAC	6.4	22	67	f
Severe cachexia cachexia (> 10 % weight loss) tumor (CAC > 10%)	DC	13	25	61	m
	AEG	15	20	61	m
	CRC	12	35	76	m
	PDAC	14	28	56	m
	PDAC	15	23	77	f

3.8.2 Thawing of PACs

Since the cryoprotectant DMSO, which ensures the survival of cells during freezing process by displacing the water inside the cells, is precisely for this reason dangerous and apoptosis increasing while thawing, the thawing protocol had to be well prepared before getting the cells out of the liquid nitrogen and rapidly performed.

For thawing, one 50 ml plastic tube as well as a 15 ml tube were set up, the 50 ml tube filled with 18 ml of proliferation medium, the 15 ml tube with 1 ml of medium. One cryo vial at a time was taken out of the liquid nitrogen and quickly thawed by holding it into a 37 °C water bath. To buffer the still sensitive cells and protect them from shear forces, 1 ml of proliferation medium was taken out of the 50 ml tube by a 5 ml serological pipette, followed by the 1 ml cell suspension out of the cryo vial, again followed by addition of 1 ml of medium out of the 50 ml tube. This had to be performed very carefully and slowly to avoid any air bubbles disrupting the buffering layers. Afterwards, all three layers were slowly pipetted into the 50 ml tube. The 1 ml in the 15 ml tube was used to rinse the cryo vial, the remaining cells were transferred into the 50 ml tube and the suspension was gently mixed and divided among two T25 flasks with a final volume of 10 ml each. This protocol resulted in 250,000 cells/T25, being the double amount as during conventional proliferation culture. Cells were incubated at 37 °C and 5 % carbon dioxide and medium was completely changed 24 h after to remove excess DMSO and

dead cells. After reaching confluence, cells were passaged once more using T25 flasks as described under 3.7.2 before splitting them into 6 well plates for adipogenic differentiation.

3.8.3 Adipogenic differentiation

When PACs reached around 90 % confluence in the 6 well plates, proliferation medium (Table 7) was replaced by induction medium (Table 10) containing the FFAs linoleic and oleic acid to further promote differentiation. This day during the differentiation process is referred to as day 0 (d0). Three days after (d3) induction medium was completely removed and cells were stimulated with differentiation medium (Table 9) until day 14 (d14) with medium changes twice a week.

3.8.4 Harvesting procedure

By harvesting cells at different time points, changes in for example mRNA expression, vitality or the progress of differentiation visible by the accumulation of lipid droplets inside the cell could be examined, not only regarding the different time points, but also in view of different patients or depots. In this project it was decided to harvest the cells on d0, d3 and d14, at which PACs are fully differentiated when using FFA medium. For each harvesting day, a full 6 well plate was used according to the following scheme:

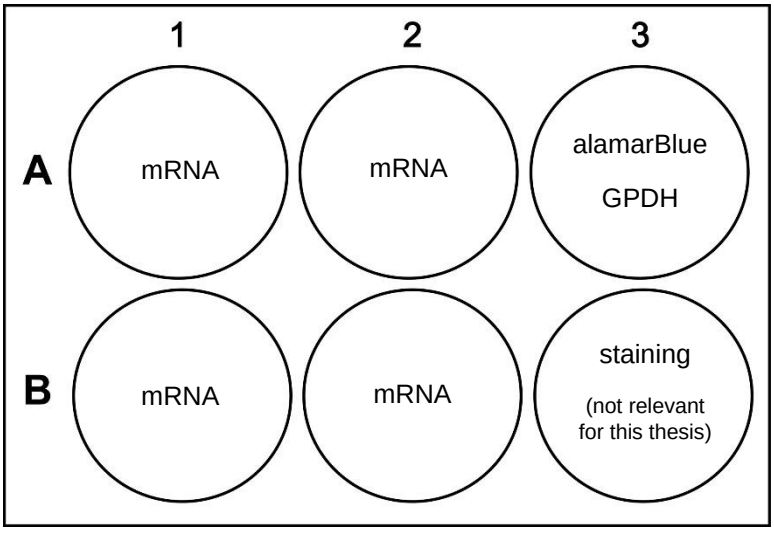

Figure 6: Harvesting scheme.

Since the cells didn't have to be kept alive for the ongoing procedure, the whole harvesting process could be proceeded under non-sterile conditions and non-sterile reagents could be used.

3.8.4.1 Harvesting for mRNA isolation

To be able to analyze mRNA expression among different time points, patients or depots, four wells had to be harvested on every harvesting day. At first, medium was removed and cells were washed three times with cold PBS. In one of the wells 350 µl of RNA harvesting solution was added and cells were scraped off by using a cell scraper. Due to β-mercaptoethanol contained in the RNA harvesting solution, the harvest was performed under the fume hood. The gained cell suspension was transferred into the second well and the procedure was repeated. The combined amount of two wells was mixed by pipetting to avoid any clumps, given into a 2 ml Eppendorf® DNA LoBind tube and shortly stored on ice until the exact same procedure was repeated with the remaining two wells. Immediately after harvesting, the 2 ml tubes were stored at -80 °C until later mRNA isolation. Emptied wells were washed three times with 70 % EtOH to erase evaporation of remaining β-mercaptoethanol.

3.8.4.2 Alamar Blue assay

The Alamar Blue assay is a method to analyze the viability of cells via their capability to reduce the blue colored alamarBlue Cell Viability Reagent's component resazurin into the red colored resofurin, whose fluorescence can be measured by a photometer (Csepregi et al., 2018). For that reason, the higher the increase in fluorescence over a certain amount of time, the higher is the cells' metabolic activity and thus viability.

To start the process 200 µl of alamarBlue Cell Viability Reagent was added to the 6 well containing cells and 2 ml of medium, shaken quickly und incubated at 37 °C. Exactly every 5 min a 200 µl aliquot was taken out in duplicates and transferred into a 96 well strip plate provided by Brand (order no. 782300). After 20 min fluorescence was measured at an excitation wavelength of 560 nm with the Tecan© Infinite® M200 PRO photometer. The primary endpoint of this measurement was considered as the time point at which the photometer wasn't able to quantify the intensity of fluorescence anymore. In case this endpoint couldn't be reached within these 20 min, another aliquot was taken after 25 min and measured again.

Results of this method will not be displayed any further since it was exclusively used to attest the viability of cells during the period of differentiation.

3.8.4.3 Harvesting for GPDH measurement

For cell harvesting in regards of GPDH measurement, the well earlier used for the Alamar Blue assay was chosen. Remaining alamarBlue Cell Viability Reagent was removed and cells were

twice washed with cold PBS. Cells were overlaid with 800 µl of GPDH harvesting solution, scraped off, transferred into a 1.5 ml Eppendorf® tube and frozen at -80 °C.

3.8.5 GPDH measurement

GPDH is highly expressed in mature adipocytes and for that reason widely used as a marker for late adipogenic differentiation in cell culture (Sottile & Seuwen, 2001). In this assay GPDH's enzymatic activity was determined in the first step whereas in the second step the results were normalized to total protein taking into account that not all harvested wells contained the exact same number of cells. The samples of the three harvesting days (d0, d3, d14) were measured in three different approaches in the assumption that all samples of a single harvesting day would behave in a similar manner during the assay. Furthermore, it is important to know that once the samples were thawed, the measurement of GPDH had to be finished at the same day, since refreezing would have destroyed the enzyme. For later determination of total protein, refreezing was unproblematic.

The samples were thawed on ice and cells were disrupted by ultrasound for 7 s at 29 % (device strength) with the help of an ultrasonic device and centrifuged at 10,000 x g for 10 min at 4 °C. The required volume of master mix was produced according to Table 19 with 50 % overhang and without adding DHAP buffer to it, since it was injected by the photometer later on. Since priming of the photometer's injectors needed a separate amount of volume, additional 1.75 ml of DHAP buffer were prepared next to the needed 10 µl per sample.

Table 19: Components of GPDH master mix.

	Number of samples			
Components of master mix	**1**	**20**	**40**	**100**
TRAM buffer	50 µl	1000 µl	2000 µl	5000 µl
ß-mercaptoethanol solution	10 µl	200 µl	400 µl	1000 µl
NADH buffer	5 µl	100 µl	200 µl	500 µl
Total volume of master mix	**65 µl**	**1300 µl**	**2600 µl**	**6500 µl**
DHAP buffer	10 µl	200 µl	400 µl	1000 µl

Sixty-five µl of master mix per sample were given into a 48 well plate, as well as the relevant volume of sample and distilled water for dilution as shown in Table 20.

Cells harvested at d0 were regarded as undifferentiated, whereas cells harvested at d3 and d14 were considered as being differentiated. To note, the first run was always carried out with the highest dilution option shown, meaning 80 µl sample volume for d0 and 40 µl for d3 and d14, and samples were measured in single determination.

Table 20: Dilution options for GPDH measurement in cells in different stages of differentiation.

	Undifferentiated cells (d0)							Differentiated cells (d3, d14)	
Sample volume	80 µl	100 µl	150 µl	180 µl	200 µl	250 µl	425 µl	40 µl	50 µl
ddH_2O	345 µl	325 µl	275 µl	245 µl	225 µl	175 µl	/	385 µl	375 µl
Master mix	65 µl								
DHAP buffer	10 µl								
Volume/well	500 µl								
Dilution factor	6.25	5	3.33	2.78	2.5	2	1.18	12.5	10
Absorption coefficient (340 nm)	496	397	265	220	198	159	93.4	992	794

The measurement was performed with the Tecan© Infinite® M200 PRO photometer. Prior to the measurement the injectors had to be washed and filled with DHAP buffer before giving in the 48 well plate with the samples. According to its protocol the photometer heated up to 37 °C, injected 10 µl of DHAP buffer into each well, mixed the solution by shaking and measured fluorescence every 20 s at an excitation wavelength of 340 nm for 5 min. Immediately after the measurement, the values had to be plotted in order to calculate the mathematical slope for each sample over the time of measurement. A negative slope, meaning less fluorescence over time, represented the direct activity of GPDH in the samples. Concluding, generated values were accepted in case the resulting graph showed a negative mathematical slope and a linearity that covered at least 50 % of the graph. In case this was not available, single samples had to be repeated using a different dilution option until proper resulting graphs were obtained. Fluorescence values were offset with the absorption coefficient at 340 nm and the dilution factor to receive the absolute GPDH activity in mU. Remaining samples were frozen at -80 °C.

In order to obtain relative GPDH activity, absolute GPDH activity had to be normalized to total protein by a BCA measurement using the Pierce™ Microplate BCA Protein Assay Kit – Reducing Agent Compatible provided by Thermo Fisher Scientific™ (order no. 23250). The standard as well as the blank and 10 % of the samples were measured in duplicates.

Prior to sample treatment, a standard dilution series was prepared out of the BSA solution in H_2O resulting in final BSA concentrations of 2mg/ml, 1 mg/ml, 0.5 mg/ml, 0.25 mg/ml, 0.125 mg/ml, 0.0625 mg/ml, 0.03125 mg/ml and an additional blank consisting of GPDH harvesting solution. Samples were thawed on ice and centrifuged at 10,000 x g for 1 min at 4 °C. Hamilton© Microlab VANTAGE pipetting robot (Hamilton Company©; USA) was used to pipet 9 µl of either standard, blank or sample into a 96 well plate, followed by 4 µl of Compatibility Reagent Solution into every well. The plate was sealed, shaken for 30 s at 600 rpm and incubated for 15 min at 37 °C. Subsequently the robot added 260 µl of Working Reagent to every well before sealing and shaking the plate for 30 s at 600 rpm. The plate was

incubated at 37 °C and the first measurement took place 30 min after at 340 nm by the help of the Tecan© Infinite® M200 PRO photometer. Additional measurements were performed every following 15 min until the highest standard reached an OD of at least 1.2 to 1.4.

For analysis, mean blank was subtracted from sample ODs of the last measurement done and protein concentrations in mg/ml were calculated using the interpolated values originating from the standard curve using GraphPad© Prism© software, version 5.02. Protein concentrations were used to calculate the final GPDH activity in mU/mg.

3.8.6 Preparation of muscle, liver and fat tissue

Since muscle and liver tissue was dry frozen in one piece and sc as well as om fat tissue was frozen in RNA harvesting solution directly after resection during surgery, tissue sections had to be prepared for later RNA isolation.

A tissue piece of around 100 mg was cut from each of the 20 patients' muscle and liver biospecimens. In order to do that, a petri dish was placed on a metal plate stored in -80 °C that rested in a box filled with dry ice, so that the tissue could be cut by means of a scalpel. This procedure prevented the tissue from thawing, which could harm the integrity of mRNA. Since sc and om fat tissue was already cut into small pieces during the sample procedure, no additional dissection was necessary. To further support the upcoming mRNA isolation, all tissue types had to be pulverized by pestle and mortar. As for the cutting procedure, an in -80 °C cooled metal plate was laid in a box containing dry ice, on which the mortar was placed and once filled with liquid nitrogen prior to use. After cool down, the muscle, liver or fat pieces of a single patient was crushed to powder under constant refilling with liquid nitrogen to avoid thawing. Once pulverized, the powder was transferred into a precooled 2 ml Eppendorf® DNA LoBind tube, covered with 700 µl of Lysis Buffer provided by the mirVana™ miRNA Isolation Kit (see 3.8.7.1) and the lid was left open for a couple of minutes to let excessive liquid nitrogen evaporate. Samples were stored at -80 °C.

3.8.7 Gene expression analysis

3.8.7.1 Isolation of mRNA

For isolation of mRNA the mirVana™ miRNA Isolation Kit purchased from Thermo Fisher Scientific™ (order no. AM1561) was used to isolate mRNA as well as miRNA out of the samples according to the manufacturer's protocol. To note, miRNA isolation is not part of this thesis, since analysis was done elsewhere.

Cell lysates obtained during the harvesting procedure or pulverized tissue samples in Lysis Buffer were thawed on ice and 350 µl of Lysis Buffer was added only to cell lysates, bringing all samples to a uniform amount of 700 µl each. 35 µl of Homogenate Additive was added, the samples inverted several times and incubated for 10 min on ice. After incubation 350 µl of acid-phenol:chloroform was added, being careful to aspirate the lower phase of the bottle instead of the upper aqueous phase. Samples were vortexed for 1 min and centrifuged at 10,000 x g for 5 min at RT. The centrifugation step led to three different phases in the tube: the upper aqueous phase, the middle interphase und the lower organic phase. Since mRNA is part of the aqueous phase, the whole phase was transferred into a 5 ml tube without disturbing the interphase or organic phase. The aqueous phase was mixed with 1.25 times the amount of EtOH absolute and inverted for several times. A filter cartridge provided by the kit was placed into a 2 ml tube and 700 µl of the mixture was added to the filter and incubated for 1 min at RT. The tube was centrifuged at 10,000 x g for 15 s at RT to press the liquid through the filter and let the mRNA bind to it. The filtrate was collected separately, since it contained the miRNA. The filter loading, incubation and centrifugation steps were repeated until all liquid was run through the filter. Since the filter now contained all available mRNA, it was topped with 700 µl of Wash Solution 1 and centrifuged at 10,000 x g for 10 s at RT and the flow-through was discarded. Next, 500 µl of Wash Solution 2/3 was added, the tube was centrifuged at 10,000 x g for 10 s at RT and the flow-through was discarded. The washing step with Wash Solution 2/3 was repeated and after further emptying the tube it was dry-centrifuged at 10,000 x g for 1 min at RT. The filter was placed in a 1.5 ml collection tube provided by the kit and 50 µl of at 95 °C preheated Elution Solution was given directly onto the center of the filter. After incubation for 1 min at RT, the tube was centrifuged at 16,000 x g for 20 s at RT. The filtrate was aspirated, placed onto the same filter and incubated for 1 min at RT before filtering it again by a centrifugation step at 16,000 x g for 30 s at RT. Afterwards, the filter cartridge was discarded and the tube was incubated for 5 min on ice with an open lid to let EtOH residues evaporate. Finally, 2 µl of eluate was removed for quality check (RIN and DV_{200}) via Bioanalyzer (Agilent Technologies, Inc©; USA) and mRNA concentration was immediately determined by the Tecan© Infinite® M200 PRO photometer before freezing the samples at -80 °C.

3.8.7.2 Synthesis of cDNA

For later qPCR analysis, the isolated mRNA had to be transcribed into cDNA using the High-Capacity cDNA Reverse Transcription Kit provided by Applied Biosystems™ (order no. 4368814) according to the manufacturer's protocol. The prior determined mRNA concentrations were used to calculate the needed amount of mRNA and PCR grade water to

gain 400 ng of cDNA for PACs, liver and muscle tissue or 200 ng of cDNA for sc and om fat, respectively. The required volume of master mix is shown in Table 21. PCR grade water served as negative control.

Table 21: Components of cDNA master mix.

Components of master mix	Volume per mRNA sample
10X RT Buffer	2.0 µ*l*
10X RT Random Primers	2.0 µl
25X dNTP Mix (100 mM)	0.8 µl
MultiScribe Reverse Transcriptase (50 U/µL)	1.0 µl
PCR grade water	4.2 µl
Total volume of master mix	**10.0 µl**

The master mix was pipetted manually, whereas the pipetting robot was used to combine master mix, mRNA samples and water for their dilution into 200 µl strips provided by Thermo Fisher Scientific™ (AB1112). Reverse transcription was performed with the Eppendorf® Mastercycler® (Eppendorf SE; Germany) with a cycling profile of 10 min at 25 °C, 2 h at 37 °C and 5 min at 85 °C before cooling down to 4 °C. The gained 400 ng of cDNA in 20 µl of volume and the 200 ng in 20 µl, respectively, was diluted to a concentration of 5 ng/µl with PCR grade water, transferred to 1.5 ml tubes and frozen at -20 °C.

3.8.7.3 Quantitative polymerase chain reaction

To analyze the expression of certain genes in the cell culture approach and sampled tissues, real-time quantitative polymerase chain reaction (RT-qPCR) was performed. The measured genes according to the target tissues as well as corresponding housekeepers and positive controls are depicted in Table 22.

Table 22: Target genes and primer sequences.

Tissue type	Target gene	Primer sequences (5' – 3')	Positive control
sc PACs d0, d3, d14 + om PACs d0, d3, d14	*UCP1*	F: TGTCCTGGGAACAATCACCG R: TGCTTCCTAAACTAGGTGCTGT	Huh7
	PRDM16	F: TCCTGAAGACATTCCGATCC R: CCGAAGTCTGTCTCCTTTGC	Huh7
	ARID5B	F: TCCACCTTGAAGGCAAACCA R: TGGAGCTCCGCTATGCAAAT	Huh7
	IRX3	F: AGACAGACACCGACACACAC R: GGGCTAAGTAAGGCAGCCAA	Huh7
	IRX5	F: CCGTGTGTGGCCATGTCCTAT R: CTGGAGGTGCGAGTTGTAGC	Huh7
	C/EBPα	F: CCAGAAAGCTAGGTCGTGGG R: TCCTAGGCAATGCTGAAGGC	Huh7
Housekeeper	*GAPDH*	F: GATCATCAGCAATGCCTCCTGC R: ACAGTCTTCTGGGTGGCAGTGA	Huh7
	IPO8	F: CGGATTATAGTCTCTGACCATGTG R: TGTGTCACCATGTTCTTCAGG	Huh7
sc PACs d14	*MT-CO2*	F: CTGAACCTACGAGTACACCG R: TTAATTCTAGGACGATGGGC	Huh7

Tissue type	Target gene	Primer sequences (5' – 3')	Positive control
+ om PACs d14	*18S*	F: GCGAAAGCATTTGCCAAGAA R: CATCACAGACCTGTTATTGC	Huh7
	ZAG	F: AAGCAAGGGTTGGAGGCAAT R: CTGTGGTTCAGCTCCCACAT	Huh7
	IL-6	F: ATCTGGATTCAATGAGGAGACTTG R: GCAGGAACTGGATCAGGACTT	Huh7
Housekeeper	*GAPDH*	F: GATCATCAGCAATGCCTCCTGC R: ACAGTCTTCTGGGTGGCAGTGA	Huh7
	IPO8	F: CGGATTATAGTCTCTGACCATGTG R: TGTGTCACCATGTTCTTCAGG	Huh7
Muscle tissue	*ZAG*	F: AAGCAAGGGTTGGAGGCAAT R: CTGTGGTTCAGCTCCCACAT	Pooled PACs
	Myostatin	F: GTAGTAGACCGCTGTGGGTG R: AGGCCTATAGCCTGTGGTACT	Pooled PACs
	IL-6	F: ATCTGGATTCAATGAGGAGACTTG R: GCAGGAACTGGATCAGGACTT	Pooled PACs
Housekeeper	*GAPDH*	F: GATCATCAGCAATGCCTCCTGC R: ACAGTCTTCTGGGTGGCAGTGA	Pooled PACs
	RPS20	F: GCGACTCATTGACTTGCACA R: TCAAAGTGTACTGCTGGCCC	Pooled PACs
Liver tissue	*ZAG*	F: AAGCAAGGGTTGGAGGCAAT R: CTGTGGTTCAGCTCCCACAT	Pooled PACs
	IL-6	F: ATCTGGATTCAATGAGGAGACTTG R: GCAGGAACTGGATCAGGACTT	Pooled PACs
Housekeeper	*GAPDH*	F: GATCATCAGCAATGCCTCCTGC R: ACAGTCTTCTGGGTGGCAGTGA	Pooled PACs
	ABCC2	F: TGAGCAAGTTTGAAACGCACAT R: AGCTCTTCTCCTGCCGTCTCT	Pooled PACs
sc adipose tissue + om adipose tissue	*ZAG*	F: AAGCAAGGGTTGGAGGCAAT R: CTGTGGTTCAGCTCCCACAT	Huh7
	IL-6	F: ATCTGGATTCAATGAGGAGACTTG R: GCAGGAACTGGATCAGGACTT	Huh7
	PTHrP	F: CTCTTTCAGCCAGAAGAGCAGA R: TCGTTAGATCTGAAGGGGGA	Huh7
Housekeeper	*GAPDH*	F: GATCATCAGCAATGCCTCCTGC R: ACAGTCTTCTGGGTGGCAGTGA	Huh7
	IPO8	F: CGGATTATAGTCTCTGACCATGTG R: TGTGTCACCATGTTCTTCAGG	Huh7

Each qPCR run was performed with a regular negative control using PCR grade water and additionally with a cDNA negative control to assure the integrity of the transcribed cDNA. Beforehand, all primer pairs were tested for functionality and to confirm their operation capacity at an annealing temperature of 60 °C during the amplification cycle. The master mixes, each containing the Maxima™ SYBR™ Green/ROX qPCR Master Mix (2X) ready-to-use solution provided by Thermo Fisher Scientific™, PCR grade water and the relevant primer pairs were prepared as depicted in Table 23.

Table 23: Components of qPCR master mix.

Components of master mix	Volume per cDNA sample
Maxima™ SYBR™ Green/ROX qPCR Master Mix (2X)	5.0 µl
Primer forward (10 µM)	0.3 µl
Primer reverse (10 µM)	0.3 µl
PCR grade water	2.4 µl
Total volume of master mix	**8.0 µl**

For all measured qPCR plates the pipetting robot was used to pipet 8 µl of master mix and 2 µl of cDNA, concentrated in 5 ng/µl, in a FrameStar® 384 well plate provided by 4titude (order no. 4ti-0381) according to the plate's layout. After loading the plate, it was sealed, centrifuged for 30 s at 1500 rpm at RT and qPCR was run by LightCycler®480. The setting of the qPCR program included 2 min of pretreatment at 50 °C and an initial denaturation for 10 min at 95 °C, followed by the 40 times repeated cycle, which consisted of 15 s at 95 °C for cDNA denaturation, 30 s of 60 °C for primer annealing and again 30 s at 72 °C for synthesis of the template. After the actual detection of fluorescence intensity over the cycles, a melting curve was performed as inner control for correctly amplified fragments. The LightCycler® software was used for further data processing and calculation of the crossing point (Cp-value) of each sample. The results were normalized to the expression of the used housekeeper genes. Expression data was BMI and age adjusted as well as log10 transformed.

3.9 Statistics

Scatterplots, bar graphs, boxplots, progression charts and heatmaps were created using GrapPad Prism 9. Beforehand, Shapiro-Wilk-Tests were used to test for/against normality leading to testing for/against differences between groups by either Mann-Whitney-U-Test (two groups; non-parametric) or by two-way ANOVA (> two groups). To investigate the positive or negative association between continuous variables, correlation analyses were conducted via IBM® SPSS® using Spearman correlation. In case a set of correlations or comparisons was performed at a time, Bonferroni correction was utilized to coadjust for multiple testing. Addressing survival, Kaplan-Meier curves were created in IBM® SPSS® referring to analysis-dependent cut-offs calculated by the statistics program R using LogRank-statistics within the packages "survival" and "maxstat". In all analyses p-values < 0.05 were considered significant.

Following points were performed in a team of two:

- Cohort establishment, primary cell culture, DNA isolation and FTO genotyping
- Performance of the differentiation experiment including cell harvest, Almar Blue assay as well as mRNA isolation and cDNA synthesis

Following points were performed exclusively by myself:

- IL-6 ELISA with plasma
- GPDH measurement
- Quantitative polymerase chain reaction (qPCR)
- All (statistical) analyses, evaluations and interpretations of the results of this thesis

4 Results

4.1 Tissue biobank: cohort description

The cohort was recruited from August 2016 until September 2019 at the Clinic and Policlinic of the *Klinikum rechts der Isar* in Munich. Up to this point, 114 patients were enrolled, a cohort description divided into the most common disease categories regarding gastrointestinal conditions is shown in Table 24. Since the patient groups for periampullary cancer, upper GI cancer, controls with benign pancreatic diseases and controls with non-inflammatory diseases each consisted of different main diagnoses, a lineup of occurring diagnoses is shown in Table 25.

Table 24: Patient characteristics of the cachexia cohort.

	all	PDAC	CRC	Periampullary cancer	Upper GI cancer	Control benign pancreatic disease	Control non-inflammatory disease
N	114	38	18	21	17	14	6
Age [years]	64.1 ± 13.7* (20 – 88)	67.1 ± 13.3 (42 – 88)	66.3 ± 10.7 (47 – 81)	64.8 ± 15.7 (20 – 84)	64.0 ± 9.7 (47 – 78)	58.1 ± 14.3 (34 – 78)	50.0 ± 17.5 (29 – 72)
Male Female	65 (57.0 %) 49 (43.0 %)	13 (34.2 %) 25 (65.8 %)	13 (72.2 %) 5 (27.8 %)	17 (81.0 %) 4 (19.0 %)	13 (76.5 %) 4 (23.5 %)	7 (50.0 %) 7 (50.0 %)	2 (33.3 %) 4 (66.7 %)
Weight surgery day [kg]	75.0 ± 16.4 (42.0 – 127.0)	68.4 ± 13.3 (47.0 – 100.0)	82.0 ± 16.6 (61.0 – 127.0)	80.7 ± 16.8 (42.0 – 118.3)	72.9 ± 16.1 (47.3 – 112.0)	77.8 ± 18.9 (50.0 – 109.0)	76.2 ± 15.4 (54.0 – 98.0)
BMI surgery day [kg/m^2]	25.7 ± 4.5 (16.2 – 41.9)	24.0 ± 3.0 (17.9 – 30.9)	27.9 ± 5.2 (21.4 – 41.9)	26.8 ± 4.9 (16.2 – 37.8)	24.9 ± 4.5 (16.7 – 33.8)	26.2 ± 5.4 (17.9 – 35.2)	27.2 ± 4.3 (21.0 – 33.1)
Weight loss Δ 6 months [%]	7.1 ± 7.2 (0 – 35.0)	9.1 ± 8.8 (0 – 35.0)	5.1 ± 6.4 (0 – 19.3)	6.6 ± 5.6 (0 – 16.0)	7.1 ± 6.3 (0 – 26.0)	7.1 ± 6.3 (0 – 14.8)	1.5 ± 1.4 (0 – 2.99)
Non-cachectic Cachectic	70 (61.4 %) 29 (25.4 %)	22 (57.9 %) 12 (31.6 %)	13 (72.2 %) 4 (22.2 %)	11 (52.4 %) 5 (23.8 %)	13 (76.5 %) 3 (17.6 %)	6 (42.9 %) 5 (35.7 %)	5 (83.3 %) 0 (0.0 %)
Non-sarcopenic Sarcopenic	41 (36.0 %) 46 (40.4 %)	15 (39.5 %) 22 (57.9 %)	10 (55.6 %) 4 (22.2 %)	7 (33.3 %) 7 (33.3 %)	6 (35.3 %) 9 (52.9 %)	1 (7.1 %) 3 (21.4 %)	2 (33.3 %) 1 (16.7 %)
FTO CT *FTO TT* *FTO CC*	63 (55.3 %) 29 (25.4 %) 13 (11.4 %)	19 (50.0 %) 13 (34.2 %) 3 (7.9 %)	13 (72.2 %) 1 (5.6 %) 2 (11.1 %)	14 (66.7 %) 6 (28.6 %) 1 (4.8 %)	6 (35.3 %) 4 (23.5 %) 5 (29.4 %)	8 (57.1 %) 3 (21.4 %) 2 (14.3 %)	3 (50.0 %) 2 (33.3 %) 0 (0.0 %)

* Mean ± SD, min - max (all such values)

Table 25: Diagnoses of patient groups of the cachexia cohort.

Patient group	Main diagnosis	N
Periampullary cancer	Bile duct cancer	8
	Papilla vateri adenocarcinoma	5
	NET of pancreas	4
	Duodenal cancer	2
	MCAC	1
	NEC head of the pancreas	1
Upper GI cancer	AEG	10
	Stomach cancer	5
	SCC esophagus	2
Control benign pancreatic disease	CP	9
	IPMN	3
	Pancreatic cyst	2
Control non-inflammatory disease	Controls (e.g. hernias, removal descendostoma)	5
	Colon adenoma	1

The mean age of the 114 patients in this cohort was 64.1 (± 13.7) ranging from 20 to 88 years without any significant differences between the groups. Among all the patients recruited 65 were male (57.0 %) and 49 were female (43.0 %). Regarding the subgroups with cancerous diseases the sex distribution was uneven showing a higher prevalence of female patients in the PDAC group (25 individuals / 65.8 % female vs. 13 individuals / 34.2 % male) and a higher prevalence of male patients in the CRC (13 individuals / 72.2 % male vs. 5 individuals / 27.8 % female), the periampullary cancer (17 individuals / 81.0 % male vs. 4 individuals / 19.0 % female) and the upper GI cancer group (13 individuals / 76.5 % male vs. 4 individuals / 23.5 % female), respectively (Figure 7).

The patients' mean weight at the day of surgery as well as the mean BMI were 75.0 kg (± 16.4 kg) and 25.7 kg/m^2 (± 4.5 kg/m^2), respectively. Patients with PDAC showed a significantly lower weight at the day of surgery (68.4 kg ± 13.3 kg) compared to patients with CRC (82.0 kg ± 16.6 kg; p = 0.049) and this effect was still visible considering the patients' mean BMI (p = 0.035). The mean weight loss of all patients calculated as delta of weight six months before surgery to the day of surgery was 6.9 % (± 6.0 %). Although mean weight loss was in tendency lower in the control group with non-inflammatory diseases compared to the other groups, results were found not to be significant. Throughout the whole cohort 29 patients (25.4 %) were cachectic according to the cut-off of 10 % weight loss in the last six months before surgery whereas 70 patients (61.4 %) were considered as non-cachectic (15 individuals/13.2 % not known). The distribution of cachectic patients in the subgroups ranged from 17.6 % among Upper GI patients to 35.7 % among patients with benign pancreatic diseases. In the control group with non-inflammatory diseases cachectic patients were absent (Figure 7).

A total number of 46 individuals (40.4 %) was defined as sarcopenic whereas 41 patients (36.0 %) did not have sarcopenia (27 individuals/23.7 % not known). The highest prevalence

of sarcopenia was found in patients with PDAC (57.9 % sarcopenic) and upper GI cancer (52.9 % sarcopenic) (Figure 7). Regarding the distribution of the *FTO* genotype (CT heterozygous genotype, TT wildtype and CC risk allele respectively) in the whole cohort, 63 patients owned the CT genotype (55.3 %) whereas 29 patients had the TT genotype (25.4 %) and 13 patients the CC genotype (11.4 %).

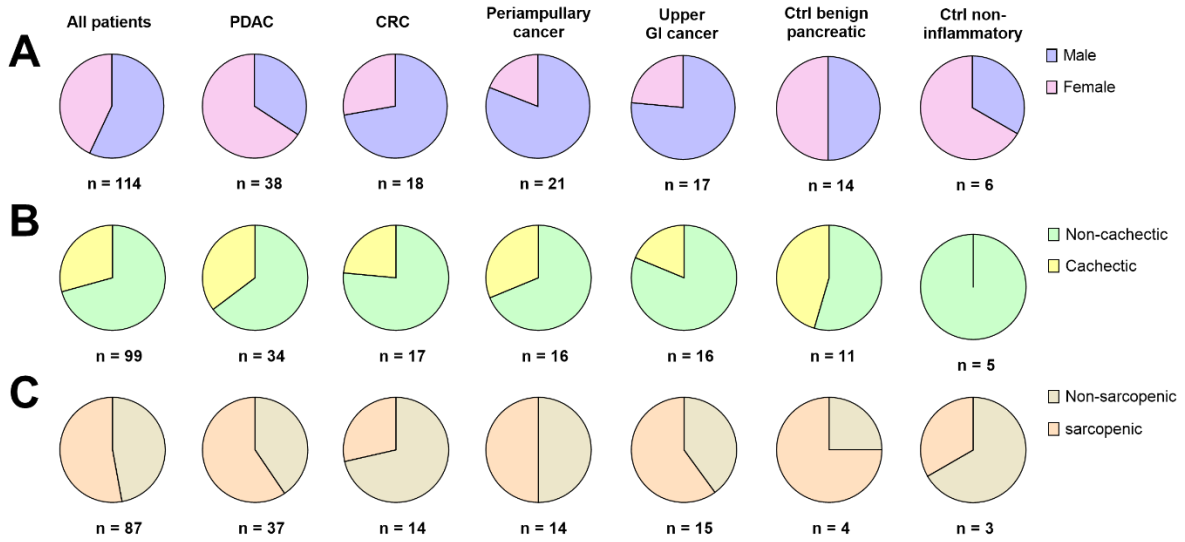

Figure 7: Sex, cachexia status and sarcopenia status among patient groups.
Pie charts demonstrating data of Table 24. **(A)** Sex distribution of whole cohort and disease subgroups. **(B)** cachexia status of whole cohort and disease subgroups. **(C)** sarcopenia status of whole cohort and disease subgroups.

The focus of this cohort was not only on the gathering of clinical data of the patients but mainly on the collection of tissue (sc adipose tissue, om adipose tissue, muscle tissue and liver tissue) as well as blood samples. Therefore, this cohort was the starting point for the differentiation experiment and 20 individuals were picked out of this pool. Selection criteria and approach are described under 3.8.1.

4.2 Plasma biobank: cohort description

Due to the fact that IL-6 is one of the most frequently measured inflammatory markers and has already been in consideration of being a biomarker for cachexia and/or sarcopenia in diverse studies (Bian et al., 2017; Eskiler et al., 2019; Han et al., 2018), it was decided to measure IL-6 in all available plasma samples of the patients of the newly established cohort to verify recent studies on the role of IL-6 in the context of cachexia. To increase statistical power the opportunity to elevate cohort size was used. The original cohort of 114 patients was scaled up by human plasma samples of a similar biobank located at the *Klinikum rechts der Isar* which also focused on the recruitment of patients with gastrointestinal cancer and suitable controls. Plasma IL-6 was therefore measured in a total number of 189 patients. The described

population was termed as “expanded cancer cohort”. The description and details of this cohort and the division into main diagnoses are shown in Table 26 and Table 27.

Table 26: Patient characteristics of the expanded cancer cohort

	all	PDAC	CRC	Periampullary cancer	Upper GI cancer	Control benign pancreatic disease	Control non-inflammatory disease
N	189	64	45	20	18	21	21
Age [years]	65.3 ± 12.8* (20 – 91)	67.8 ± 11.0 (42 – 88)	69.5 ± 10.3 (52 – 86)	62.6 ± 15.3 (20 – 78)	64.1 ± 9.3 (47 – 78)	56.4 ± 13.5 (34 – 78)	61.1 ± 16.3 (29 – 91)
Male Female	106 (56.1 %) 83 (43.9 %)	27 (42.2 %) 37 (57.8 %)	30 (66.7 %) 15 (33.3 %)	16 (80.0 %) 4 (20.0 %)	12 (66.7 %) 6 (33.3 %)	12 (57.1 %) 9 (42.9 %)	9 (42.9 %) 12 (57.1 %)
Weight surgery day [kg]	75.9 ± 17.6 (42.0 – 130.0)	70.6 ± 14.3 (42.0 – 101.0)	80.7 ± 19.5 (43.0 – 127.0)	81.0 ± 16.0 (52.0 – 118.3)	70.2 ± 17.0 (47.3 – 112.0)	77.5 ± 18.0 (47.0 – 109.0)	80.7 ± 19.5 (47.0 – 130.0)
BMI surgery day [kg/m^2]	25.8 ± 5.2 (15.8 – 43.9)	24.3 ± 4.3 (16.4 – 39.7)	27.2 ± 6.2 (15.8 – 41.9)	27.1 ± 4.5 (19.8 – 37.8)	24.6 ± 4.7 (16.7 – 33.8)	25.3 ± 5.5 (17.2 – 35.2)	27.7 ± 5.5 (18.8 – 43.9)
Weight loss Δ 6 months [%]	5.9 ± 6.4 (0 – 35.0)	7.9 ± 6.9 (0 – 35.0)	4.5 ± 6.6 (0 – 28.8)	6.2 ± 4.9 (0 – 15.5)	6.1 ± 6.7 (0 – 26.0)	6.0 ± 6.7 (0 – 16.1)	2.5 ± 3.2 (0 – 9,1)
Non-cachectic Cachectic	124 (65.6 %) 40 (21.2 %)	34 (53.1 %) 22 (34.4 %)	36 (80.0 %) 5 (11.1 %)	11 (55.0 %) 4 (20.0 %)	14 (77.8 %) 3 (16.7 %)	10 (47.6 %) 6 (28.6 %)	19 (90.5 %) 0 (0.0 %)
Non-sarcopenic Sarcopenic	62 (32.8 %) 95 (50.3 %)	23 (35.9 %) 37 (57.8 %)	16 (35.6 %) 26 (57.8 %)	7 (35.0 %) 8 (40.0 %)	5 (27.8 %) 12 (66.7 %)	6 (28.6 %) 8 (38.1 %)	5 (23.8 %) 4 (19.0 %)
FTO CT *FTO TT* *FTO CC*	19.7 ± 69.2 (0 – 566.3)	14.8 ± 32.8 (0 – 182.0)	33.5 ± 103.4 (0 – 533.3)	37.2 ± 127.4 (0 – 566.3)	7.6 ± 13.8 (0 – 53.6)	14.2 ± 35.3 (0 – 140.0)	3.7 ± 6.6 (0 – 27.1)

* Mean ± SD, min - max (all such values)

Table 27: Diagnoses of patient groups of the expanded cancer cohort.

Patient group	Main diagnosis	N
Periampullary cancer	Bile duct cancer	8
	NET of pancreas	5
	Papilla vateri adenocarcinoma	4
	Duodenal cancer	2
	MCAC	1
Upper GI cancer	AEG	10
	Stomach cancer	6
	SCC esophagus	2
Control benign pancreatic disease	CP	11
	IPMN	8
	Pancreatic cyst	2
Control non-inflammatory disease	Controls (e.g. hernias, removal descendostoma)	17
	Colon adenoma	4

The mean age of the 189 patients of the expanded cancer cohort was 65.3 (± 12.8) with the youngest patient being 20 and the oldest being 91 years old. The patients' mean age was found to be lowest in the control group with benign pancreatic diseases with a significant difference in comparison to PDAC and CRC patients respectively ($p = 0.004$; $p = 0.001$) (Table 26). Among all patients recruited 106 were male (56.1 %) and 83 were female (43.9 %). Trends in sex distribution were similar to the original cohort mentioned in Table 24, with the most pronounced sex differences in the periampullary cancer group in which 16 patients (80 %) were male, whereas only 4 (20.0 %) were female.

The patients' mean weight at the day of surgery as well as the mean BMI were 75.9 kg (±17.6 kg) and 25.8 kg/m^2 (± 5.2 kg/m^2) respectively. Regarding mean BMI there were no significant differences between the groups, although PDAC patients had a significantly lower mean weight at the day of surgery (70.6 kg ± 14.3 kg) compared to CRC patients (80.7 kg ± 19.5 kg; $p = 0.04$). The mean weight loss of all patients was 5.9 % (± 6.4 %). Patients with PDAC revealed a significantly higher mean weight loss over a six months' period than control patients with non-inflammatory diseases ($p = 0.021$). Throughout the whole cohort 40 patients (21.2 %) were cachectic, whereas 124 patients (65.6 %) were considered as non-cachectic (25 individuals/13.2 % not known). The distribution of cachectic patients in the subgroups ranged from 11.1 % among CRC patients to 34.4 % among patients with PDAC. In the control group with non-inflammatory diseases cachectic patients were absent. A total number of 95 individuals (50.3 %) were defined as sarcopenic, whereas 62 patients (32.8 %) did not have sarcopenia (32 individuals/16.9 % not known). The highest prevalence of sarcopenia was found in patients with upper GI cancer (66.7 % sarcopenic).

Mean plasma levels of IL-6 were 19.7 pg/ml with a high standard deviation of 69.2 pg/ml and the subgroups with CRC and periampullary cancer revealed the highest amount of IL-6, namely 33.5 pg/ml (± 103.4 pg/ml) and 37.2 pg/ml (± 127.4 pg/ml), respectively (Figure 8). Differences between the groups were not found to be significant.

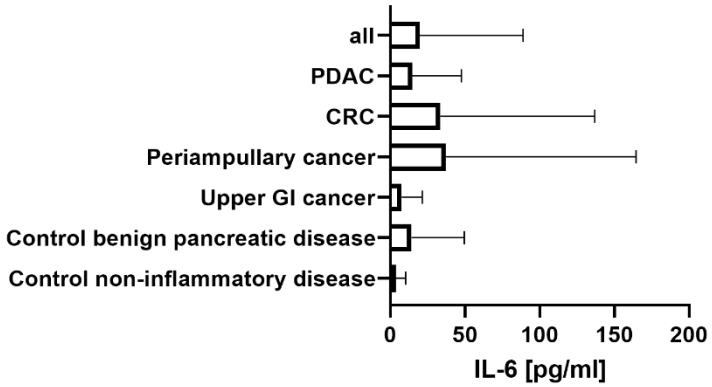

Figure 8: IL-6 plasma levels in the expanded cancer cohort according to diagnosis.
IL-6 plasma levels in pg/ml in the total cohort ("all") and the subgroups. Data displayed as mean and ± SD.

The description of the two cohorts regarding age, sex, weight and BMI at the day of surgery was collected and added to the biobank's basic information. Delta weight loss comprising 6 months before surgery as well as the cachectic and sarcopenic status according to disease groups completed the knowledge about the health status of the patients. The distribution of *FTO* genotypes and IL-6 plasma measurements were conducted in order to search for possible biomarkers and predictors of cachexia. To further perform correlation analyses of plasma IL-6 with routine laboratory parameters are shown in the following.

4.3 Correlation analysis of IL-6 in the extended cancer cohort

In Table 28 correlation analyses of IL-6 with body composition parameters are shown. No parameter revealed significant results. "BMI pre OP" as well as "weight loss in %" showed tendencies towards a negative correlation ($p = 0.054$; $r = -0.140$) or rather a positive correlation ($p = 0.076$; $r = 0.139$) with plasma IL-6.

Table 28: Correlations of IL-6 with body composition parameters.

Correlations IL-6 plasma	Correlation coefficient	p-value	N
Hip circumference pre OP	-0.052	0.599	105
Waist circumference pre OP	0.046	0.601	133
Waist-to-hip-ratio pre OP	0.091	0.375	98
BMI 5 years pre OP	-0.040	0.634	141
BMI 12 months pre OP	-0.064	0.432	152
BMI 6 months pre OP	-0.064	0.414	164
BMI 3 months pre OP	-0.105	0.182	164
BMI pre OP	-0.140	0.054	189
BMI 3 months post OP	-0.043	0.669	100
BMI 6 months post OP	-0.006	0.951	95
BMI 12 months post OP	-0.048	0.728	54
Weight loss in %	0.139	0.076	164
SMAI pre OP	-0.076	0.343	157

In Table 29 correlation analyses of IL-6 with hematological parameters are shown. Only parameters, which revealed significant results, are depicted. CRP, alkaline phosphatase, total serum protein, CA19-9 and the percentage occurrence of neutrophils in blood correlated positively with the inflammatory cytokine in plasma. P-values ranged from 0.049 with alkaline phosphatase to less than 0.001 with CRP. Albumin, cholinesterase, total cholesterol, hemoglobin, iron and the percentage occurrence of lymphocytes in blood correlated negatively with IL-6. P-values ranged from 0.033 with total cholesterol to 0.001 with cholinesterase, hemoglobin as well as iron.

Table 29: Correlations of IL-6 with hematological parameters.

Correlations IL-6 plasma	Correlation coefficient	p-value	N
Albumin	-0.236	0.002**	172
CRP	0.338	< 0.001***	133
Cholinesterase	-0.407	0.000***	141
Cholesterol total	-0.259	0.033*	68
Hemoglobin	-0.247	0.001***	189
Iron	-0.370	0.001***	81
Alkaline phosphatase	0.148	0.049*	178
Total serum protein	0.217	0.014*	127
CA19-9	0.263	0.009**	97
Neutrophils %	0.237	0.021*	95
Lymphocytes %	-0.290	0.004**	96

Statistical significance is depicted as follows: * $p < 0.05$; ** $p < 0.01$; *** $p < 0.001$

Plasma levels of IL-6 of the expanded cancer cohort were not only taken into account regarding the correlation with routine laboratory parameters but also as a possible predictor of overall survival. Results of survival analyses are shown below.

4.4 Survival analysis of IL-6 plasma cohort

Survival time was presented in days, which was calculated using the day of surgery as starting point and the day of data analysis as endpoint. During this time frame, either an event occurred - meaning the reported death of a patient - or data was registered as being censored. Censored data covers the known survival of a patient even beyond the endpoint or the unknown survival status at the endpoint. This occurred in case the last contact with a patient took place before the analyzed time period was closed.

Cut-offs for either the whole expanded cancer cohort or separate subgroups were calculated, dividing the patients into “IL-6 high” or “IL-6 low” categories. Kaplan-Meier curves were created as shown in Figure 9 and Figure 10, describing the difference in survival with regard to IL-6 plasma levels.

In Figure 9, the difference in survival between patients with either high or low plasma IL-6 is shown, all patients were included, regardless of tumor type and a group cut-off of 0.09 pg/ml was used. Altogether, 139 patients are depicted, 37 clustered as “IL-6 low” and 102 as “IL-6 high”. Until about 400 days after surgery both groups showed similar survival rates and cases of death. Beyond this turning point, IL-6 plasma levels at the day of surgery revealed an effect. Patients with low IL-6 revealed significantly better survival of 69.1 % until day 1000 after surgery compared to only 22.1 % among the patients with high IL-6 levels, resulting in a p-value of 0.071.

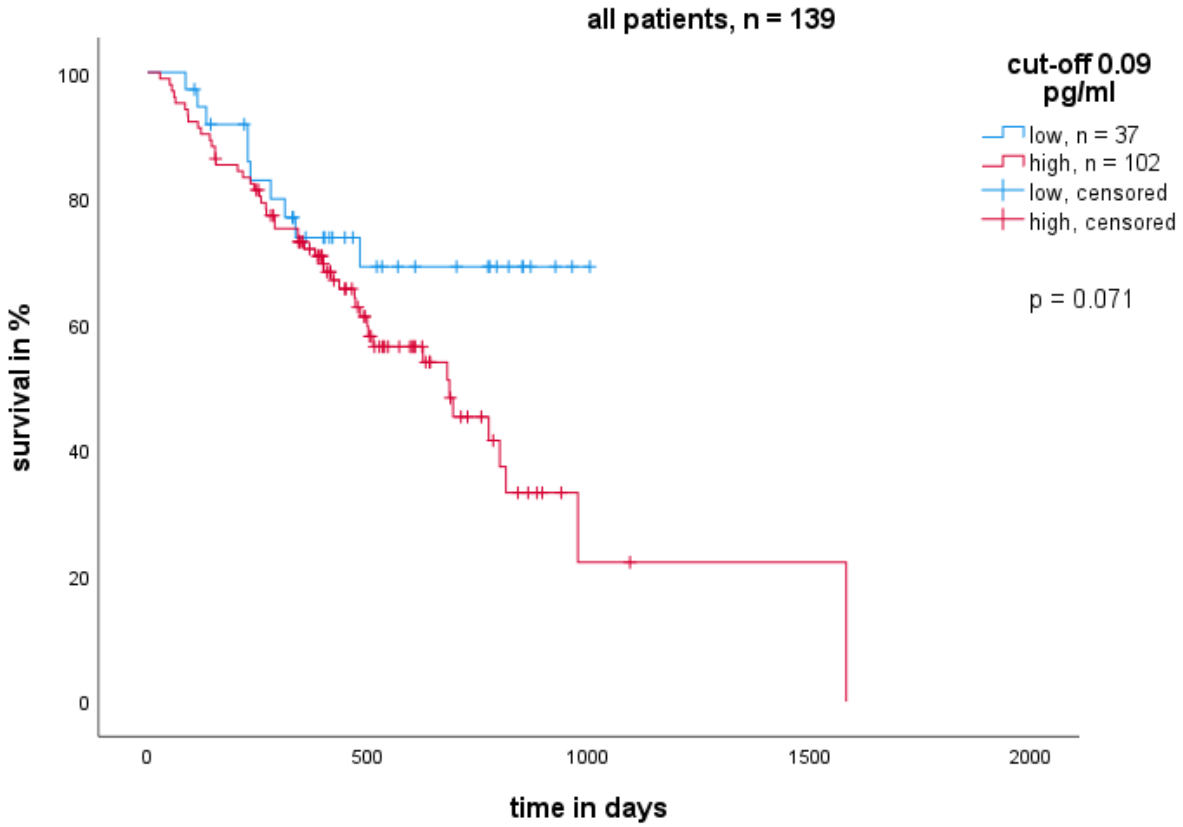

Figure 9: Kaplan-Meier survival curve of all patients dependent on plasma IL-6 levels.
X-axis shows survival in days and y-axis the survival probability in %. As cut-off between IL-6 low (blue, n = 37) and IL-6 high (green, n = 102) 0.09 pg/ml was calculated. Censoring describes an individual’s death. P = 0.071

Additionally, the Kaplan-Meier curves of patients with PDAC only are depicted in Figure 10, a cut-off of 0.09 pg/ml was calculated. Thirteen patients were grouped as “IL-6 low” and 49 as “IL-6 high”. About 500 days after surgery, 75.2 % of the PDAC patients with low IL-6 plasma levels were still alive which only applied for 44.6 % of the patients with high IL-6 levels. At day 1000 after surgery, only 8.9 % of patients with high IL-6 were still alive, still facing 75.2 % of the second group. This significant difference in survival is represented by a p-value of 0.006.

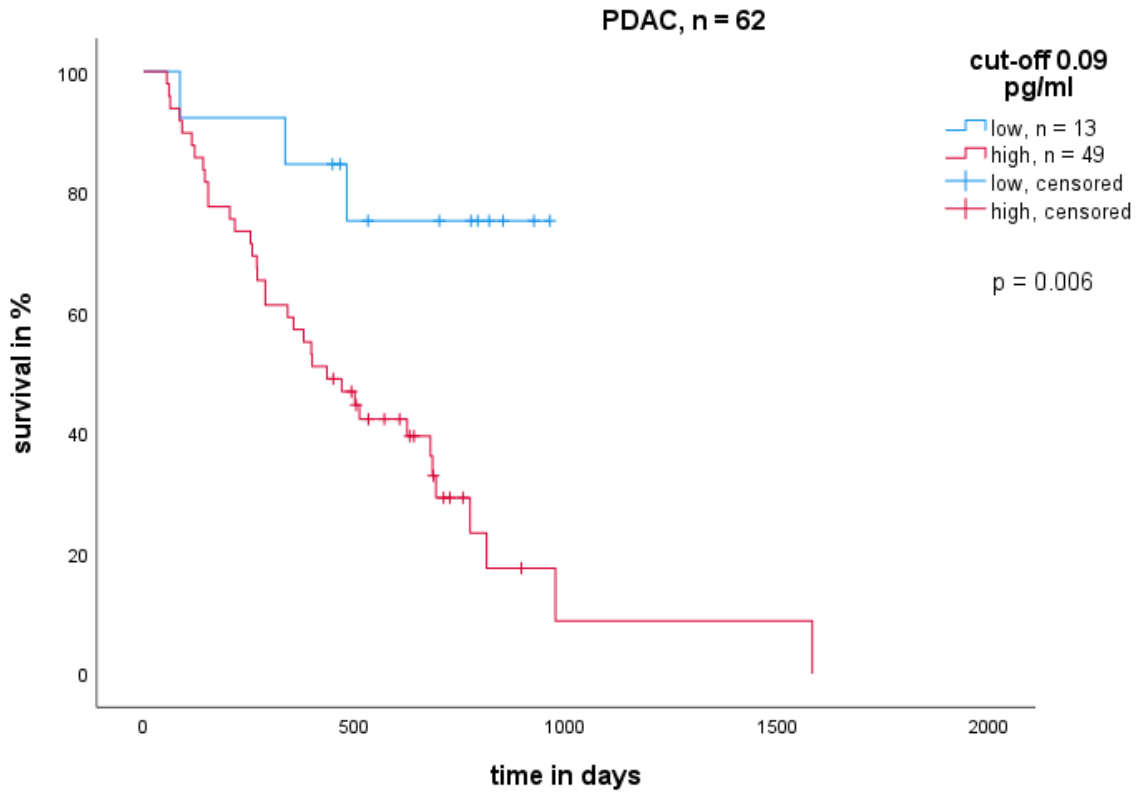

Figure 10: Kaplan-Meier survival curve of PDAC patients dependent on plasma IL-6 levels.
X-axis shows survival in days and y-axis the survival probability in %. As cut-off between IL-6 low (blue, n = 13) and IL-6 high (green, n = 49) 0.09 pg/ml was used. Censoring describes an individual's death. P = 0.006

In addition to the analyses of the whole cachexia and the expanded cancer cohort, gene expression analysis of a selected subgroup was performed. Expression was evaluated in sampled tissues and preadipocytes/adipocytes of a cell culture differentiation experiment. Results are depicted in the following.

4.5 Gene expression and differentiation experiment

4.5.1 GPDH activity

Relative GPDH activity, a marker for adipogenic differentiation, of all 20 patients included in the differentiation experiment is shown in Figure 11 and Figure 12. Represented are the results of sc and om PACs combined, since no significant differences in GPDH activity could be found among both depots (data not shown).

Figure 11 shows the relative GPDH activity of PACs during their adipogenic differentiation on d0, d3 and d14 separated according to the four different patient groups described in Table 18. In all four groups, GPDH activity rose over the measured time points reaching the highest activity level at d14. At d0, severe cachectic patients with a weight loss higher than 10 % revealed a significantly higher GPDH activity compared to both control groups (CAC > 10% to - CAC/+ ca: p = 0.008; CAC > 10% to - CAC/- ca: p = 0.05). The same effect was seen between

the patients with 5-10 % weight loss and without weight loss but cancer (p = 0.04). Even d3 and d14 revealed a higher GPDH activity of the two cachectic compared to the two control groups, with a stronger effect on d14, but the results were not significant, which was probably due to a high diversity of the differentiation progress.

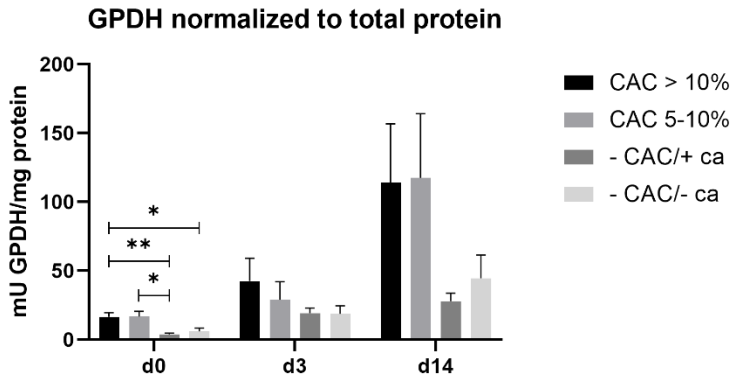

Figure 11: GPDH activity normalized to total protein on day (d) 0, d3 and d14 of adipogenic differentiation in sc and om PACs in the patient groups CAC > 10%, CAC 5-10%, -CAC/+ ca and -CAC/- ca.
Group size of n = 5. Data represent mean values ± SEM. Statistical significance calculated by a two-way ANOVA is depicted as follows: * p < 0.05; ** p < 0.01.

Furthermore, a possible effect of cachexia as well as the presence of a tumor to relative GPDH activity was investigated. When patients were grouped according to being cachectic (CAC) or non-cachectic (- CAC) it could be shown that cachectic patients had a significantly higher GPDH activity on d0 (p = 0.0001) and d14 (p = 0.02) respectively, compared to non-cachectic patients (Figure 12A). Figure 12B exclusively shows GPDH measurements of patients without cachexia. Here, no significant difference in GPDH activity could be seen between patients with and without cancer independent of the harvesting day.

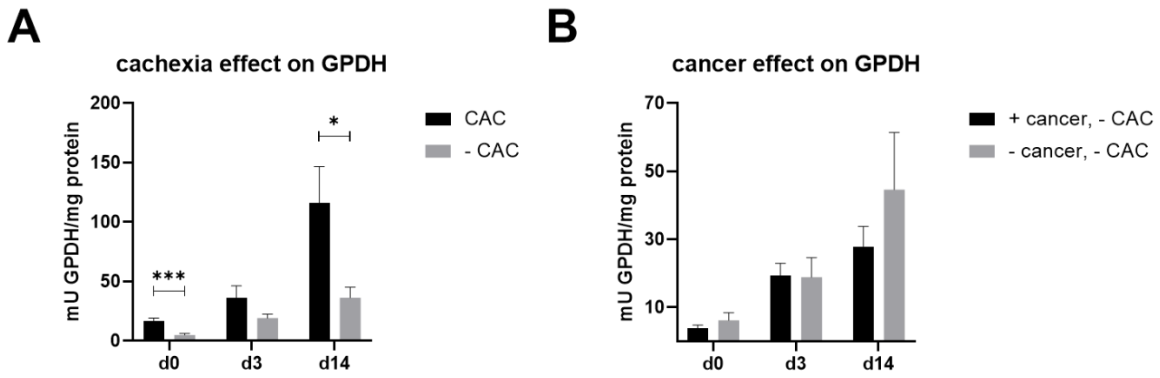

Figure 12: GPDH activity normalized to total protein on day (d) 0, d3 and d14 of adipogenic differentiation in sc and om PACs in different groupings.
Data represent mean values ± SEM. **(A)** GPDH activity in cachectic (CAC; n = 10) versus non-cachectic (- CAC; n = 10) group. **(B)** GPDH activity in cancer (n = 5) versus no cancer (n = 5) group without CAC. Statistical significance calculated by a Mann-Whitney U test is depicted as follows: * p < 0.05; *** p < 0.001

Taken together, the enzymatic activity of GPDH revealed huge interindividual differences, but showed a tendency to be higher in cachectic patients.

4.5.2 mRNA analysis of subcutaneous and omental preadipocytes

In the following, mRNA gene expression analyses of PACs originating from the sc and om depot are depicted. Unless stated otherwise, all gene expression data are displayed as fold change expression related to the - CAC/- ca control group, hence regarded as the healthy reference group/baseline. Significances towards the reference group are depicted by significance stars only, whereas significances between the three groups are additionally shown with the actual p-values. In case a marker was measured over all three harvesting days, an overview graphic of all groups and days is shown. Possible significant differences among the groups are additionally represented as scatterplots. In case a marker was only measured at d14 (see Table 22), scatterplots are shown independent of possible significances.

UCP1 and *PRDM16* mRNA expression levels in sc PACs are shown in Figure 13. Figure 13A revealed only low differences between the groups on d0 as well as on d14, but on d3 severe cachectic patients with a weight loss of at least 10 % showed a significantly lower *UCP1* expression in comparison to the group with moderate cachexia as well as healthy controls (Figure 13B). Although differences of *PRDM16* expression between the groups seemed to be highest on d0 and d3, only d0 disclosed significantly increased *PRDM16* expression in patients with moderate cachexia in comparison to the healthy group (Figure 13C, D).

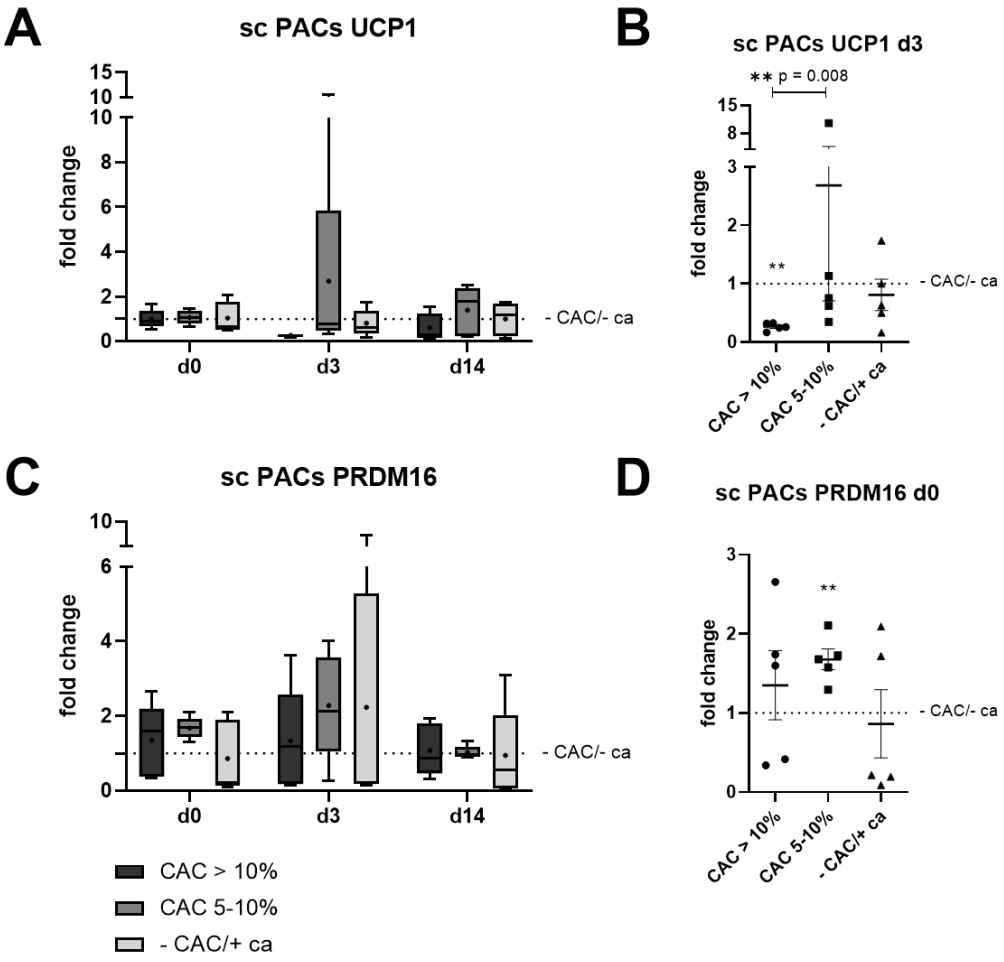

Figure 13: mRNA expression of browning markers in sc PACs on harvesting day(d)0, d3 and d14 among the patient groups CAC > 10%, CAC 5-10%, -CAC/+ ca and -CAC/- ca.
Group size of n = 5. Data represent mean values ± SEM. **(A)** fold change mRNA expression of *UCP1* on d0, d3 and d14 in all groups using -CAC/- ca as baseline **(B)** fold change mRNA expression of *UCP1* on d3 **(C)** fold change mRNA expression of *PRDM16* on d0, d3 and d14 in all groups using -CAC/- ca as baseline **(D)** fold change mRNA expression of *PRDM16* on d0; Statistical significance is depicted as follows: * $p < 0.05$; ** $p < 0.01$

The same markers were measured in om PACs. Gene expression of *UCP1* and *PRDM16* in om PACs is shown in Figure 14. The overview picture of *UCP1* revealed an increased expression of UCP1 in the cancer control group in comparison to the remaining groups as well as to baseline. This was due to outliers on each harvesting day, which could not be led back to a single individual (Figure 14A). Nonetheless, on d0, patients with severe cachexia showed a significantly lower *UCP1* expression in comparison to healthy controls (Figure 14B). *PRDM16* expression was rather homogenous between the groups and across harvesting days. Solely, a single outlier among the cancer control group was visible on d3, which led to high SEM and no significant differences (Figure 14C).

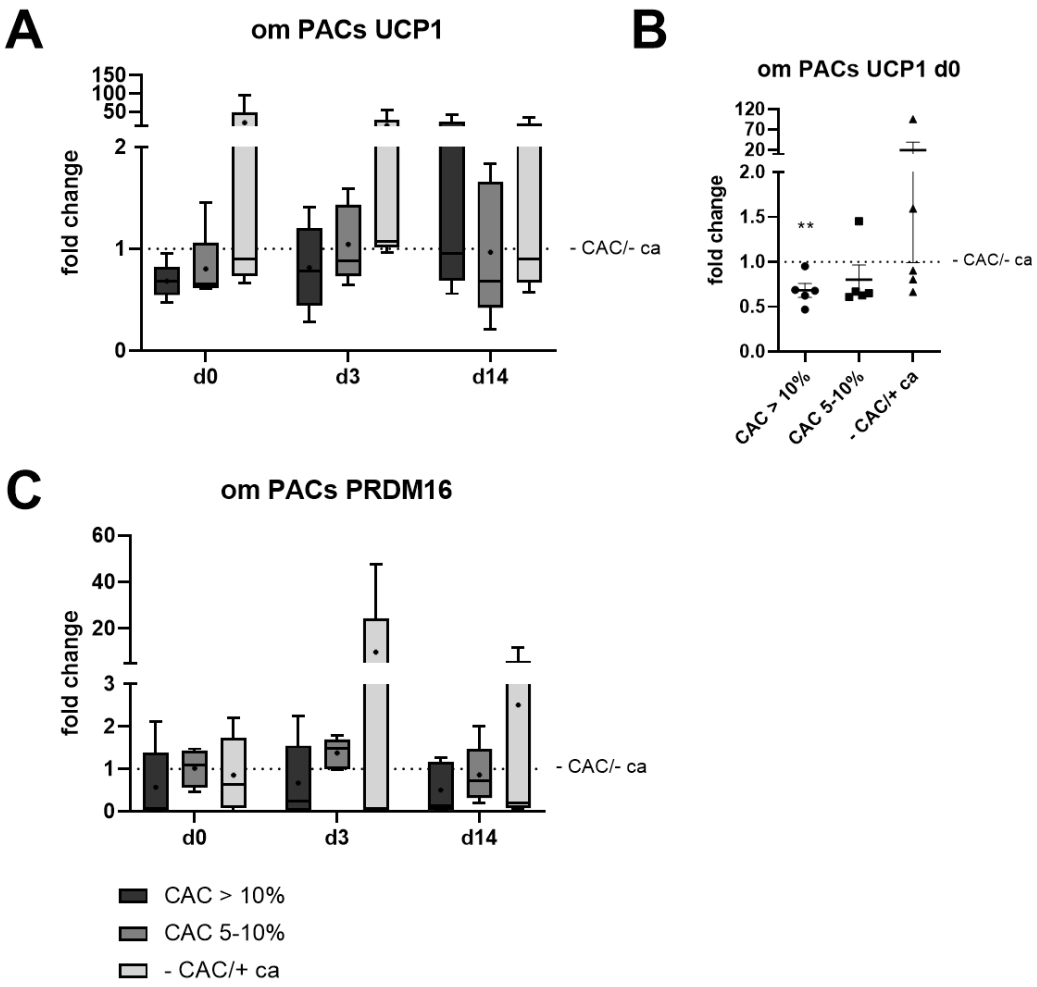

Figure 14: mRNA expression of browning markers in om PACs on harvesting day(d)0, d3 and d14 among the patient groups CAC > 10%, CAC 5-10%, -CAC/+ ca and -CAC/- ca.
Group size of n = 5. Data represent mean values ± SEM. **(A)** fold change mRNA expression of *UCP1* on d0, d3 and d14 in all groups using -CAC/- ca as baseline **(B)** fold change mRNA expression of *UCP1* on d0 **(C)** fold change mRNA expression of *PRDM16* on d0, d3 and d14 in all groups using -CAC/- ca as baseline; Statistical significance is depicted as follows: * $p < 0.05$; ** $p < 0.01$

The expression of the browning markers *UCP1* and *PRDM16* revealed huge interindividual differences in both depots. *UCP1* expression was extremely low in PACs of both depots regardless the harvesting day. Regarding *PRDM16*, a trend towards a higher expression in sc PACs among cancer patients could be shown. Besides classical browning markers, other factors contributing to thermogenesis were evaluated and are depicted below.

In Figure 15, mRNA gene expression of the *FTO*-related markers *ARID5B*, *IRX3* and *IRX5* in sc PACs is shown. Focusing on *ARID5B* it was seen that the cancer control group without cachexia (-CAC/+ca) showed significantly lower expression on d0 in comparison to the group with moderate cachexia and healthy controls (Figure 15B). On d3 patients with moderate cachexia expressed significantly less *ARID5B* compared to healthy controls (Figure 15C).

Regarding *IRX3*, mRNA gene expression of patients with moderate cachexia was significantly increased compared to both control groups (Figure 15E). On d0, a significantly higher *IRX5* expression in comparison to the cancer control group was found, whereas on d14 the expression of *IRX5* in severe cachectic patients was significantly lower compared to the healthy controls (Figure 15G, H). Comparing all three markers it should be noted that the expression levels of *IRX3* and *IRX5* were very similar (Figure 15D, F) and that on d0 patients with moderate cachexia showed a significantly increased *ARID5B*, *IRX3* and *IRX5* gene expression in comparison to cancer controls (Figure 15B, E, G). *IRX3* as well as *IRX5* revealed much higher fold change expression differences in comparison to healthy controls and a higher SEM compared to the marker *ARID5B* (mean fold change of 10.4 and 9.5 vs 1.1, respectively; Figure 15B, E, G).

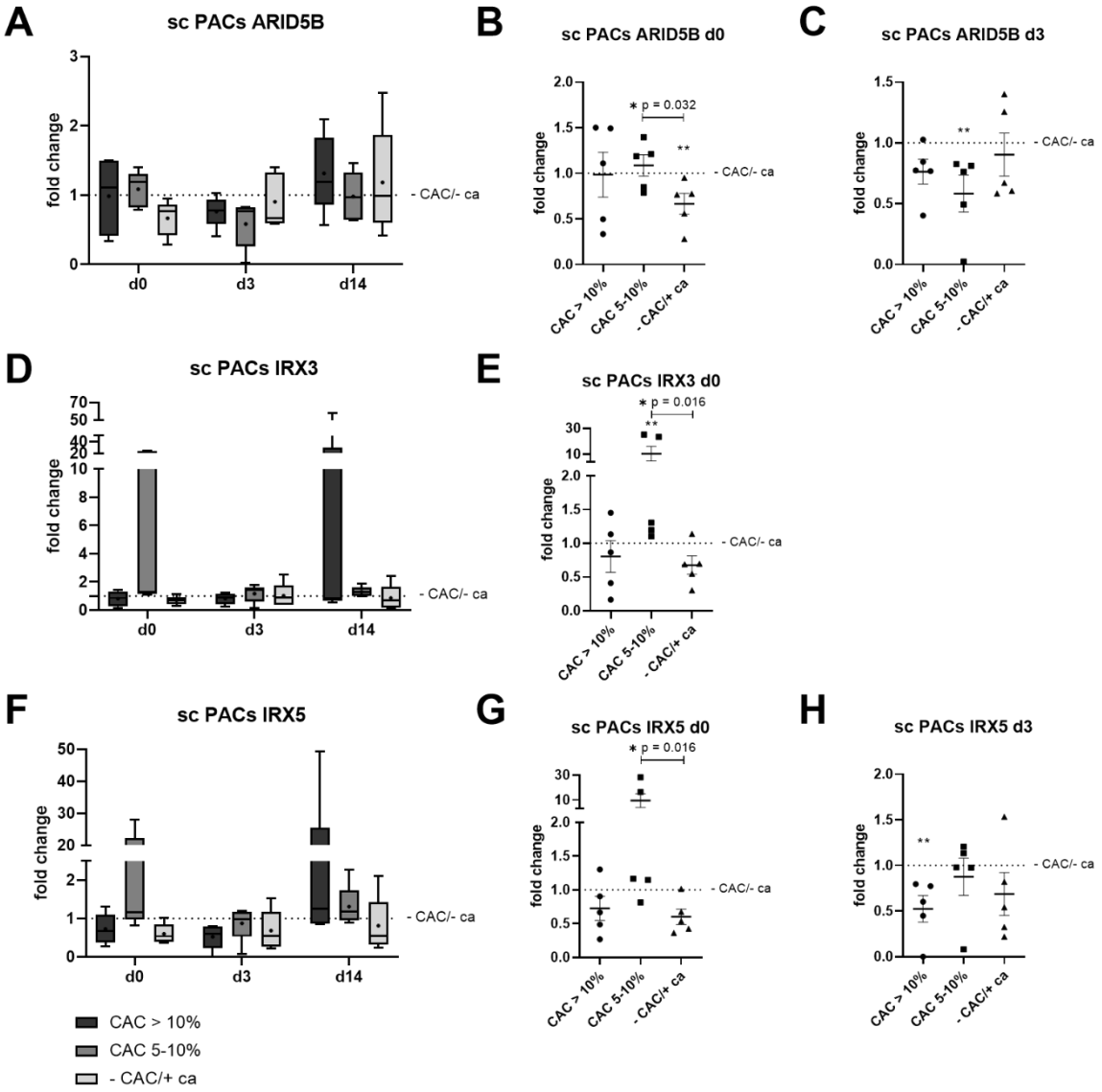

Figure 15: mRNA expression of *FTO*-related markers in sc PACs on harvesting day(d)0, d3 and d14 among the patient groups CAC > 10%, CAC 5-10%, -CAC/+ ca and -CAC/- ca.
Group size of n = 5. Data represent mean values ± SEM. **(A)** fold change mRNA expression of *ARID5B* on d0, d3 and d14 in all groups using -CAC/- ca as baseline **(B)** fold change mRNA expression of *ARID5B* on d0 **(C)** fold change mRNA expression of *ARID5B* on d3 **(D)** fold change mRNA expression of *IRX3* on d0, d3 and d14 in all groups using -CAC/- ca as baseline **(E)** fold change mRNA expression of *IRX3* on d0 **(F)** fold change mRNA expression of *IRX5* on d0, d3 and d14 in all groups using -CAC/- ca as baseline **(G)** fold change mRNA expression of IRX5 on d0 **(H)** fold change mRNA expression of *IRX5* on d3; Statistical significance is depicted as follows: * $p < 0.05$; ** $p < 0.01$

In Figure 16 mRNA gene expression of the *FTO*-related markers *ARID5B*, *IRX3* and *IRX5* in om PACs is shown. *ARID5B* revealed a significantly lower expression in both cachectic groups compared to healthy controls. This tendency was also present in the cancer control group but results were found not to be significant (Figure 16B). Results on d3, which presented a similar expression profile as on d0, again displayed a significantly decreased *ARID5B* expression in the group with severe cachexia in comparison to baseline. No significant results were found regarding the patients with moderate cachexia, although a tendency towards lower expression

compared to healthy controls was visible. (Figure 16C) As already seen in sc PACs, the gene expression profile of *IRX3* and *IRX5* in om PACs was similar, but in both cases no significant differences among the groups were present on all three harvesting days (Figure 16D, E). To note, the outlier, which caused high SEM on d3 in all three measured markers due to a fold change difference from 6.4 in *ARID5B* up to 37.4 in *IRX5* compared to baseline, was the same individual in all cases and belonged to the cancer control group (Figure 16A, D, E).

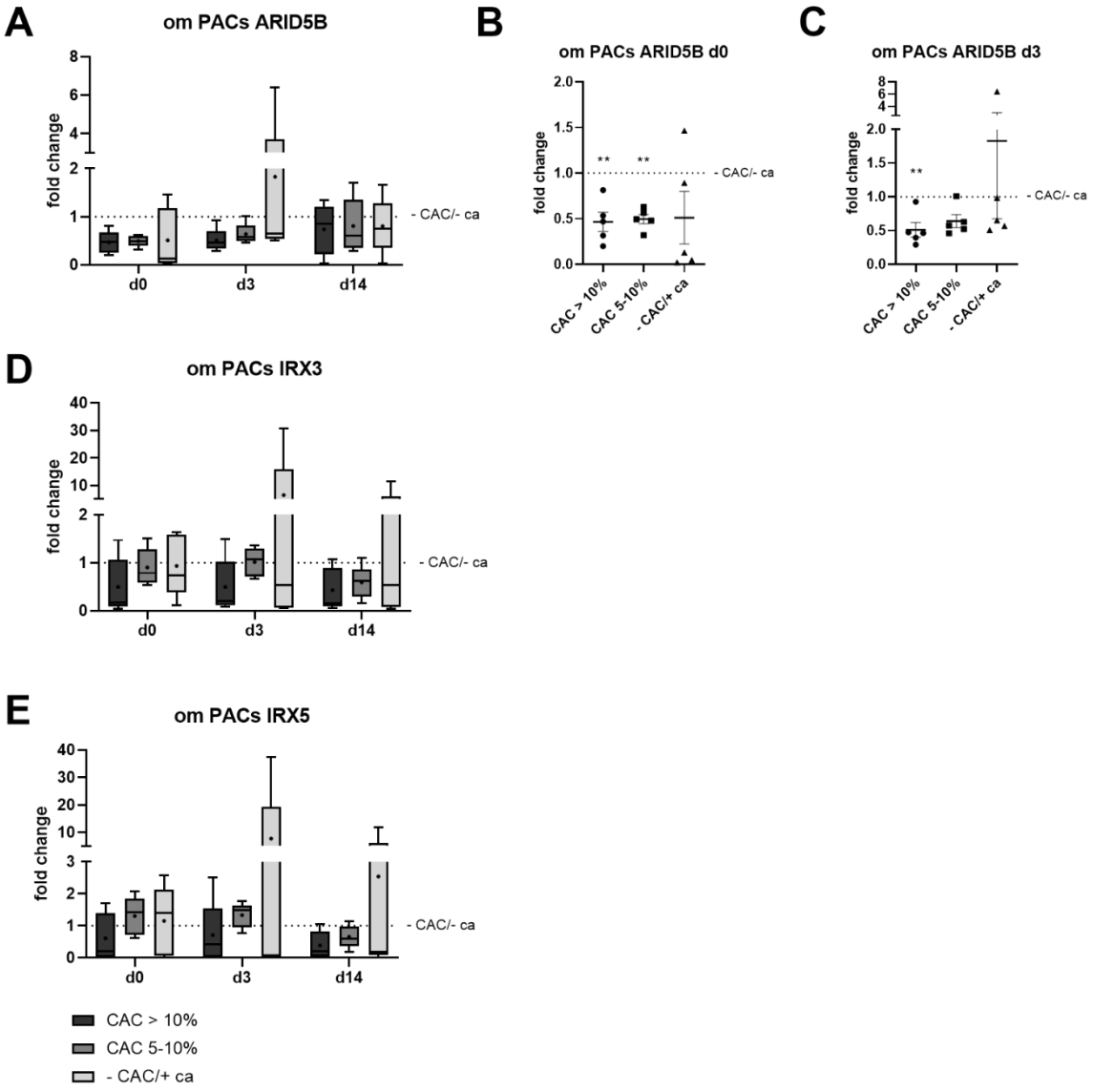

Figure 16: mRNA expression of *FTO*-related markers in om PACs on harvesting day(d)0, d3 and d14 among the patient groups CAC > 10%, CAC 5-10%, -CAC/+ ca and -CAC/- ca.
Group size of n = 5. Data represent mean values ± SEM. **(A)** fold change mRNA expression of *ARID5B* on d0, d3 and d14 in all groups using -CAC/- ca as baseline **(B)** fold change mRNA expression of *ARID5B* on d0 **(C)** fold change mRNA expression of *ARID5B* on d3 **(D)** fold change mRNA expression of *IRX3* on d0, d3 and d14 in all groups using -CAC/- ca as baseline **(E)** fold change mRNA expression of *IRX5* on d0, d3 and d14 in all groups using -CAC/- ca as baseline; Statistical significance is depicted as follows: * $p < 0.05$; ** $p < 0.01$

To directly investigate a possible effect of the three *FTO* genotypes TT, CC and CT on the expression of the *FTO*-related markers *ARID5B*, *IRX3* and *IRX5*, Figure 17 depicts the results of both depots on all three harvesting days. Among the 20 patients investigated, nine showed the heterozygous CT combination (45 %), whereas six patients revealed the TT (30 %) and five patients the CC genotype (25 %), respectively. Genotypes were evenly distributed among cachexia (TT x 2, CC x 3, CT x 5) and non-cachectic controls (TT x 4, CC x 2, CT x 4). No differences among the genotypes could be found in any of the markers, irrelevant of the harvesting day or the depot. Comparing sc and om PACs, om cells showed a higher interindividual variability of the results compared to the sc counterparts.

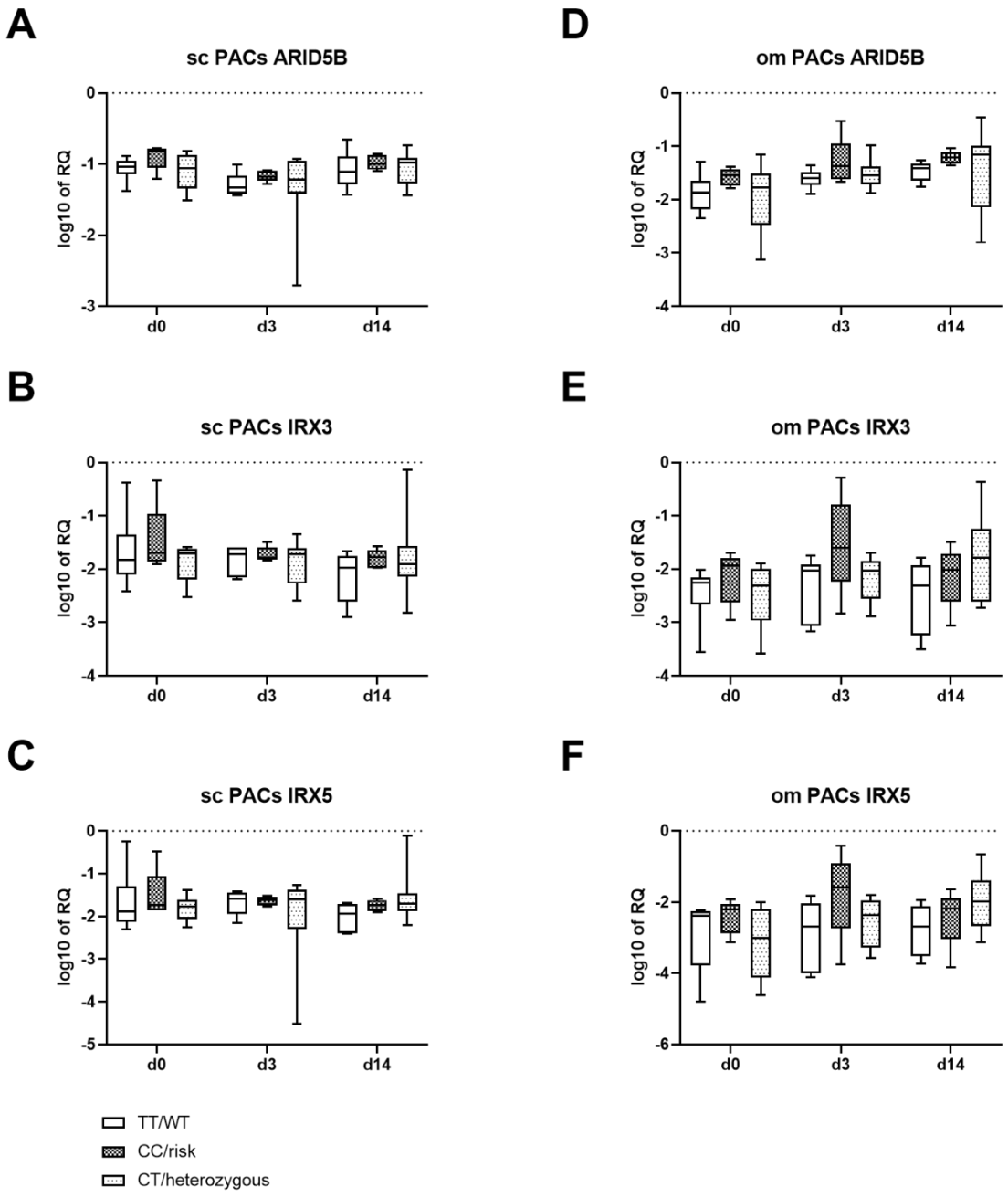

Figure 17: mRNA expression of FTO-related marker in sc and om PACs on harvesting day(d) 0, d3 and d14 according to the three FTO genotypes (TT/WT, CC/risk, CT/heterozygous).
Group size TT n = 6, CC n = 5, CT n = 9. Data represent log10 of the relative quantification (RQ) in boxplots displaying Min and Max. **(A)** log10 of RQ mRNA expression of *ARID5B* on d0, d3 and d14 in sc PACs in genotype groups TT, CC and CT **(B)** log10 of RQ mRNA expression of *IRX3* on d0, d3 and d14 in sc PACs in genotype groups TT, CC and CT **(C)** log10 of RQ mRNA expression of *IRX5* on d0, d3 and d14 in sc PACs in genotype groups TT, CC and CT **(D)** log10 of RQ mRNA expression of *ARID5B* on d0, d3 and d14 in om PACs in genotype groups TT, CC and CT **(E)** log10 of RQ mRNA expression of *IRX3* on d0, d3 and d14 in om PACs in genotype groups TT, CC and CT **(F)** log10 of RQ mRNA expression of *IRX5* on d0, d3 and d14 in om PACs in genotype groups TT, CC and CT.

In both depots *ARID5B* seemed to be downregulated in cachectic patients compared to non-cachectic controls. This effect was more pronounced in om PACs, where it was not only visible on d3 but already on d0. Patients with moderate cachexia revealed, in conjunction with *ARID5B* results, a significantly increased expression of *IRX3* and *IRX5* compared to the cancer control group in sc PACs. The *FTO* genotype was not shown to have an influence on gene expression. In addition to browning-associated markers, PACs' differentiation capacity was evaluated on the level of gene expression.

Differentiation of preadipocytes was investigated by measuring mRNA gene expression of *C/EBP*α. On d0, overall expression of *C/EBP*α was low as expected and increased until d3, a further increase until d14 was seen in the group of severe cachexia and cancer controls (Figure 18A). Analyzing the boxplot overview graphic, it was seen that, mainly on d0 and d14, single groups showed differing expression levels including high variation compared to the healthy controls with the strongest effect on d0 and d3 (Figure 18B). Therefore, a significantly higher *C/EBP*α expression was found among the group with moderate cachexia compared to both control groups on d0 (increase of 13.5 mean fold change compared to baseline) and, inversely, a significantly lower expression of the severe cachectic group and the cancer control group in relation to healthy controls on d3 (Figure 18C, D). On d14, no significant differences among the groups were found.

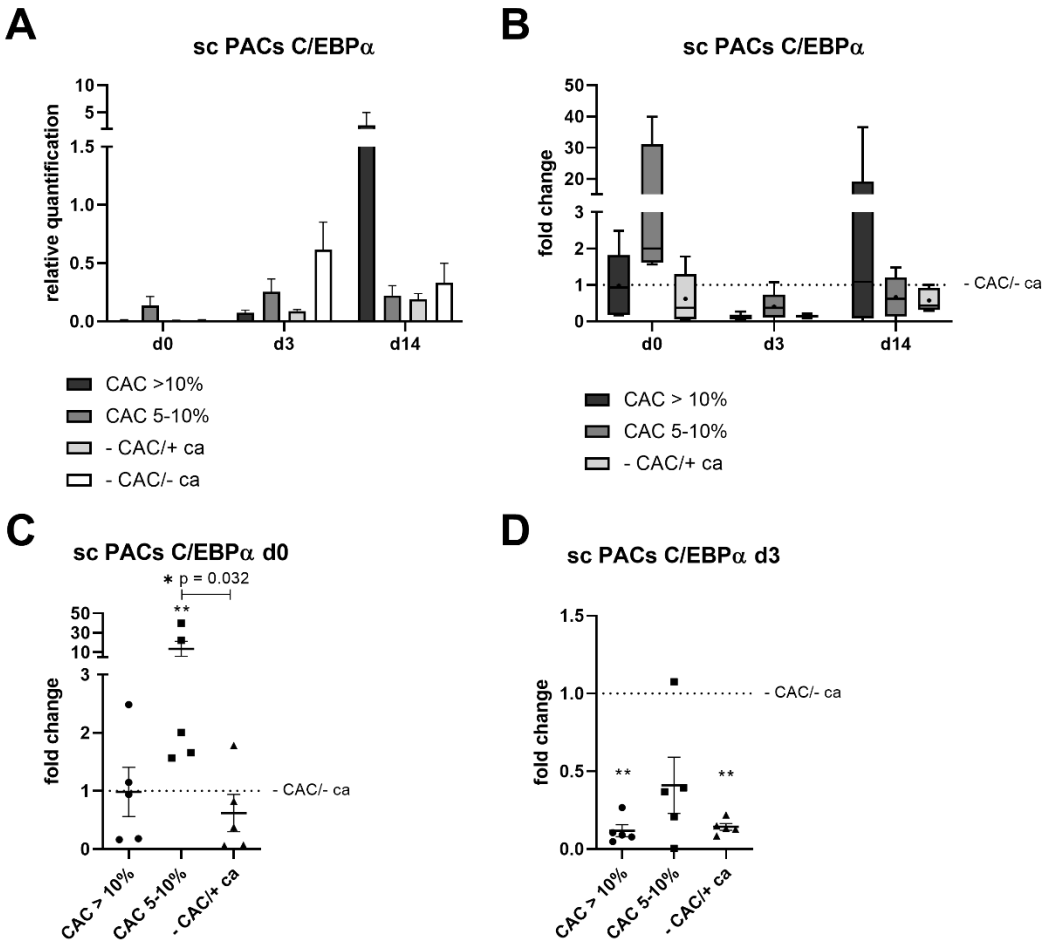

Figure 18: mRNA expression of the differentiation marker C/EBPα in sc PACs on harvesting day(d)0, d3 and d14 among the patient groups CAC > 10%, CAC 5-10%, -CAC/+ ca and -CAC/- ca.
Group size of n = 5. Data represent mean values ± SEM. **(A)** relative quantification of mRNA expression of *C/EBPα* on d0, d3 and d14 in all groups **(B)** fold change mRNA expression of *C/EBPα* on d0, d3 and d14 in all groups using -CAC/- ca as baseline **(C)** fold change mRNA expression of *C/EBPα* on d0 **(D)** fold change mRNA expression of *C/EBPα* on d3; Statistical significance is depicted as follows: * $p < 0.05$; ** $p < 0.01$

Fold change expression of the differentiation marker *C/EBPα* in om PACs over all three harvesting days is shown in Figure 19. Figure 19A demonstrates an increase in *C/EBPα* expression from d0 until d14. Regarding the cancer control group, *C/EBPα* expression reached its peak already on d3. On d0 as well as on d14, all three groups displayed a similar expression as the baseline, whereas on d3 a single individual revealed a 30.2-fold increase in expression compared to healthy controls. This extreme value couldn't be explained by any patient characteristics and resulted in a high SEM but did not lead to a statistical significance.

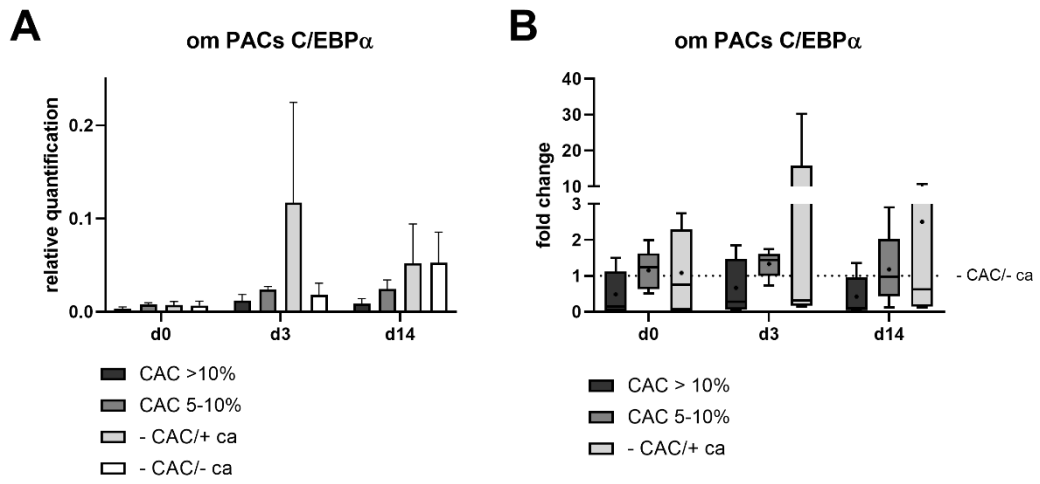

Figure 19: mRNA expression of the differentiation marker C/EBPα in om PACs on harvesting day(d)0, d3 and d14 among the patient groups CAC > 10%, CAC 5-10%, -CAC/+ ca and -CAC/- ca.
Group size of n = 5. Data represent mean values ± SEM. **(A)** relative quantification of mRNA expression of *C/EBPα* on d0, d3 and d14 in all groups **(B)** fold change mRNA expression of *C/EBPα* on d0, d3 and d14 in all groups using -CAC/- ca as baseline; Statistical significance is depicted as follows: * $p < 0.05$; ** $p < 0.01$

Since browning markers, as well as differentiation markers themselves, are known to vary in the level of expression during adipose differentiation, they were measured on all three harvesting days. This was not valid for the following markers, hence they were measured at d14 to gain highest possible expression rates.

The mRNA gene expression of the cachexia-related markers *MT-CO2*/*18S*, *ZAG* and *IL-6* at d14 in sc PACs is shown in Figure 20. *MT-CO2*/*18S* represents the quotient between *MT-CO2*, a gene involved in mitochondrial activity and *18S* ribosomal RNA which was used to calculate the relative number of mitochondria per sample. As seen in Figure 20A, interindividual differences were high and no significances between the groups or to baseline were available. Figure 20B shows a significantly lower expression of *ZAG* in cancer controls compared to the healthy control group, whereas mean fold change of cachectic patients nearly hit the baseline. Regarding *IL-6,* all groups revealed a decreased gene expression in comparison to the healthy controls, but differences were only significant among the group with moderate cachexia as well as the cancer control group (Figure 20C).

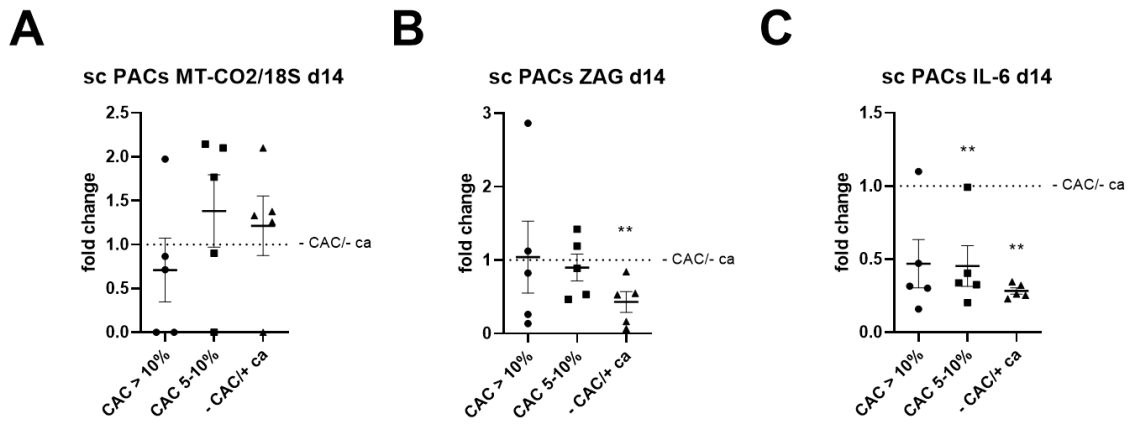

Figure 20: mRNA expression of a cachexia-related markers in sc PACs on harvesting day(d)0, d3 and d14 among the patient groups CAC > 10%, CAC 5-10%, -CAC/+ ca and -CAC/- ca.
Group size of n = 5. Data represent mean values ± SEM. **(A)** fold change mRNA expression of *MT-CO2/18S* on d14 in all groups using -CAC/- ca as baseline **(B)** fold change mRNA expression of *ZAG* on d14 in all groups using -CAC/- ca as baseline **(C)** fold change mRNA expression of *IL-6* on d14 in all groups using -CAC/- ca as baseline; Statistical significance is depicted as follows: * $p < 0.05$; ** $p < 0.01$

In om PACs, the quotient of *MT-CO2/18S* as indicator of mitochondria revealed no significant differences between the groups or compared to the baseline situation, although single individuals in the group with severe cachexia as well as in the cancer control group showed a strongly increased expression compared to baseline (Figure 21A). Regarding *ZAG* and *IL-6,* no significant differences were found among the groups or compared to baseline as represented by healthy controls (Figure 21B, C).

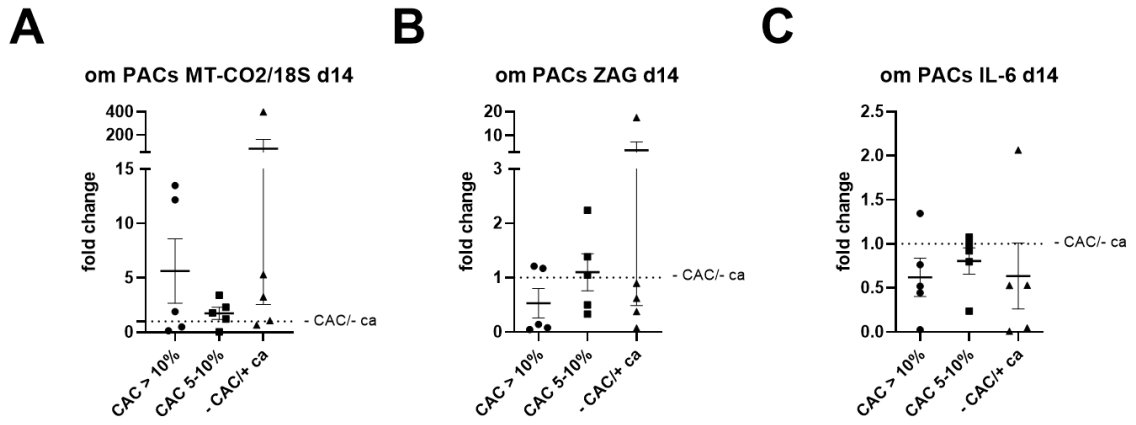

Figure 21: mRNA expression of a cachexia-related markers in om PACs on harvesting day(d)0, d3 and d14 among the patient groups CAC > 10%, CAC 5-10%, -CAC/+ ca and -CAC/- ca.
Group size of n = 5. Data represent mean values ± SEM. **(A)** fold change mRNA expression of *MT-CO2/18S* on d14 in all groups using -CAC/- ca as baseline **(B)** fold change mRNA expression of *ZAG* on d14 in all groups using -CAC/- ca as baseline **(C)** fold change mRNA expression of *IL-6* on d14 in all groups using -CAC/- ca as baseline; Statistical significance is depicted as follows: * $p < 0.05$; ** $p < 0.01$

Taken together, mRNA expression analysis of sc and om PACs revealed some differences regarding browning, differentiation and cachexia. *UCP1* expression was low in both depots over the whole period of differentiation, whereas *PRDM16* seemed to be elevated in sc PACs of cancer patients. The *FTO* genotype did not have an influence on the expression of these markers. *ARID5B* was found to be moderately downregulated under cachexia, whereas the expression of *IRX3* and *IRX5* was promoted in sc PACs from patients with moderate cachexia. In sc PACs, the expression of *C/EBP*α was decreased in cancer patients, an effect which could not be confirmed in om PACs. Analyses of cachexia-related markers was inconsistent due to high scattering of individual samples, but *ZAG* as well as *IL-6* seemed to be slightly downregulated compared to healthy controls.

To expand the analysis, gene expression of related tissues of the same 20 patients was performed. This setup included the investigation of liver, muscle as well as sc and om adipose tissue. All biopsies were taken during the initial surgery. In the following, heat maps containing all four patient groups are presented to get a tissue-overriding overview. Additionally, results are displayed as fold change expression compared to the healthy controls.

4.5.3 mRNA analysis of tissues

Gene expression data of the four tissues are displayed as $\log_{10}$ of RQ values and colored from low expression in green to high expression in red (Figure 22). Since the heat maps function as overview graphics, scatterplots showing fold change expression are only shown in case of possible significances (Figure 23 and Figure 24).

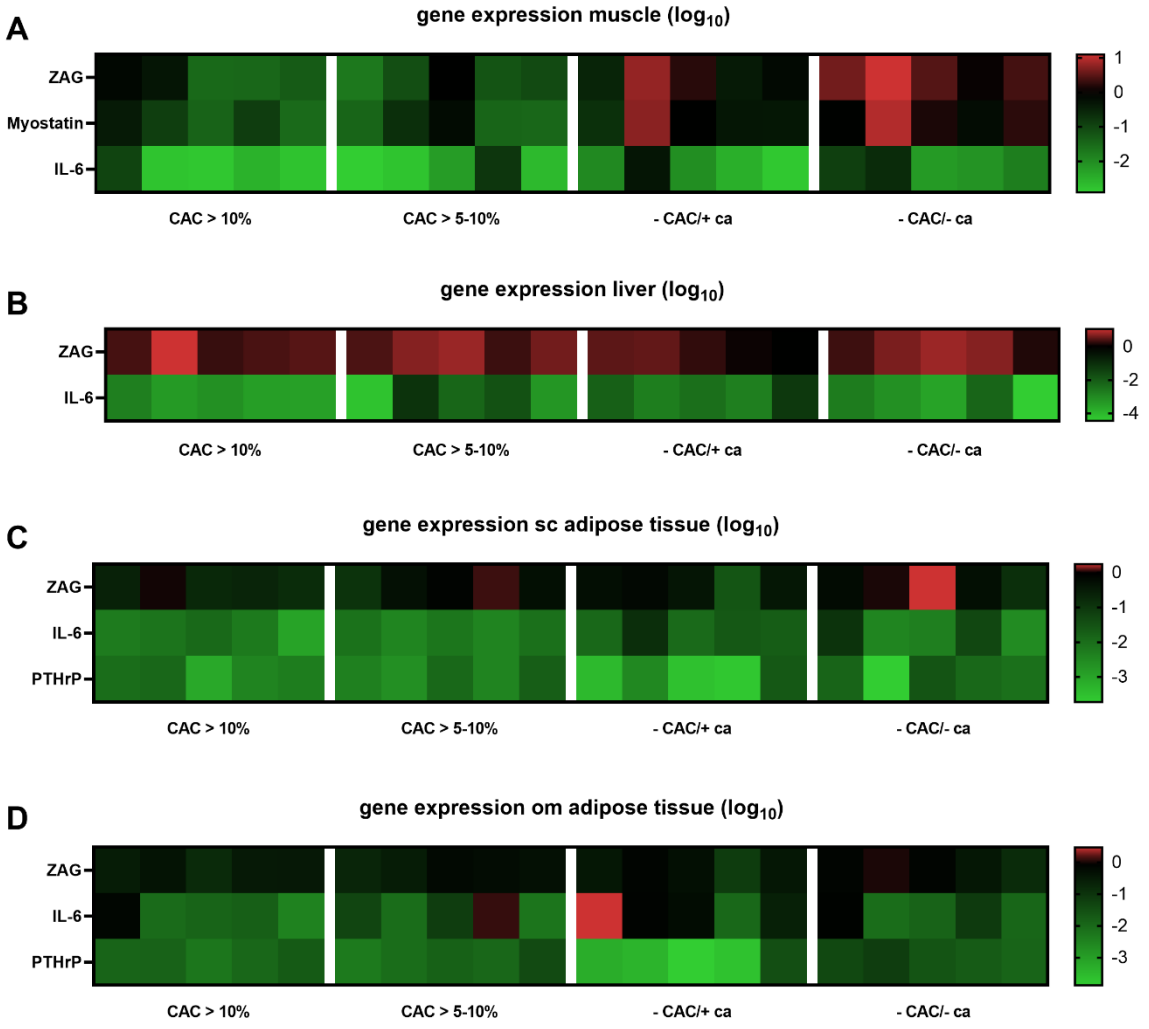

Figure 22: Overview of mRNA expression of cachexia-related markers in muscle, liver, sc and om adipose tissue.
Data is shown as log10 of RQ values and split according to the patient groups CAC > 10%, CAC 5-10%, -CAC/+ ca and -CAC/- ca. Low expression levels are depicted in green versus high expression levels in red. Group size of n = 5. **(A)** mRNA expression of *ZAG*, *myostatin* and *IL-6* in muscle tissue **(B)** mRNA expression of *ZAG* and *IL-6* in liver tissue **(C)** mRNA expression of *ZAG*, *IL-6* and *PTHrP* in sc adipose tissue **(D)** mRNA expression of *ZAG*, *IL-6* and *PTHrP* in om adipose tissue.

Figure 23 displays significant results regarding gene expression of muscle and liver tissue. In Figure 23A, *ZAG* is noticeably less expressed in muscle tissue of all cancer patients in comparison to the healthy controls without cancer, but due to an outlier among the cancer controls the effect was only significant regarding the two cachexia groups. Measurement of the muscle growth inhibitor *myostatin* revealed that cachectic patients show a significantly decreased gene expression compared to the healthy controls. Additionally, patients with severe cachexia had a significantly lower *myostatin* expression in comparison to the cancer control group, whose mean expression was again elevated by the same outlier already found among *ZAG* analysis. (Figure 23B) Regarding gene expression of *IL-6* no significant differences between the groups or compared to controls were found (data not shown). *ZAG*

fold change expression in liver tissue revealed that most of the patients were in the range of the control group, but nevertheless the cancer control group was found to express significantly less *ZAG* than healthy controls (Figure 23C). In Figure 23D it can be seen that patients with severe cachexia showed a significantly decreased *IL-6* gene expression in comparison to both control groups. Due to interindividual differences in *IL-6* expression, the same tendency was present between the two cachectic subgroups, but results were found not to be significant (Figure 23D).

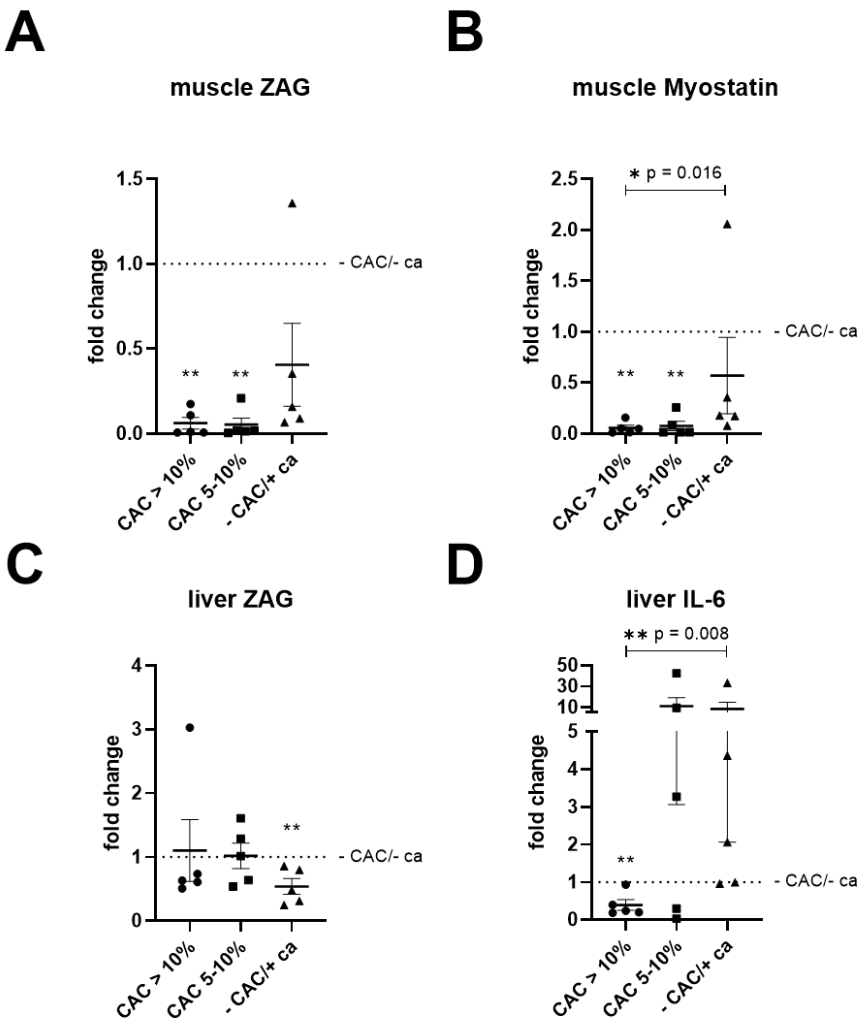

Figure 23: mRNA expression of cachexia-related markers in muscle and liver tissue dry frozen on the day of surgery among the patient groups CAC > 10%, CAC 5-10%, -CAC/+ ca and -CAC/- ca.
Group size of n = 5. Data represent mean values ± SEM. **(A)** fold change mRNA expression of *ZAG* in muscle tissue using -CAC/-ca as baseline **(B)** fold change mRNA expression of *myostatin* in muscle tissue using -CAC/-ca as baseline **(C)** fold change mRNA expression of *ZAG* in liver tissue using -CAC/-ca as baseline **(D)** fold change mRNA expression of *IL-6* in liver tissue using -CAC/-ca as baseline; Statistical significance is depicted as follows: * $p < 0.05$; ** $p < 0.01$

Additionally to gene expression results of muscle and liver tissue, the results regarding sc and om adipose tissue were more precisely examined in the following.

Figure 24 describes the results of gene expression analysis in sc as well as in om adipose tissue. Regarding the expression of *IL-6* in sc adipose tissue a clear distinction between the groups could be made: both cachectic groups, the moderate and severe manifestation of cachexia, showed significantly lower *IL-6* mRNA expression in comparison to both control groups (Figure 24A). Additionally, the expression of *ZAG* was significantly decreased among the cancer control group compared to the healthy control group in sc adipose tissue (Figure 24B). Relating to *PTHrP* in sc adipose tissue, no significant differences between the groups or in comparison to the healthy control group were found (data not shown). The analysis of gene expression in om adipose tissue revealed that patients with severe cachexia had a significantly lower *ZAG* as well as *PTHrP* expression in comparison to healthy controls (Figure 24C, D). Regarding *PTHrP*, this effect was also detected among the cancer control group (Figure 24D). The expression of *IL-6* in om adipose tissue did not differ between the groups or healthy controls, hence data were not shown.

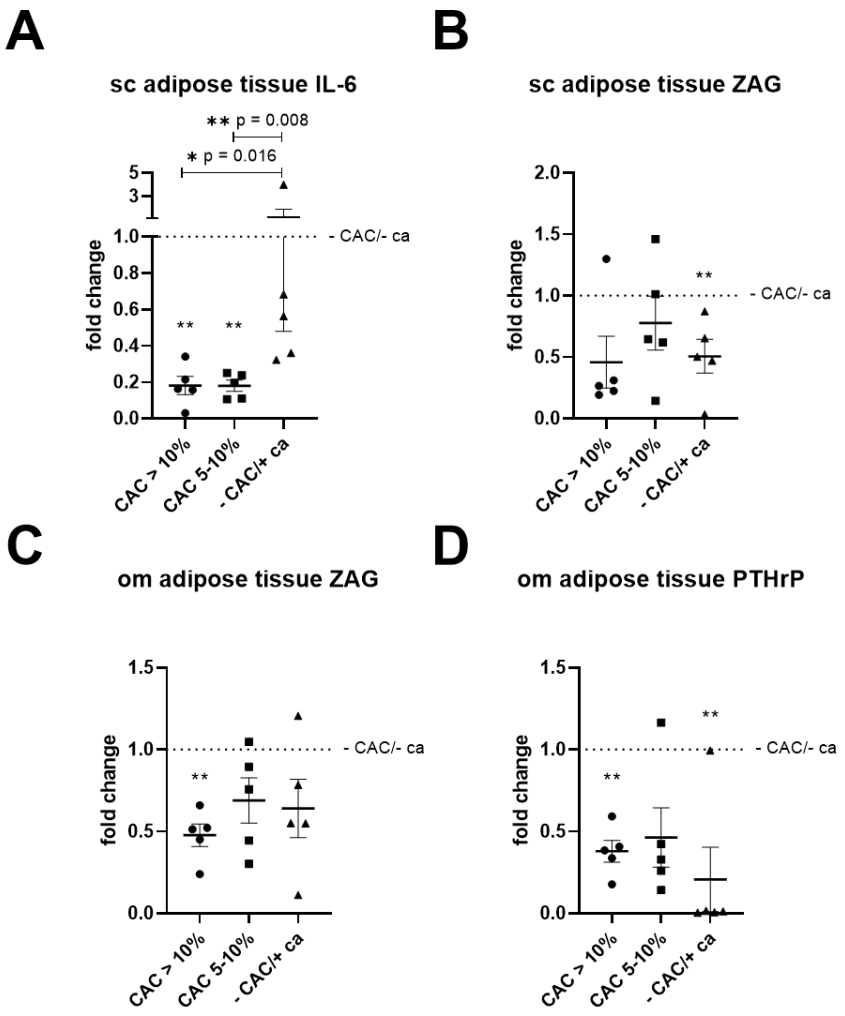

Figure 24: mRNA expression of cachexia-related markers in sc and om adipose tissue among the patient groups CAC > 10%, CAC 5-10%, -CAC/+ ca and -CAC/- ca.
Group size of n = 5. Data represent mean values ± SEM. **(A)** fold change mRNA expression of *IL-6* in sc adipose tissue using -CAC/-ca as baseline **(B)** fold change mRNA expression of *ZAG* in sc adipose tissue using -CAC/-ca as baseline **(C)** fold change mRNA expression of *ZAG* in om adipose tissue using -CAC/-ca as baseline **(D)** fold change mRNA expression of *PTHrP* in om adipose tissue using -CAC/-ca as baseline; Statistical significance is depicted as follows: * $p < 0.05$; ** $p < 0.01$

Summarizing the gene expression results of related tissues, *ZAG* and *myostatin* were down-regulated in all three cancer groups. Results were significant in both cachectic groups compared to the healthy control group. *ZAG* expression in liver was similar in all measured individuals, nevertheless the cancer control group showed significantly decreased values compared to the healthy controls. Due to large scattering of individuals, *IL-6* expression in liver only delivered significant results regarding the group with severe cachexia, where a down-regulation was found compared to both control groups. In sc adipose tissue both cachectic groups revealed a significant decrease in *IL-6* expression compared to the non-cachectic patients. *ZAG* and *PTHrP* expression tended to be reduced under cancer

conditions. Regarding *ZAG,* this effect applied for both depots, whereas *PTHrP* showed stronger results in om tissue.

To bring together the results of the cell culture differentiation experiments and the measurement of mRNAs in whole tissues, the markers *ZAG*, *IL-6* and *PTHrP* are shown in Figure 25. Each heat map represents gene expression of a single marker in all available tissue types or cell culture approaches among all 20 patients.

ZAG, which was not only measured on d14 in the cell culture differentiation experiment but also in all four related whole tissues, showed the highest rate of expression in liver tissue. The intensity of expression of *ZAG* in muscle tissue was similar to liver tissue, but was mainly observed in the two control groups. The lowest ZAG expression was found among PACs with decreased expression in om PACs compared to sc PACs (Figure 25A). Expression of *IL-6* was lowest in muscle and liver tissue, respectively, and by trend elevated in both cell types of the differentiation experiment including one outlier among the healthy control group of sc PACs (Figure 25B). Since *PTHrP* was merely measured in cell culture, Figure 25C shows a direct comparison between *PTHrP* expression in sc and om PACs. *PTHrP* expression was lowest in the cancer control group, whereas the healthy controls revealed higher amounts of *PTHrP* (Figure 25C).

All results shown in these heat maps are being completed by the already described analyses of Figure 20 to Figure 24.

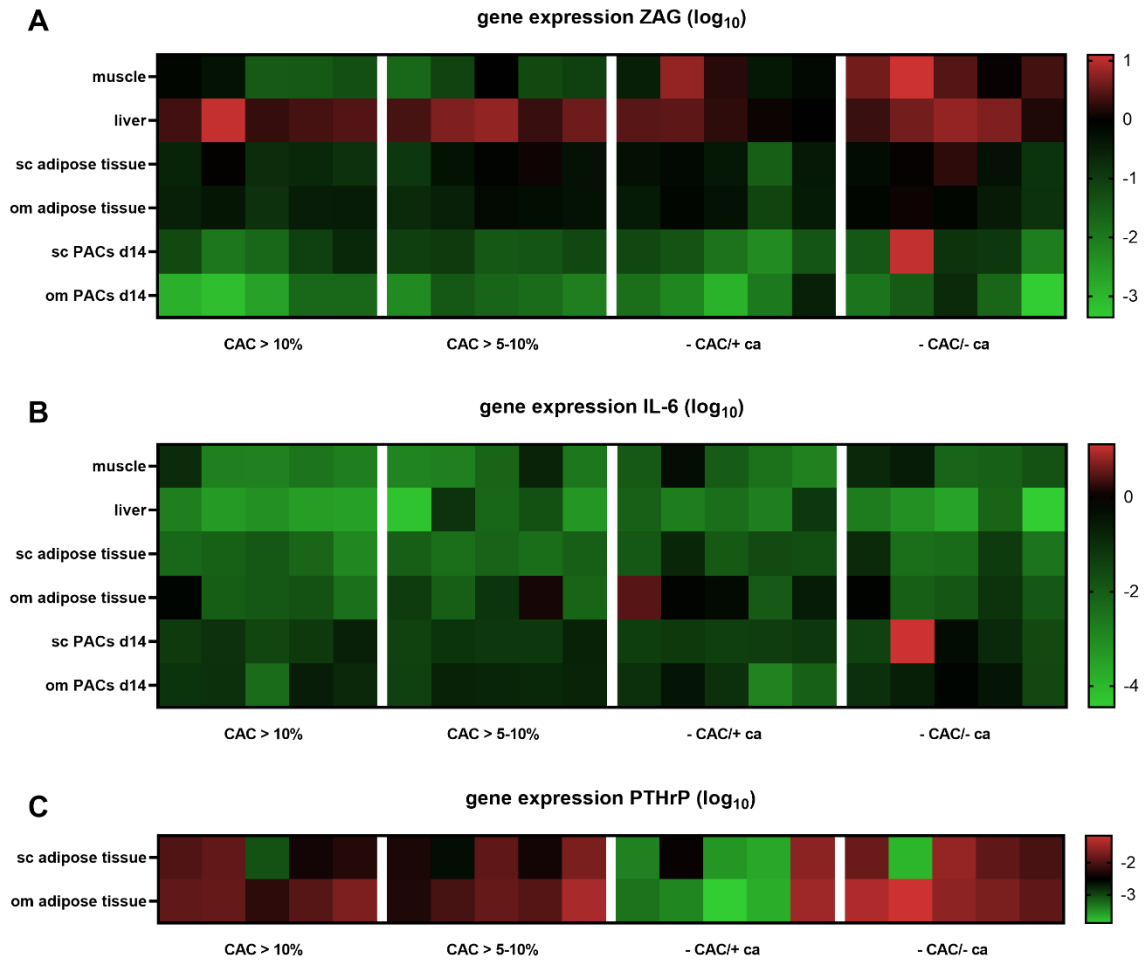

Figure 25: Overview of mRNA expression of *ZAG*, *IL-6* and *PTHrP* among different tissue types.
Data is shown as log10 of RQ values and split according to the patient groups CAC > 10%, CAC 5-10%, -CAC/+ ca and -CAC/- ca. Low expression levels are depicted in green versus high expression levels in red. Group size of n = 5. **(A)** mRNA expression of *ZAG* in muscle tissue, liver tissue, sc adipose tissue, om adipose tissue, sc PACs harvested on d14 and om PACs harvested on d14 **(B)** mRNA expression of *IL-6* in muscle tissue, liver tissue, sc adipose tissue, om adipose tissue, sc PACs harvested on d14 and om PACs harvested on d14 **(C)** mRNA expression of *PTHrP* in sc and om adipose tissue.

The results of this study were obtained from patients with not only malign, but also benign diseases of the gastrointestinal tract. The manifold collection of liver, muscle and adipose tissue as well as the isolation of PACs helped to provide a solid basis for gene expression analysis in the context of cachexia and sarcopenia. Additionally, the analysis of blood and the successful follow-up gave us the possibility to predict patients' survival across the whole cohort and PDAC in particular, which might be a promising tool in future clinical practice.

5 Discussion

5.1 Contribution of browning to cachexia

Browning of WAT in adult humans has widely positive connotations due to its association with increased energy expenditure which can lead to a metabolic improvement by ameliorating insulin sensitivity and supporting weight loss (Tamucci et al., 2017). But under a cachectic state, where loss of muscle and adipose tissue mass worsens the physical condition, browning and increased energy expenditure could play an essential role in cancer-associated cachexia as shown in multiple studies (Kir et al., 2014; Petruzzelli et al., 2014). *Petruzzelli et al.* revealed WAT browning in mice happening in early stages of cachexia and increasing energy expenditure by an IL-6-dependent upregulation of *UCP1* (Petruzzelli et al., 2014). This effect could not be confirmed by the experiments in human tissue described here, where *IL-6* as well as *UCP1* expression in sc PACs was lower in the groups of severe cachexia, moderate cachexia and the cancer control, respectively, compared to the healthy controls. To note, *UCP1* indeed generated significant group differences, but the initial expression level in both adipose tissue depots and at all three harvesting days of cultured preadipocytes was so low that the results lack any biological significance. This circumstance is not surprising, since the expression of *UCP1* in WAT (in contrast to BAT) is known for being close to or under the detection limit (Oliver et al., 2001). Additionally, the actual validity of the *UCP1* expression analysis was further decreased by single outliers, in both sc and om PACs (Figure 13; Figure 14).

To our knowledge, UCP1 expression measurements under cachexia were not performed in human adipocytes before. According to the results of this study, UCP1-mediated thermogenesis in WAT is not a driver of cancer cachexia in humans. In 2021, *Rupert et al.* showed that IL-6 is derived from tumor cells, since in an *in vivo* approach PDAC cells triggered *IL-6* expression in muscle cells and, thereby, induced adipose tissue lipolysis and wasting. The cell culture approach instead was dependent on the administration of soluble IL-6 to gain similar effects and could be a possible explanation for the absent browning effect in the here shown experiment (Rupert et al., 2021). Besides UCP1 and IL-6, ZAG has been characterized as a possible mediator of browning under cachexia. Previous research revealed that ZAG, mainly expressed in heart, kidney, liver and BAT, stimulates the expression of *PPARγ*, early B cell factor 2 and is the promoter of *PRDM16* (leading to increased expression of *PRDM16* itself) which causes browning as well as energy wasting in mice (Elattar et al., 2018). In the here shown approach, *ZAG* expression was measured in sc and om adipose tissue, sc and om PACs, as well as in muscle and liver tissue. Findings in adipose tissue (Figure 24) were not conclusive due to high interindividual variance, but there was a trend towards higher *ZAG*

expression in healthy individuals compared to the other groups (Figure 24), an effect which was to a similar extent found in muscle tissue, where both cachectic groups revealed a significantly lower *ZAG* expression than the healthy control group (Figure 23). Supported by literature, the overall expression of *ZAG* was highest in liver tissue (Figure 23) (Elattar et al., 2018). Murine knock-out studies suggest an involvement of ZAG in UCP1-driven thermogenesis (through activation) on the basis of gene expression measurements in the gastrocnemius muscle (Fan et al., 2021). In the here shown approach, both cachectic groups had significantly lower *ZAG* expression in muscle than the healthy control group (Figure 23). Consequently, the findings of this thesis did not support the theory of ZAG activating thermogenesis in cachectic muscle. Hypothesizing the strong disturbance of muscular metabolism due to muscle wasting under a cachectic state might disrupt features usually shown by tissues of healthy subjects. In the here shown approach, *ZAG* expression was lower in PACs compared to whole adipose tissue (Figure 25). Therefore, an external factor (possibly liver-driven) was hypothesized to stimulate *ZAG* expression in WAT. This interaction got lost under cell culture conditions and, hence, failed to activate *UCP1* expression in PACs. Cell culture experiments with stimulation of PACs by ZAG should, therefore, be carried out to elucidate the role of ZAG in PAC browning and thermogenesis. In contrast, *PRDM16* expression in sc PACs of patients with moderate cachexia was significantly increased compared to healthy controls (Figure 13). This supports research indicating PRDM16 functioning as a transcriptional driver of brown fat determination not only in BAT but also in WAT (Seale et al., 2007).

Not only alterations in gene expression, also possible genotypic effects of the *FTO* gene were investigated in the context of browning. Several risk alleles connected to obesity have been discovered so far, for example rs9939609 as well as rs1421085 (Claussnitzer et al., 2015; Karra et al., 2013). The fact that the manifestation of the *FTO* risk allele rs1421085 verifiably leads to increased obesity through its linkage to thermogenesis in humans brings up the question whether the risk genotype CC may protect from cachexia by preventing adipose tissue loss through the downregulation of browning (Claussnitzer et al., 2015). Independent of the risk allele genotype and concentrating on the differentiation experiment's initial groups, the results of this thesis indicate an influence of cachexia and/or the presence of a tumor to the overall expression of genes influenced by *FTO*. In om PACs both cachectic groups showed a strongly decreased expression of *ARID5B* compared to healthy controls on d0 and d3 (significance available in most combinations; Figure 16) whereas in sc PACs this effect was delayed and only visible on d3 (Figure 15). The cachectic phenotype seems *vice versa* not only to decrease *ARID5B* but to promote the expression of *IRX3* and *IRX5* since in sc PACs patients with moderate cachexia show a significantly higher *IRX3* expression compared to both

control groups on d0 and regarding *IRX5* to the cancer control group without cachexia on d0 (Figure 15). Tendencies in om PACs were similar with an elevated expression of *IRX5* in patients with moderate cachexia compared to healthy controls, but results were found not to be significant (data not shown). Interestingly, sc PACs of patients with severe cachexia express significantly less *IRX5* on d3 compared to healthy controls which can possibly be referred to the effects of *FTO* on cell fate and the beige lineage only occurring in the very early phase of differentiation (Claussnitzer et al., 2015). Additionally, gene expression data was analyzed by means of the three rs1421085 genotypes TT, CC and CT. Relating to the pathway already elucidated by *Claussnitzer* and coworkers, CC patients were expected to show a decreased expression of *ARID5B* and an increased expression of *IRX3* and *IRX5* but both could not be confirmed in our study (Claussnitzer et al., 2015). In none of the two depots and none of the three markers, the genotypes revealed significant results compared to one another (Figure 17).

In the data of this thesis, the hypothesis that CC risk allele carriers are potentially protected from cachexia could not be confirmed. However, *FTO* might nevertheless be a promising target. Research revealed that certain risk alleles, such as rs9939609 and rs1477196, are strongly connected to certain cancer types like pancreatic and breast cancer, respectively, and might therefore give answers to the origin of cachexia (Kaklamani et al., 2011; Lin et al., 2013). Additionally, our research gave a hint about differences in *FTO*-related expression regarding the two depots, a distinction is therefore indispensable in future research.

Although classical browning markers were evaluated in this approach, the findings could not confirm a direct involvement of WAT browning in the process of cachexia formation. The inconsistent findings regarding marker expression were probably due to low n-numbers (5 individuals per group), a circumstance which gives outliers a stronger terminal effect, and the disease heterogeneity of the chosen patients since it's already known that gene expression incorporates a huge variability dependent on the tumor type (Kong et al., 2010). Furthermore, the process of browning is orchestrated by a large number of genes and only a few were analyzed so far. Varying experimental conditions as well as differing cell culture techniques and the long duration of differentiation experiments can cause discrepancies in gene signature. (Perdikari et al., 2018)

5.2 Lipolysis, lipogenesis and fatty acid storage under cachexia

Since loss of adipose tissue mass is, besides the loss of muscle mass, one of the key symptoms of cancer-associated cachexia, it seems obvious that either increased lipolysis or decreased *de novo* lipogenesis might be involved in the molecular process. Hence, several studies addressed the topic of enhanced lipolysis and found out that *ZAG* overexpression in

adipose tissue as well as external administration of ZAG leads to the activation of lipolysis in WAT of mice by activating β3-adrenergic receptors and HSL (Elattar et al., 2018; Hirai et al., 1998; Khan & Tisdale, 1999; Russell et al., 2002). In regards of lipolysis, IL-6 was shown to decrease LPL activity in mice which results in an impaired fatty acid uptake in murine WAT (Greenberg et al., 1992). Thereupon, the hypothesis was set that *ZAG* and *IL-6* expression in WAT is increased in cachectic patients which would consequently drive lipolysis and reduce internal fatty acid uptake, respectively. Across tissue types, *ZAG* expression in cachectic patients (moderate and severe cachexia) was not increased compared to both control groups which was in part, at least in sc and om PACs and adipose tissues, due to high interindividual differences (Figure 20; Figure 21; Figure 23; Figure 24). Obese patients are known to express less *ZAG* in sc and vc WAT compared to their lean counterparts (Mracek et al., 2010; Selva et al., 2009). Only five out of 20 patients had a BMI over 30 kg/m^2 in the approach of this study. Although they were evenly distributed among the patient groups, a BMI effect on *ZAG* cannot be excluded. Leaving cachexia aside, patients with cancer but without cachexia revealed significantly less *ZAG* expression in liver than healthy subjects (Figure 23). The fact that liver tissue from cancer patients shows less *ZAG* expression than healthy liver tissue of the same subjects as published by *Huang et al.* in 2012, combined with the results of our study, clearly points out the strong influence of a tumor on the expression of *ZAG* (Y. Huang et al., 2012). Summarizing, ZAG regulated lipolytic pathways in humans seem to be influenced by the individual tumor environment rather than by cachexia.

Regarding IL-6, external administration in cell culture was shown to activate the STAT3 pathway and to induce lipolysis in murine 3T3 cells as well as to stimulate lipolysis through the reduction of triglyceride synthesis in human breast adipocytes (Hu et al., 2019; Päth et al., 2001). In humans, circulating levels of IL-6 were demonstrated to correlate with lipolysis in adipose tissue, but the *IL-6* expression patterns in WAT did not differ between cachectic and weight-stable patients (Rydén et al., 2008). In the here shown cell culture approach, sc PACs of all groups with cancer revealed decreased expression of *IL-6* compared to healthy controls (Figure 20) and similar results were found among sc adipose tissue (Figure 24). This finding suggests that IL-6, which in several murine and human studies caused lipolysis in WAT, is not deriving from WAT itself, but from other peripheral organs or from the tumor. Besides the involvement in lipolysis, IL-6 was demonstrated to decrease LPL in murine 3T3 cells which in turn leads to a restricted fatty acid uptake in WAT which could be a contributor to cachexia (Greenberg et al., 1992). For that reason, the future measurement of lipogenesis- and also lipolysis-related enzymes in our biobank material such as LPL, adipose triglyceride lipase, HSL and monoglycerol lipase, respectively, could be a promising tool to further investigate adipose tissue function under cachexia.

5.3 Myostatin, a possible biomarker for cachexia or sarcopenia?

Since myostatin involvement in the regulation of muscle tissue mass is well-established, its inhibiting properties have been investigated to elucidate a possible role in muscle tissue atrophy under cachexia and sarcopenia. Common opinion is that myostatin induces cachexia and muscle atrophy by regulating *FoxO* transcription factors leading to enhanced activity of UPS which causes degradation of muscular proteins (McFarlane et al., 2006; Sakuma et al., 2017). Surprisingly, the results of this thesis are contradictory: *Myostatin* expression in *musculus rectus abdominis* of patients with severe and also moderate cachexia was significantly decreased compared to the healthy control group (Figure 23). Similar results were generated by *Bonetto et al.* in 2013 in a human cohort of gastric cancer, where patients with the disease and an average weight loss of 5.3 % revealed significantly less *myostatin* expression in the abdominal muscle compared to the control group. This effect was explained by posttranscriptional mechanisms meaning that, although *myostatin* expression in cachectic muscle might not be increased as expected, downstream protein synthesis could still be induced and degradation of the protein myostatin reduced, respectively (Bonetto et al., 2013). Discrepancies between *myostatin* mRNA and protein levels were indeed reported earlier. *In vivo* experiments in rats showed that fasting during existing sepsis leads to reduced *myostatin* mRNA expression, whereas protein levels remain unchanged in comparison to a control group (Smith et al., 2010). Other studies suggest that myostatin is auto-regulating its own expression via a negative feedback loop where, at least in cattle, the exogenous myostatin protein binds to its receptor ActRIIB and, thereby, represses *myostatin* promoter activity leading to a downregulation of corresponding endogenous mRNA (Forbes et al., 2006). An alternative negative feedback mechanism was detected by *McFarlane* and coworkers revealing myostatin, via Smad3 signaling, is regulating miR-27a/b, an miRNA which owns the capability to decrease *myostatin* expression in mice (McFarlane et al., 2014). In the context of sarcopenia in elderly, myostatin was shown to be increased in older males compared to younger individuals, whereas studies in mice could not demonstrate an age-related effect on sarcopenia development (Léger et al., 2008; Morissette et al., 2009). An age-related effect influencing the here shown gene expression measurements can be excluded since all gene expression values were adjusted for BMI as well as age. In summary, research on this topic shows a lot of inconsistency when it comes to study design: results and hypotheses strongly vary according to the *in vivo* animal model or the underlying cancer type in human *in vitro* biopsies. This reflects the limitations of our study, since the cohort was heterogeneous by cancer type and tumor staging as well as grading. All these factors can possibly influence *myostatin* expression in muscle tissue and, therefore, need further investigation in larger studies.

5.4 IL-6 as key player in inflammation and overall survival

In our expanded cancer cohort of 189 individuals IL-6 was measured in plasma samples that were drawn during anesthesia but before the surgical intervention. The data obtained were analyzed intra as well as inter group-wise and the focus was laid on cytokine correlation to body composition data additionally collected, hematological parameters as well as survival data. The highest IL-6 levels were found in the patients with CRC and periampullary cancer with mean values of 33.5 pg/ml and 37.2 pg/ml, respectively (Table 26; Figure 8). Outliers were found in these two groups, resulting not only in high mean values, but also increased SD. In case of exclusion of extreme outliers, mean group levels of IL-6 were similar among the PDAC, CRC, periampullary cancer and control benign pancreatic disease group (data not shown). The upper GI tumor group as well as the control group containing non-inflammatory diseases revealed lower IL-6 levels, but none of the mentioned group differences were found to be significant which can possibly be traced to high SD. Patients with PDAC and patients with benign pancreatic diseases had similar IL-6 plasma levels (14.8 pg/ml vs. 14.2 pg/ml) and hence supported the theory of PDAC and certain kinds of pancreatitis being difficult to distinguish just by clinical parameters due to a similar inflammatory background and sharing the extent of manifestation of certain blood markers (Elsherif et al., 2020).

Regarding body composition data, no significant correlation was found. BMI before surgery showed a tendency towards a negative correlation with IL-6 levels ($r = -0.140$, $p = 0.054$), whereas weight loss (6 months before surgery to the day of surgery) evinced a tendency towards a positive correlation ($r = 0.139$, $p = 0.076$) (Table 28). This correlation between IL-6 plasma levels and initial weight loss is coherent with the literature showing that IL-6 is a mediator of weight loss, not only in murine cancer models, but also under rheumatoid arthritis in humans (Chen et al., 2016; Tournadre et al., 2017). Although IL-6 levels were positively correlated with BMI in PDAC patients, the results of this thesis are contradictory (Babic et al., 2018). The tendency of a negative correlation between IL-6 and BMI on the day of surgery points to a protective function of body weight and BMI against inflammation under cachexia, at least to a certain extent. In the context of hematological parameters IL-6 plasma levels *inter alia* positively correlated with the inflammation marker CRP and the tumor progression marker CA19-9. A negative correlation was detected towards albumin and oxygen transport indicators such as hemoglobin and iron (Table 29). Since CRP and albumin are the two elements of the GPS it is not surprising that studies were conducted trying to link inflammation markers such as IL-6 to this cachexia staging. Investigation of GPS itself is inconsistent. Depending on the cohort, the score was associated with soluble IL-6 levels in CRC patients or failed to (R. Sharma et al., 2008; Yu et al., 2021). CRP as a separate inflammation marker was identified as a possible mediator of the IL-6 triggered JAK/STAT pathway and was shown to

link IL-6 to the acute-phase response (K. C. Fearon et al., 1991; Socha et al., 2021). These assumptions were confirmed by the results of this study. The Kaplan-Meier curves were generated to stratify patients into “IL-6 high” vs. “IL-6 low” to predict survival. For the whole cohort and for the separated PDAC subgroup a cut-off of 0.09 pg/ml was calculated. Results revealed that IL-6 was negatively correlated with survival and, therefore, was identified as a strong prognostic factor (Figure 9). The prognostic effect regarding mortality was even stronger within the PDAC group (Figure 10), which is in agreement with similar results additionally linked to CA19-9 published earlier (Babic et al., 2018; Bellone et al., 2006; Schultz et al., 2013). The negative correlation between soluble IL-6 and survival was additionally demonstrated in cohorts with CRC patients only (Chung & Chang, 2003). In 2021, *Rupert et al.* published a theory about the role of IL-6 in the crosstalk of tumor, adipose and muscle tissue in PDAC-associated cachexia. According to their research IL-6 secreted from the tumor leads not only to increased expression of IL-6 itself and stimulates lipolysis in adipose tissue. It also enhances expression of the surface-bound *IL-6R* as well as the soluble receptor for *sIL-6R* in muscle. This leads to an inter-tissue crosstalk resulting in wasting of both adipose and muscle tissue (Rupert et al., 2021). Although this hypothesis could not be confirmed by the here shown *IL-6* gene expression results, the determination of expression of *sIL-6R* in muscle as well as its presence in blood may be a promising concept for future research not only in PDAC, but also for other gastrointestinal tumor types.

Since most human studies investigating the role of IL-6 in cancer and cachexia are based on small cohorts with a single tumor entity and a single evaluation technique (such as plasma IL-6 or gene expression patterns), their explanatory power is limited and the results of these studies little coherent. However, our cohort and experimental setup raises the possibility to look at *IL-6* on a systemic level and across organs. The data clearly suggests that IL-6 is indeed a prognostic factor regarding survival in patients with gastrointestinal tumor diseases, especially for PDAC, but requires the additional measurement of hematological parameters such as CRP, albumin and CA19-9 to permit conclusions regarding the cachectic and sarcopenic status as well as the patient’s overall health condition.

5.5 Integrity of fat cells under cachexia: differentiation capacity

The enzyme GPDH catalyzes the conversion of dihydroxyacetone phosphate into glycerol-3-phosphate which supports the formation of TGs. For this reason, the measurement of GPDH activity in cell culture has been considered as a marker of adipogenic differentiation for many decades (Hauner et al., 1989; Sato et al., 2020). Although, to our knowledge, studies investigating GPDH activity under cachexia and sarcopenia are not available, one might set up the hypothesis of GPDH being less active in cachectic patients, causing a lack of lipid

accumulation and impaired differentiation from PACs to adipocytes which could possibly contribute to a reduction of WAT in general. Less GPDH activity in mature adipocytes could, furthermore, be a hint towards an impaired activity to store FFAs. In the experimental setup of this thesis, GPDH activity was shown to increase during differentiation with the highest levels on d14. Surprisingly, preadipocytes of cachectic patients (weight loss of 5-10 % or over 10 %) revealed an overall higher GPDH activity compared to the ones from non-cachectic patients, statistically significant on d0 and also d14 (Figure 11; Figure 12A). The results on d0 are little biologically relevant, since GPDH is known to be a late marker for adipogenic differentiation. Although results were not significant, GPDH activity in cells from cancer patients was increased throughout the whole differentiation process. A cancer effect on GPDH was already detected in the liver of rats, where GPDH increased in rats with hepatic carcinomas compared to the control group (Lorenzetti et al., 2020). Human studies in this context are rare, but publications of the 1980s revealed a tumor effect on the activity of GPDH, not only depending on the tumor type, but also on its staging and grading which possibly influenced the results of this thesis as well (Kudriavtsev, 1980; Meyer et al., 1983; Mitchell et al., 1989). Since GPDH is associated with TG formation rather than WAT atrophy characteristic for cachexia, the underlying mechanisms should be urgently elucidated for a better understanding and the expression levels of GPDH should be more deeply investigated besides the role of this enzyme in WAT development.

Gene expression measurements of the differentiation marker C/EBPα led to the assumption that sc PACs, obtained from a tumor-affected donor, show lower *C/EBPα* expression (Figure 18). These results match published reports. In both murine and human studies, *C/EBPα* was shown to be decreased by a cachexia-inducing tumor, accompanied by a reduction of *C/EBPβ*, *PPARγ* and *SREB-1c* (on mRNA and protein levels) which leads to a disturbance of the differentiation process in human preadipocytes (C. Bing et al., 2006; D. Sun et al., 2021). On d0 (Figure 18), the large scattering of individual values resulted in a significant upregulation of *C/EBPα* in the group of moderate cachexia compared to baseline and the cancer control group, but this effect was interpreted not to have any biological relevance, since C/EBPα is not known to be one of the very first drivers of differentiation such as C/EBPβ (Tang & Lane, 2012). Regarding om PACs, no significant differences in *C/EBPα* expression were found between groups, independent of the harvesting day (Figure 19). The inter-depot differences in our study are not surprising, since *C/EBPα* expression as well as its protein levels were found to vary even intra-depot wise, with significant differences between retroperitoneal, epididymal and mesenteric WAT (all parts of vc adipose tissue). This shows that the resistance towards any kind of fat-reducing effect is indeed dependent on the location of adipose tissue and should be taken into account (Batista et al., 2012).

To receive robust and reliable results in the differentiation experiment of this study, the media used were modified. The used induction as well as differentiation medium contained additional fatty acids to further stimulate adipogenesis which, as seen in pre-experiments and also confirmed by literature findings, can be a challenge, especially in vc PACs (Grandl et al., 2016). Based on literature research, it was decided to use oleic and linoleic acid in a final concentration of 100 µM. Oleic acid, a mono-unsaturated n-9 fatty acid, and linoleic acid, a poly-unsaturated n-6 fatty acid, are both prominent components of the human diet and serve as energy sources. They can be esterified into phospholipids, cholesterol esters as well as triacylglycerols, as which they become part of the adipogenic metabolism (Fayezi et al., 2018; Whelan & Fritsche, 2013). Multiple studies dealt with possible implications of these two fatty acids on adipogenic cells in culture. They were identified to increase differentiation and lipogenesis not only in murine and bovine cells, but also in stromal-vascular cells of chicken by, amongst others, the stimulation of glucose uptake or the enhanced expression of *PPAR*γ and *GLUT4* (Kokta et al., 2008; Regassa et al., 2017; Tsuchiya et al., 2014; Yanting et al., 2018). Leading over to GPDH, a cell culture study in chicken showed an activity enhancement through the combination of oleic and linoleic acid with FBS in differentiation medium, respectively, which can obviously have an effect on measurements of enzymatic activities (Regassa et al., 2017). In summary, the usage of oleic and linoleic acid in human preadipocyte cell cultures seems to be a promising approach to maximize the differentiation capacity of sc, but in particular also of vc cells.

5.6 General limitations of the study

Although human biobanks are essential to address central issues of medical research and to either confirm or disprove hypotheses originating from animal experiments they nevertheless come along with a variety of limitations, for instance the cohort itself, the sampling procedure or the cell culture setting. The framework conditions of every human study are set by the composition of the patient cohort. A very heterogeneous cohort can either be an advantage, looking at the broad possible spectrum of individual cases, or a disadvantage due to indispensable subgrouping which may be necessary, but at the same time strongly decreases statistical power. Our cachexia cohort consisted of 114 individuals, whereas the expanded cancer cohort included 189 patients. All participants shared the fact of suffering either from a malign or a benign disease of the gastrointestinal tract, nevertheless, tumor types as well as staging and grading varied strongly. In view of different cancerous diseases the presence of muscle and adipose tissue loss is not equally distributed under cachexia (and/or sarcopenia), but appears mainly in pancreatic and liver cancer, whereas the prevalence of cachexia is rather low in prostate and skin cancer (Anker et al., 2019). Additionally, different cancer types were shown not only to trigger a particular amount of weight loss, but also to promote a distinct gene

expression profile of cachexia-inducing factors (Freire et al., 2020). This knowledge may lead to an indirect shaping of the cohort by favoring special types of cancer for biopsy taking. Most publications, for the purpose of defining cachexia, concentrate on a cut-off of 5 % weight loss in a certain time frame and combine it with BMI and SMAI data as suggested by the International Consensus paper of 2011 (K. Fearon et al., 2011). Nevertheless, next to the most important factor of benign or malign diseases of the gastrointestinal tract, it was in this case decided to concentrate on a single cachexia-related factor meaning weight loss of at least 10 % in the last six months before surgery. In our opinion, the 10 % mark ensures to highlight severe cases of cachexia and guaranties an easy embedding of the assessment into the daily clinical routine of hospitals. Milder cases of cachexia (between 5 to 10 % weight loss) were only evaluated for gene expression analyses and termed “moderate cachexia”. As seen in most cohorts, the prevalence of healthy control patients is low, since biopsies, especially from muscle, liver and vc adipose tissue, are almost impossible to get without an open surgery. Hence, included healthy individuals also suffered from chronic diseases of the gastrointestinal tract. Patients with hernias were included as well and served as optimal controls, since they were overall healthy and did not suffer from any kind of inflammatory or chronic diseases.

Although the sampling procedure was standardized as good as possible, certain aspects may have limited the outcome or affected especially the molecular biological results. For plausible reasons an impending surgery causes psychological stress for the patient which can alter the immune response on the level of interaction between T- and B-cells (Linn et al., 1988). But not only mental stress before surgery, general as well as regional anesthesia during surgery influences the immune response and can cause excessive release of inflammatory cytokines such as TNFα, IL-6 and IL-1β (Duggan et al., 2017; Rossaint & Zarbock, 2019). Additionally, to the indispensable use of anesthetic agents, dexamethasone was administered to some patients while being asleep to prevent or at least reduce postoperative nausea and vomiting, which possibly distorts blood glucose levels (“Dexamethasone Versus Standard Treatment for Postoperative Nausea and Vomiting in Gastrointestinal Surgery: Randomised Controlled Trial (DREAMS Trial),” 2017; Polderman et al., 2018). A measurable increase of IL-6 and CRP may furthermore occur as consequence of the surgical injury from the time point of first surgical incision (Watt et al., 2015). In our cohort, blood samples were mainly drawn before the surgical intervention, but in exceptional cases this procedure could not be maintained which could have influenced biomarker measurement as well as the general fact that biopsies could not be taken during the identical time point of the intervention due to diverse surgical procedures. Furthermore, the exact location of the different biopsies within one and the same organ/tissue varied according to the accessibility during the surgical process and no distinction between the regions of superficial and deep sc adipose tissue could be made, which are known to be

functionally relevant and to have a differing impact on metabolic diseases such as obesity (M.-J. Lee et al., 2013).

The experimental *in vitro* cell culture approach is to some extent a limiting factor of this thesis. Preadipocytes grew in a two-dimensional monolayer and the missing crosstalk to surrounding tissues could only partially mimic *in vivo* conditions (Li & Cui, 2014). Nevertheless, state of the art media containing not only appropriate amounts of glucose and growth factors, but also additional FFAs during induction and differentiation were used to provide defined physiological conditions. Additionally, due to the elaborate and time-consuming experimental setup, donor numbers of the cell culture part were small (20 patients, 5 per group) which led to limited statistical power. In summary, although several limitations were obvious, the defined and standardized setup of this thesis was suitable to investigate cachexia and sarcopenia in the context of gastrointestinal tumors and tumor-induced cachexia. Furthermore, this approach was unique, as various organs including functional tissue could be investigated simultaneously.

6 Conclusion

The molecular biological investigation of this human cohort consisting of sc and om adipose tissue, liver tissue, muscle tissue, blood and a diverse spectrum of corresponding clinical data revealed multiple findings in the context of cachexia and sarcopenia. Related to WAT browning *PRDM16* was shown to be a driver of cachexia in sc PACs which required no external stimulation through other tissues, although no activation of *UCP1* on the level of gene expression was detectable. The uncoupling-protein as well as *IL-6* and *ZAG* were not elevated in cachectic patients compared to controls, possibly due to missing liver stimulation in the cell culture setup. No connection could be found between the expression levels of *FTO*-related genes and the genotypes of rs1421085, but cachexia seemed to decrease *ARID5B* and to increase *IRX3* and *IRX5* in the early phase of adipocyte differentiation. In this approach, a direct involvement of browning in cachexia could not be found, but larger numbers and more detailed methods are needed to further characterize the potential role of thermogenesis due to WAT browning.

Although literature suggests stimulated lipolysis as well as impaired *de novo* lipogenesis as likely causes of WAT wasting under cachexia, direct evidence could not be found for this thesis. The expression of *ZAG* was decreased in muscle of all cancer patients pointing to a possible tumor involvement and IL-6 was hypothesized to not originate from WAT, even if it is an effective driver of lipolysis.

The differentiation capacity of preadipocytes was significantly modified by the cachectic state. The expression of *C/EBP*α was shown to be decreased in cancer and cancer-associated cachexia in sc PACs during the early onset of differentiation. Surprisingly, in this cell culture approach the enzymatic activity of GPDH was elevated in cachectic patients compared to non-cachectic controls which can possibly be explained by GPDH being affected by the tumor.

Since myostatin is a muscle inhibitor it is assumed that an overexpression contributes to muscle wasting in sarcopenia and cachexia, but the results of this thesis delivered quite the contrary: *myostatin* expression in muscle tissue of cachectic patients was decreased compared to controls which can either be explained by posttranscriptional mechanisms leading to a discrepancy between the expression level and the actual protein synthesis or a negative feedback loop due to already low muscle mass in cachectic cancer patients.

Certainly, IL-6 is one of the most intensively investigated cytokines in medical research due to its involvement in inflammation and tumor environment. In this analysis, IL-6 was positively correlated with hematological parameters such as CRP, while it was negatively correlated with albumin confirming the great importance of the Glasgow Prognostic Score as an instrument to

identify and stage cachexia. Furthermore, this study successfully demonstrated the prognostic power of IL-6 as a marker of survival, since patients of the whole cohort – but especially with PDAC – revealed significantly higher mortality in case of elevated IL-6 plasma levels at the day of surgery compared to individuals with low levels. Hence, to determine cachexia and the general health status, a combination of serum IL-6 as well as CRP, albumin and CA19-9 is a promising approach for assessment.

In conclusion, this study provides a comprehensive overview of some mechanisms of cancer-associated cachexia and sarcopenia in liver, muscle and adipose tissue based on measurements of circulating markers as well as on gene expression levels in these tissues. Although limitations are present, research using the established biobank should be continued to further unravel the molecular mechanisms in the context of tumor-induced cachexia and sarcopenia in humans.

7 References

Alves-Bezerra, M., & Cohen, D. E. (2017). Triglyceride Metabolism in the Liver. *Comprehensive Physiology*, *8*(1), 1–8. https://doi.org/10.1002/cphy.c170012.

Andersson, C., Gelin, J., Iresjö, B. M., & Lundholm, K. (1993). Acute-phase proteins in response to tumor growth. *The Journal of Surgical Research*, *55*(6), 607–614. https://doi.org/10.1006/jsre.1993.1192

Anker, M. S., Holcomb, R., Muscaritoli, M [Maurizio], Haehling, S. von, Haverkamp, W., Jatoi, A., Morley, J. E., Strasser, F., Landmesser, U., Coats, A. J. S., & Anker, S. D. (2019). Orphan disease status of cancer cachexia in the USA and in the European Union: A systematic review. *Journal of Cachexia, Sarcopenia and Muscle*, *10*(1), 22–34. https://doi.org/10.1002/jcsm.12402

Argiles, J. M., Lopez-Soriano, F. J., Toledo, M., Betancourt, A., Serpe, R., & Busquets, S [Silvia] (2011). The cachexia score (CASCO): A new tool for staging cachectic cancer patients. *Journal of Cachexia, Sarcopenia and Muscle*, *2*(2), 87–93. https://doi.org/10.1007/s13539-011-0027-5

Argilés, J. M., Busquets, S [Sílvia], Stemmler, B., & López-Soriano, F. J. (2014). Cancer cachexia: Understanding the molecular basis. *Nature Reviews. Cancer*, *14*(11), 754–762. https://doi.org/10.1038/nrc3829

Argilés, J. M., López-Soriano, J., Almendro, V., Busquets, S [Sílvia], & López-Soriano, F. J. (2005). Cross-talk between skeletal muscle and adipose tissue: A link with obesity? *Medicinal Research Reviews*, *25*(1), 49–65. https://doi.org/10.1002/med.20010

Argilés, J. M., Stemmler, B., López-Soriano, F. J., & Busquets, S [Silvia] (2015). Nonmuscle Tissues Contribution to Cancer Cachexia. *Mediators of Inflammation*, *2015*, 182872. https://doi.org/10.1155/2015/182872

Argilés, J. M., Stemmler, B., López-Soriano, F. J., & Busquets, S [Silvia] (2018). Inter-tissue communication in cancer cachexia. *Nature Reviews. Endocrinology*, *15*(1), 9–20. https://doi.org/10.1038/s41574-018-0123-0

Arner, P., & Kulyté, A. (2015). Microrna regulatory networks in human adipose tissue and obesity. *Nature Reviews. Endocrinology*, *11*(5), 276–288. https://doi.org/10.1038/nrendo.2015.25

Arnold, M., Abnet, C. C., Neale, R. E., Vignat, J., Giovannucci, E. L., McGlynn, K. A., & Bray, F. (2020). Global Burden of 5 Major Types of Gastrointestinal Cancer. *Gastroenterology*, *159*(1), 335-349.e15. https://doi.org/10.1053/j.gastro.2020.02.068

Aversa, Z., Bonetto, A [Andrea], Penna, F [Fabio], Costelli, P [Paola], Di Rienzo, G., Lacitignola, A., Baccino, F. M [Francesco M.], Ziparo, V., Mercantini, P., Rossi Fanelli, F [Filippo], & Muscaritoli, M [Maurizio] (2012). Changes in myostatin signaling in non-weight-losing cancer patients. *Annals of Surgical Oncology*, *19*(4), 1350–1356. https://doi.org/10.1245/s10434-011-1720-5

Babic, A., Schnure, N., Neupane, N. P., Zaman, M. M., Rifai, N., Welch, M. W., Brais, L. K., Rubinson, D. A., Morales-Oyarvide, V., Yuan, C., Zhang, S [S.], Poole, E. M., Wolpin, B. M., Kulke, M. H., Barbie, D. A., Wong, K., Fuchs, C. S., & Ng, K. (2018). Plasma inflammatory cytokines and survival of pancreatic cancer patients. *Clinical and Translational Gastroenterology*, *9*(4), 145. https://doi.org/10.1038/s41424-018-0008-5

Bäckdahl, J., Franzén, L., Massier, L., Li, Q., Jalkanen, J., Gao, H., Andersson, A., Bhalla, N., Thorell, A., Rydén, M., Ståhl, P. L., & Mejhert, N. (2021). Spatial mapping reveals human adipocyte subpopulations with distinct sensitivities to insulin. *Cell Metabolism*, *33*(9), 1869-1882.e6. https://doi.org/10.1016/j.cmet.2021.07.018

Barak, Y., Nelson, M. C., Ong, E. S., Jones, Y. Z., Ruiz-Lozano, P., Chien, K. R., Koder, A., & Evans, R. M. (1999). Ppar gamma is required for placental, cardiac, and adipose tissue

development. *Molecular Cell*, *4*(4), 585–595. https://doi.org/10.1016/s1097-2765(00)80209-9

Barbatelli, G., Murano, I., Madsen, L., Hao, Q., Jimenez, M., Kristiansen, K., Giacobino, J. P., Matteis, R. de, & Cinti, S [S.] (2010). The emergence of cold-induced brown adipocytes in mouse white fat depots is determined predominantly by white to brown adipocyte transdifferentiation. *American Journal of Physiology. Endocrinology and Metabolism*, *298*(6), E1244-53. https://doi.org/10.1152/ajpendo.00600.2009

Batista, M. L., Neves, R. X., Peres, S. B., Yamashita, A. S., Shida, C. S., Farmer, S. R., & Seelaender, M [M.] (2012). Heterogeneous time-dependent response of adipose tissue during the development of cancer cachexia. *The Journal of Endocrinology*, *215*(3), 363–373. https://doi.org/10.1530/JOE-12-0307

Bauer, J [Juergen], Morley, J. E., Schols, A. M. W. J., Ferrucci, L., Cruz-Jentoft, A. J., Dent, E., Baracos, V. E., Crawford, J. A., Doehner, W., Heymsfield, S. B., Jatoi, A., Kalantar-Zadeh, K., Lainscak, M., Landi, F., Laviano, A., Mancuso, M., Muscaritoli, M [Maurizio], Prado, C. M., Strasser, F., . . . Anker, S. D. (2019). Sarcopenia: A Time for Action. An SCWD Position Paper. *Journal of Cachexia, Sarcopenia and Muscle*, *10*(5), 956–961. https://doi.org/10.1002/jcsm.12483

Bellone, G., Smirne, C., Mauri, F. A., Tonel, E., Carbone, A., Buffolino, A., Dughera, L., Robecchi, A., Pirisi, M., & Emanuelli, G. (2006). Cytokine expression profile in human pancreatic carcinoma cells and in surgical specimens: Implications for survival. *Cancer Immunology, Immunotherapy : CII*, *55*(6), 684–698. https://doi.org/10.1007/s00262-005-0047-0

Bian, A.-L., Hu, H.-Y., Rong, Y.-D., Wang, J., Wang, J.-X., & Zhou, X.-Z. (2017). A study on relationship between elderly sarcopenia and inflammatory factors IL-6 and TNF-α. *European Journal of Medical Research*, *22*(1), 25. https://doi.org/10.1186/s40001-017-0266-9

Bing, C [C.], Russell, S., Becket, E., Pope, M., Tisdale, M. J [M. J.], Trayhurn, P [P.], & Jenkins, J. R. (2006). Adipose atrophy in cancer cachexia: Morphologic and molecular analysis of adipose tissue in tumour-bearing mice. *British Journal of Cancer*, *95*(8), 1028–1037. https://doi.org/10.1038/sj.bjc.6603360

Bing, C [Chen], Bao, Y., Jenkins, J., Sanders, P., Manieri, M., Cinti, S [Saverio], Tisdale, M. J [Michael J.], & Trayhurn, P [Paul] (2004). Zinc-alpha2-glycoprotein, a lipid mobilizing factor, is expressed in adipocytes and is up-regulated in mice with cancer cachexia. *Proceedings of the National Academy of Sciences of the United States of America*, *101*(8), 2500–2505. https://doi.org/10.1073/pnas.0308647100

Bonetto, A [Andrea], Penna, F [Fabio], Aversa, Z., Mercantini, P., Baccino, F. M [Francesco M.], Costelli, P [Paola], Ziparo, V., Lucia, S., Rossi Fanelli, F [Filippo], & Muscaritoli, M [Maurizio] (2013). Early changes of muscle insulin-like growth factor-1 and myostatin gene expression in gastric cancer patients. *Muscle & Nerve*, *48*(3), 387–392. https://doi.org/10.1002/mus.23798

Bora, P., & Majumdar, A. S. (2017). Adipose tissue-derived stromal vascular fraction in regenerative medicine: A brief review on biology and translation. *Stem Cell Research & Therapy*, *8*(1), 145. https://doi.org/10.1186/s13287-017-0598-y

Bossola, M [Maurizio], Marzetti, E., Rosa, F., & Pacelli, F. (2016). Skeletal muscle regeneration in cancer cachexia. *Clinical and Experimental Pharmacology & Physiology*, *43*(5), 522–527. https://doi.org/10.1111/1440-1681.12559

Bray, F., Laversanne, M., Weiderpass, E., & Soerjomataram, I. (2021). The ever-increasing importance of cancer as a leading cause of premature death worldwide. *Cancer.* Advance online publication. https://doi.org/10.1002/cncr.33587

Broekhuizen, R., Grimble, R. F., Howell, W. M., Shale, D. J., Creutzberg, E. C., Wouters, E. F., & Schols, A. M. (2005). Pulmonary cachexia, systemic inflammatory

profile, and the interleukin 1beta -511 single nucleotide polymorphism. *The American Journal of Clinical Nutrition*, *82*(5), 1059–1064. https://doi.org/10.1093/ajcn/82.5.1059

Castro, G. S. de, Simoes, E., Lima, J. D. C. C., Ortiz-Silva, M., Festuccia, W. T., Tokeshi, F., Alcântara, P. S., Otoch, J. P., Coletti, D., & Seelaender, M [Marilia] (2019). Human Cachexia Induces Changes in Mitochondria, Autophagy and Apoptosis in the Skeletal Muscle. *Cancers*, *11*(9). https://doi.org/10.3390/cancers11091264

Center, M. M., Jemal, A., Smith, R. A., & Ward, E. (2009). Worldwide variations in colorectal cancer. *CA: A Cancer Journal for Clinicians*, *59*(6), 366–378. https://doi.org/10.3322/caac.20038

Chen, J. L., Walton, K. L., Qian, H., Colgan, T. D., Hagg, A., Watt, M. J., Harrison, C. A., & Gregorevic, P. (2016). Differential Effects of IL6 and Activin A in the Development of Cancer-Associated Cachexia. *Cancer Research*, *76*(18), 5372–5382. https://doi.org/10.1158/0008-5472.CAN-15-3152

Cheng, C. K., Bakar, H. A., Gollasch, M., & Huang, Y [Yu] (2018). Perivascular Adipose Tissue: The Sixth Man of the Cardiovascular System. *Cardiovascular Drugs and Therapy*, *32*(5), 481–502. https://doi.org/10.1007/s10557-018-6820-z

Chung, Y.-C., & Chang, Y.-F. (2003). Serum interleukin-6 levels reflect the disease status of colorectal cancer. *Journal of Surgical Oncology*, *83*(4), 222–226. https://doi.org/10.1002/jso.10269

Cinti, S [Saverio] (2012). The adipose organ at a glance. *Disease Models & Mechanisms*, *5*(5), 588–594. https://doi.org/10.1242/dmm.009662

Claussnitzer, M., Dankel, S. N., Kim, K.-H., Quon, G., Meuleman, W., Haugen, C., Glunk, V., Sousa, I. S., Beaudry, J. L., Puviindran, V., Abdennur, N. A., Liu, J [Jannel], Svensson, P.-A., Hsu, Y.-H., Drucker, D. J., Mellgren, G., Hui, C.-C., Hauner, H [Hans], & Kellis, M. (2015). Fto Obesity Variant Circuitry and Adipocyte Browning in Humans. *The New England Journal of Medicine*, *373*(10), 895–907. https://doi.org/10.1056/NEJMoa1502214

Costelli, P [P.], Muscaritoli, M [M.], Bonetto, A [A.], Penna, F [F.], Reffo, P., Bossola, M [M.], Bonelli, G [G.], Doglietto, G. B [G. B.], Baccino, F. M [F. M.], & Rossi Fanelli, F [F.] (2008). Muscle myostatin signalling is enhanced in experimental cancer cachexia. *European Journal of Clinical Investigation*, *38*(7), 531–538. https://doi.org/10.1111/j.1365-2362.2008.01970.x

Cruz-Jentoft, A. J., Baeyens, J. P., Bauer, J. M., Boirie, Y., Cederholm, T., Landi, F., Martin, F. C., Michel, J.-P., Rolland, Y., Schneider, S. M., Topinková, E., Vandewoude, M., & Zamboni, M. (2010). Sarcopenia: European consensus on definition and diagnosis: Report of the European Working Group on Sarcopenia in Older People. *Age and Ageing*, *39*(4), 412–423. https://doi.org/10.1093/ageing/afq034

Cruz-Jentoft, A. J., Bahat, G., Bauer, J., Boirie, Y., Bruyère, O., Cederholm, T., Cooper, C., Landi, F., Rolland, Y., Sayer, A. A., Schneider, S. M., Sieber, C. C., Topinkova, E., Vandewoude, M., Visser, M., & Zamboni, M. (2019). Sarcopenia: Revised European consensus on definition and diagnosis. *Age and Ageing*, *48*(1), 16–31. https://doi.org/10.1093/ageing/afy169

Csepregi, R., Lemli, B., Kunsági-Máté, S., Szente, L., Kőszegi, T., Németi, B., & Poór, M. (2018). Complex Formation of Resorufin and Resazurin with B-Cyclodextrins: Can Cyclodextrins Interfere with a Resazurin Cell Viability Assay? *Molecules (Basel, Switzerland)*, *23*(2). https://doi.org/10.3390/molecules23020382

Daas, S. I., Rizeq, B. R., & Nasrallah, G. K. (2018). Adipose tissue dysfunction in cancer cachexia. *Journal of Cellular Physiology.* Advance online publication. https://doi.org/10.1002/jcp.26811

Davidson, W., Ash, S., Capra, S., & Bauer, J [Judith] (2004). Weight stabilisation is associated with improved survival duration and quality of life in unresectable pancreatic cancer.

Clinical Nutrition (Edinburgh, Scotland), *23*(2), 239–247. https://doi.org/10.1016/j.clnu.2003.07.001

Dexamethasone versus standard treatment for postoperative nausea and vomiting in gastrointestinal surgery: Randomised controlled trial (DREAMS Trial) (2017). *BMJ (Clinical Research Ed.)*, *357*, j1455. https://doi.org/10.1136/bmj.j1455

Dogra, C., Changotra, H., Wedhas, N., Qin, X., Wergedal, J. E., & Kumar, A. (2007). Tnf-related weak inducer of apoptosis (TWEAK) is a potent skeletal muscle-wasting cytokine. *FASEB Journal : Official Publication of the Federation of American Societies for Experimental Biology*, *21*(8), 1857–1869. https://doi.org/10.1096/fj.06-7537com

D'Orlando, C., Marzetti, E., François, S., Lorenzi, M., Conti, V., Di Stasio, E., Rosa, F., Brunelli, S., Doglietto, G. B [Giovan Battista], Pacelli, F., & Bossola, M [Maurizio] (2014). Gastric cancer does not affect the expression of atrophy-related genes in human skeletal muscle. *Muscle & Nerve*, *49*(4), 528–533. https://doi.org/10.1002/mus.23945

Douglas, E., & McMillan, D. C [Donald C.] (2014). Towards a simple objective framework for the investigation and treatment of cancer cachexia: The Glasgow Prognostic Score. *Cancer Treatment Reviews*, *40*(6), 685–691. https://doi.org/10.1016/j.ctrv.2013.11.007

Duggan, E. W., Carlson, K., & Umpierrez, G. E. (2017). Perioperative Hyperglycemia Management: An Update. *Anesthesiology*, *126*(3), 547–560. https://doi.org/10.1097/ALN.0000000000001515

Dumas, J.-F., Goupille, C., Julienne, C. M., Pinault, M., Chevalier, S., Bougnoux, P., Servais, S., & Couet, C. (2011). Efficiency of oxidative phosphorylation in liver mitochondria is decreased in a rat model of peritoneal carcinosis. *Journal of Hepatology*, *54*(2), 320–327. https://doi.org/10.1016/j.jhep.2010.08.012

Duncan, R. E., Ahmadian, M., Jaworski, K., Sarkadi-Nagy, E., & Sul, H. S. (2007). Regulation of lipolysis in adipocytes. *Annual Review of Nutrition*, *27*, 79–101. https://doi.org/10.1146/annurev.nutr.27.061406.093734

Elattar, S., Dimri, M., & Satyanarayana, A. (2018). The tumor secretory factor ZAG promotes white adipose tissue browning and energy wasting. *FASEB Journal : Official Publication of the Federation of American Societies for Experimental Biology*, *32*(9), 4727–4743. https://doi.org/10.1096/fj.201701465RR

El-Jack, A. K., Hamm, J. K., Pilch, P. F., & Farmer, S. R. (1999). Reconstitution of insulin-sensitive glucose transport in fibroblasts requires expression of both PPARgamma and C/EBPalpha. *The Journal of Biological Chemistry*, *274*(12), 7946–7951. https://doi.org/10.1074/jbc.274.12.7946

Elkina, Y., Haehling, S. von, Anker, S. D., & Springer, J. (2011). The role of myostatin in muscle wasting: An overview. *Journal of Cachexia, Sarcopenia and Muscle*, *2*(3), 143–151. https://doi.org/10.1007/s13539-011-0035-5

Elsherif, S. B., Virarkar, M., Javadi, S., Ibarra-Rovira, J. J., Tamm, E. P., & Bhosale, P. R. (2020). Pancreatitis and PDAC: Association and differentiation. *Abdominal Radiology (New York)*, *45*(5), 1324–1337. https://doi.org/10.1007/s00261-019-02292-w

Eskiler, G. G., Bezdegumeli, E., Ozman, Z., Ozkan, A. D., Bilir, C., Kucukakca, B. N., Ince, M. N., Men, A. Y., Aktas, O., Horoz, Y. E., Akpinar, D., Genc, I., & Kaleli, S. (2019). Il-6 mediated JAK/STAT3 signaling pathway in cancer patients with cachexia. *Bratislavske Lekarske Listy*, *66*(11), 819–826. https://doi.org/10.4149/BLL_2019_136

Fan, G., Li, Y [Yanfei], Ma, F., Zhao, R., & Yang, X. (2021). Zinc-α2-glycoprotein promotes skeletal muscle lipid metabolism in cold-stressed mice. *Endocrine Journal*, *68*(1), 53–62. https://doi.org/10.1507/endocrj.EJ20-0179

Fayezi, S., Leroy, J. L. M. R., Ghaffari Novin, M., & Darabi, M. (2018). Oleic acid in the modulation of oocyte and preimplantation embryo development. *Zygote (Cambridge, England)*, *26*(1), 1–13. https://doi.org/10.1017/S0967199417000582

Fearon, K. C., McMillan, D. C [D. C.], Preston, T., Winstanley, F. P., Cruickshank, A. M., & Shenkin, A. (1991). Elevated circulating interleukin-6 is associated with an acute-phase response but reduced fixed hepatic protein synthesis in patients with cancer. *Annals of Surgery*, *213*(1), 26–31. https://doi.org/10.1097/00000658-199101000-00005

Fearon, K., Strasser, F., Anker, S. D., Bosaeus, I., Bruera, E., Fainsinger, R. L., Jatoi, A., Loprinzi, C., MacDonald, N., Mantovani, G., Davis, M., Muscaritoli, M [Maurizio], Ottery, F., Radbruch, L., Ravasco, P., Walsh, D., Wilcock, A., Kaasa, S., & Baracos, V. E. (2011). Definition and classification of cancer cachexia: An international consensus. *The Lancet Oncology*, *12*(5), 489–495. https://doi.org/10.1016/S1470-2045(10)70218-7

Fearon, K. C. H., Glass, D. J., & Guttridge, D. C. (2012). Cancer cachexia: Mediators, signaling, and metabolic pathways. *Cell Metabolism*, *16*(2), 153–166. https://doi.org/10.1016/j.cmet.2012.06.011

Ferrari, P., Jenab, M., Norat, T., Moskal, A., Slimani, N., Olsen, A., Tjønneland, A., Overvad, K., Jensen, M. K., Boutron-Ruault, M.-C., Clavel-Chapelon, F., Morois, S., Rohrmann, S., Linseisen, J., Boeing, H., Bergmann, M., Kontopoulou, D., Trichopoulou, A., Kassapa, C., . . . Riboli, E. (2007). Lifetime and baseline alcohol intake and risk of colon and rectal cancers in the European prospective investigation into cancer and nutrition (EPIC). *International Journal of Cancer*, *121*(9), 2065–2072. https://doi.org/10.1002/ijc.22966

Forbes, D., Jackman, M., Bishop, A., Thomas, M., Kambadur, R., & Sharma, M. (2006). Myostatin auto-regulates its expression by feedback loop through Smad7 dependent mechanism. *Journal of Cellular Physiology*, *206*(1), 264–272. https://doi.org/10.1002/jcp.20477

Forrest, L. M., McMillan, D. C [D. C.], McArdle, C. S [C. S.], Angerson, W. J [W. J.], & Dunlop, D. J. (2003). Evaluation of cumulative prognostic scores based on the systemic inflammatory response in patients with inoperable non-small-cell lung cancer. *British Journal of Cancer*, *89*(6), 1028–1030. https://doi.org/10.1038/sj.bjc.6601242

Frayling, T. M., Timpson, N. J., Weedon, M. N., Zeggini, E., Freathy, R. M., Lindgren, C. M., Perry, J. R. B., Elliott, K. S., Lango, H., Rayner, N. W., Shields, B., Harries, L. W., Barrett, J. C., Ellard, S., Groves, C. J., Knight, B., Patch, A.-M., Ness, A. R., Ebrahim, S., . . . McCarthy, M. I. (2007). A common variant in the FTO gene is associated with body mass index and predisposes to childhood and adult obesity. *Science (New York, N.Y.)*, *316*(5826), 889–894. https://doi.org/10.1126/science.1141634

Freire, P. P., Fernandez, G. J., Moraes, D. de, Cury, S. S., Dal Pai-Silva, M., Dos Reis, P. P., Rogatto, S. R., & Carvalho, R. F. (2020). The expression landscape of cachexia-inducing factors in human cancers. *Journal of Cachexia, Sarcopenia and Muscle*, *11*(4), 947–961. https://doi.org/10.1002/jcsm.12565

Freytag, S. O., Paielli, D. L., & Gilbert, J. D. (1994). Ectopic expression of the CCAAT/enhancer-binding protein alpha promotes the adipogenic program in a variety of mouse fibroblastic cells. *Genes & Development*, *8*(14), 1654–1663. https://doi.org/10.1101/gad.8.14.1654

Frigolet, M. E., & Gutiérrez-Aguilar, R. (2020). Los colores del tejido adiposo [The colors of adipose tissue]. *Gaceta Medica De Mexico*, *156*(2), 142–149. https://doi.org/10.24875/GMM.M20000356

Gesta, S., Tseng, Y.-H., & Kahn, C. R. (2007). Developmental origin of fat: Tracking obesity to its source. *Cell*, *131*(2), 242–256. https://doi.org/10.1016/j.cell.2007.10.004

Grandl, G., Müller, S., Moest, H., Moser, C., Wollscheid, B., & Wolfrum, C. (2016). Depot specific differences in the adipogenic potential of precursors are mediated by

collagenous extracellular matrix and Flotillin 2 dependent signaling. *Molecular Metabolism*, *5*(10), 937–947. https://doi.org/10.1016/j.molmet.2016.07.008

Gray, S., Feinberg, M. W., Hull, S., Kuo, C. T., Watanabe, M., Sen-Banerjee, S., DePina, A., Haspel, R., & Jain, M. K. (2002). The Krüppel-like factor KLF15 regulates the insulin-sensitive glucose transporter GLUT4. *The Journal of Biological Chemistry*, *277*(37), 34322–34328. https://doi.org/10.1074/jbc.M201304200

Greenberg, A. S., Nordan, R. P., McIntosh, J., Calvo, J. C., Scow, R. O., & Jablons, D. (1992). Interleukin 6 reduces lipoprotein lipase activity in adipose tissue of mice in vivo and in 3T3-L1 adipocytes: A possible role for interleukin 6 in cancer cachexia. *Cancer Research*, *52*(15), 4113–4116.

Guo, D., Wang, C., Wang, Q., Qiao, Z., & Tang, H. (2017). Pantoprazole blocks the JAK2/STAT3 pathway to alleviate skeletal muscle wasting in cancer cachexia by inhibiting inflammatory response. *Oncotarget.* Advance online publication. https://doi.org/10.18632/oncotarget.17387

Han, J., Meng, Q., Shen, L., & Wu, G. (2018). Interleukin-6 induces fat loss in cancer cachexia by promoting white adipose tissue lipolysis and browning. *Lipids in Health and Disease*, *17*(1), 14. https://doi.org/10.1186/s12944-018-0657-0

Hauner, H [H.], Entenmann, G., Wabitsch, M., Gaillard, D., Ailhaud, G., Negrel, R., & Pfeiffer, E. F. (1989). Promoting effect of glucocorticoids on the differentiation of human adipocyte precursor cells cultured in a chemically defined medium. *Journal of Clinical Investigation*, *84*(5), 1663–1670. https://doi.org/10.1172/JCI114345

Hauner, H [H.], Petruschke, T., Russ, M., Röhrig, K., & Eckel, J. (1995). Effects of tumour necrosis factor alpha (TNF alpha) on glucose transport and lipid metabolism of newly-differentiated human fat cells in cell culture. *Diabetologia*, *38*(7), 764–771. https://doi.org/10.1007/s001250050350

Hauner, H [H.], Schmid, P., & Pfeiffer, E. F. (1987). Glucocorticoids and insulin promote the differentiation of human adipocyte precursor cells into fat cells. *The Journal of Clinical Endocrinology and Metabolism*, *64*(4), 832–835. https://doi.org/10.1210/jcem-64-4-832

Hensley, C. T., Wasti, A. T., & DeBerardinis, R. J. (2013). Glutamine and cancer: Cell biology, physiology, and clinical opportunities. *Journal of Clinical Investigation*, *123*(9), 3678–3684. https://doi.org/10.1172/JCI69600

Hirai, K., Hussey, H. J., Barber, M. D., Price, S. A., & Tisdale, M. J [M. J.] (1998). Biological evaluation of a lipid-mobilizing factor isolated from the urine of cancer patients. *Cancer Research*, *58*(11), 2359–2365.

Hollands, M. A., & Cawthorne, M. A. (1981). Important sites of lipogenesis in the mouse other than liver and white adipose tissue. *The Biochemical Journal*, *196*(2), 645–647. https://doi.org/10.1042/bj1960645

Horton, J. D. (2002). Sterol regulatory element-binding proteins: Transcriptional activators of lipid synthesis. *Biochemical Society Transactions*, *30*(Pt 6), 1091–1095. https://doi.org/10.1042/bst0301091

Hu, W., Ru, Z., Zhou, Y., Xiao, W., Sun, R., Zhang, S [Santao], Gao, Y., Li, X [Xiang], Zhang, X., & Yang, H. (2019). Lung cancer-derived extracellular vesicles induced myotube atrophy and adipocyte lipolysis via the extracellular IL-6-mediated STAT3 pathway. *Biochimica Et Biophysica Acta. Molecular and Cell Biology of Lipids*, *1864*(8), 1091–1102. https://doi.org/10.1016/j.bbalip.2019.04.006

Huang, H., Song, T.-J., Li, X [Xi], Hu, L., He, Q., Liu, M., Lane, M. D., & Tang, Q.-Q. (2009). Bmp signaling pathway is required for commitment of C3H10T1/2 pluripotent stem cells to the adipocyte lineage. *Proceedings of the National Academy of Sciences of the United States of America*, *106*(31), 12670–12675. https://doi.org/10.1073/pnas.0906266106

Huang, Y [Yan], Li, L.-Z., Zhang, C. Z.-Y., Yi, C., Liu, L.-L., Zhou, X [Xuan], Xie, G.-B., Cai, M.-Y., Li, Y [Yan], & Yun, J.-P. (2012). Decreased expression of zinc-alpha2-glycoprotein in hepatocellular carcinoma associates with poor prognosis. *Journal of Translational Medicine*, *10*, 106. https://doi.org/10.1186/1479-5876-10-106

Ilic, M., & Ilic, I. (2016). Epidemiology of pancreatic cancer. *World Journal of Gastroenterology*, *22*(44), 9694–9705. https://doi.org/10.3748/wjg.v22.i44.9694

Julienne, C. M., Tardieu, M., Chevalier, S., Pinault, M., Bougnoux, P., Labarthe, F., Couet, C., Servais, S., & Dumas, J.-F. (2014). Cardiolipin content is involved in liver mitochondrial energy wasting associated with cancer-induced cachexia without the involvement of adenine nucleotide translocase. *Biochimica Et Biophysica Acta*, *1842*(5), 726–733. https://doi.org/10.1016/j.bbadis.2014.02.003

Kaklamani, V., Yi, N., Sadim, M., Siziopikou, K., Zhang, K., Xu, Y., Tofilon, S., Agarwal, S., Pasche, B., & Mantzoros, C. (2011). The role of the fat mass and obesity associated gene (FTO) in breast cancer risk. *BMC Medical Genetics*, *12*, 52. https://doi.org/10.1186/1471-2350-12-52

Kalantar-Zadeh, K., Rhee, C., Sim, J. J., Stenvinkel, P., Anker, S. D., & Kovesdy, C. P. (2013). Why cachexia kills: Examining the causality of poor outcomes in wasting conditions. *Journal of Cachexia, Sarcopenia and Muscle*, *4*(2), 89–94. https://doi.org/10.1007/s13539-013-0111-0

Karra, E., O'Daly, O. G., Choudhury, A. I., Yousseif, A., Millership, S., Neary, M. T., Scott, W. R., Chandarana, K., Manning, S., Hess, M. E., Iwakura, H., Akamizu, T., Millet, Q., Gelegen, C., Drew, M. E., Rahman, S., Emmanuel, J. J., Williams, S. C. R., Rüther, U. U., . . . Batterham, R. L. (2013). A link between FTO, ghrelin, and impaired brain food-cue responsivity. *Journal of Clinical Investigation*, *123*(8), 3539–3551. https://doi.org/10.1172/JCI44403

Karsli-Uzunbas, G., Guo, J. Y., Price, S., Teng, X., Laddha, S. V., Khor, S., Kalaany, N. Y., Jacks, T., Chan, C. S., Rabinowitz, J. D., & White, E. (2014). Autophagy is required for glucose homeostasis and lung tumor maintenance. *Cancer Discovery*, *4*(8), 914–927. https://doi.org/10.1158/2159-8290.CD-14-0363

Khan, S., & Tisdale, M. J [M. J.] (1999). Catabolism of adipose tissue by a tumour-produced lipid-mobilising factor. *International Journal of Cancer*, *80*(3), 444–447. https://doi.org/10.1002/(sici)1097-0215(19990129)80:3<444::aid-ijc18>3.0.co;2-u

Kir, S., White, J. P., Kleiner, S., Kazak, L., Cohen, P., Baracos, V. E., & Spiegelman, B. M [Bruce M.] (2014). Tumour-derived PTH-related protein triggers adipose tissue browning and cancer cachexia. *Nature*, *513*(7516), 100–104. https://doi.org/10.1038/nature13528

Klingenspor, M., Herzig, S., & Pfeifer, A. (2012). Brown fat develops a brite future. *Obesity Facts*, *5*(6), 890–896. https://doi.org/10.1159/000346337

Kokta, T. A., Strat, A. L., Papasani, M. R., Szasz, J. I., Dodson, M. V., & Hill, R. A. (2008). Regulation of lipid accumulation in 3T3-L1 cells: Insulin-independent and combined effects of fatty acids and insulin. *Animal : An International Journal of Animal Bioscience*, *2*(1), 92–99. https://doi.org/10.1017/S1751731107000936

Kong, B., Michalski, C. W., Hong, X., Valkovskaya, N., Rieder, S., Abiatari, I., Streit, S., Erkan, M., Esposito, I., Friess, H [H.], & Kleeff, J. (2010). Azgp1 is a tumor suppressor in pancreatic cancer inducing mesenchymal-to-epithelial transdifferentiation by inhibiting TGF-β-mediated ERK signaling. *Oncogene*, *29*(37), 5146–5158. https://doi.org/10.1038/onc.2010.258

Kudriavtsev, I. V. (1980). Gisto-tsitospektrofotometricheskaia kharakteristika raka legkogo [Histocytospectrophotometric characteristics of lung cancer]. *Arkhiv patologii*, *42*(11), 20–27.

Kurahara, H., Maemura, K., Mataki, Y., Sakoda, M., Iino, S., Hiwatashi, K., Kawasaki, Y., Arigami, T., Ishigami, S., Kijima, Y., Shinchi, H., Takao, S., & Natsugoe, S. (2015). Prognostication by inflammation-based score in patients with locally advanced pancreatic cancer treated with chemoradiotherapy. *Pancreatology : Official Journal of the International Association of Pancreatology (IAP) … [Et Al.]*, *15*(6), 688–693. https://doi.org/10.1016/j.pan.2015.09.015

Lecker, S. H., Jagoe, R. T., Gilbert, A., Gomes, M., Baracos, V., Bailey, J., Price, S. R., Mitch, W. E., & Goldberg, A. L. (2004). Multiple types of skeletal muscle atrophy involve a common program of changes in gene expression. *FASEB Journal : Official Publication of the Federation of American Societies for Experimental Biology*, *18*(1), 39–51. https://doi.org/10.1096/fj.03-0610com

Lee, J. H., Park, A., Oh, K.-J., Lee, S. C., Kim, W. K [Won Kon], & Bae, K.-H. (2019). The Role of Adipose Tissue Mitochondria: Regulation of Mitochondrial Function for the Treatment of Metabolic Diseases. *International Journal of Molecular Sciences*, *20*(19). https://doi.org/10.3390/ijms20194924

Lee, M.-J., Wu, Y., & Fried, S. K. (2013). Adipose tissue heterogeneity: Implication of depot differences in adipose tissue for obesity complications. *Molecular Aspects of Medicine*, *34*(1), 1–11. https://doi.org/10.1016/j.mam.2012.10.001

Léger, B., Derave, W., Bock, K. de, Hespel, P., & Russell, A. P. (2008). Human sarcopenia reveals an increase in SOCS-3 and myostatin and a reduced efficiency of Akt phosphorylation. *Rejuvenation Research*, *11*(1), 163-175B. https://doi.org/10.1089/rej.2007.0588

Li, Z., & Cui, Z. (2014). Three-dimensional perfused cell culture. *Biotechnology Advances*, *32*(2), 243–254. https://doi.org/10.1016/j.biotechadv.2013.10.006

Lin, Y., Ueda, J., Yagyu, K., Ishii, H., Ueno, M., Egawa, N., Nakao, H., Mori, M., Matsuo, K., & Kikuchi, S. (2013). Association between variations in the fat mass and obesity-associated gene and pancreatic cancer risk: A case-control study in Japan. *BMC Cancer*, *13*, 337. https://doi.org/10.1186/1471-2407-13-337

Linn, B. S., Linn, M. W., & Klimas, N. G. (1988). Effects of psychophysical stress on surgical outcome. *Psychosomatic Medicine*, *50*(3), 230–244. https://doi.org/10.1097/00006842-198805000-00002

Liu, C.-M., Yang, Z., Liu, C.-W., Wang, R., Tien, P., Dale, R., & Sun, L.-Q. (2008). Myostatin antisense RNA-mediated muscle growth in normal and cancer cachexia mice. *Gene Therapy*, *15*(3), 155–160. https://doi.org/10.1038/sj.gt.3303016

Lorenzetti, F., Capiglioni, A. M., Marinelli, R. A., Carrillo, M. C., & Alvarez, M. d. L. (2020). Hepatic glycerol metabolism is early reprogrammed in rat liver cancer development. *Biochimie*, *170*, 88–93. https://doi.org/10.1016/j.biochi.2020.01.002

Martignoni, M. E., Dimitriu, C., Bachmann, J [Jeaninne], Krakowski-Rosen, H., Ketterer, K., Kinscherf, R., & Friess, H [Helmut] (2009). Liver macrophages contribute to pancreatic cancer-related cachexia. *Oncology Reports*, *21*(2), 363–369.

McFarlane, C., Plummer, E., Thomas, M., Hennebry, A., Ashby, M., Ling, N., Smith, H., Sharma, M., & Kambadur, R. (2006). Myostatin induces cachexia by activating the ubiquitin proteolytic system through an NF-kappaB-independent, FoxO1-dependent mechanism. *Journal of Cellular Physiology*, *209*(2), 501–514. https://doi.org/10.1002/jcp.20757

McFarlane, C., Vajjala, A., Arigela, H., Lokireddy, S., Ge, X., Bonala, S., Manickam, R., Kambadur, R., & Sharma, M. (2014). Negative auto-regulation of myostatin expression is mediated by Smad3 and microRNA-27. *PloS One*, *9*(1), e87687. https://doi.org/10.1371/journal.pone.0087687

McMillan, D. C [Donald C.], Crozier, J. E. M., Canna, K., Angerson, W. J [Wilson J.], & McArdle, C. S [Colin S.] (2007). Evaluation of an inflammation-based prognostic score

(GPS) in patients undergoing resection for colon and rectal cancer. *International Journal of Colorectal Disease*, *22*(8), 881–886. https://doi.org/10.1007/s00384-006-0259-6

Meyer, R. D., Preston, S. L., & McMorris, F. A. (1983). Glycerol-3-phosphate dehydrogenase is induced by glucocorticoids in hepatocytes and hepatoma cells in vitro. *Journal of Cellular Physiology*, *114*(2), 203–208. https://doi.org/10.1002/jcp.1041140209

Miller, A., McLeod, L., Alhayyani, S., Szczepny, A., Watkins, D. N., Chen, W., Enriori, P., Ferlin, W., Ruwanpura, S., & Jenkins, B. J. (2017). Blockade of the IL-6 trans-signalling/STAT3 axis suppresses cachexia in Kras-induced lung adenocarcinoma. *Oncogene*, *36*(21), 3059–3066. https://doi.org/10.1038/onc.2016.437

Mitchell, I., Hayward, S., Deshpande, N., & Towler, J. M. (1989). Enzyme studies in human transitional cell carcinoma of the urinary bladder. *The Journal of Urology*, *141*(5), 1234–1237. https://doi.org/10.1016/s0022-5347(17)41228-6

Morissette, M. R., Stricker, J. C., Rosenberg, M. A., Buranasombati, C., Levitan, E. B., Mittleman, M. A., & Rosenzweig, A. (2009). Effects of myostatin deletion in aging mice. *Aging Cell*, *8*(5), 573–583. https://doi.org/10.1111/j.1474-9726.2009.00508.x

Mracek, T., Ding, Q., Tzanavari, T., Kos, K., Pinkney, J., Wilding, J., Trayhurn, P [P.], & Bing, C [C.] (2010). The adipokine zinc-alpha2-glycoprotein (ZAG) is downregulated with fat mass expansion in obesity. *Clinical Endocrinology*, *72*(3), 334–341. https://doi.org/10.1111/j.1365-2265.2009.03658.x

Mulligan, H. D., & Tisdale, M. J [M. J.] (1991). Lipogenesis in tumour and host tissues in mice bearing colonic adenocarcinomas. *British Journal of Cancer*, *63*(5), 719–722. https://doi.org/10.1038/bjc.1991.162

Murphy, M. G., Négrel, R., & Ailhaud, G. (1981). Lipoprotein lipase and monoacylglycerol lipase activities during maturation of ob17 preadipocytes. *Biochimica Et Biophysica Acta*, *664*(2), 240–248. https://doi.org/10.1016/0005-2760(81)90046-1

Muscaritoli, M [Maurizio], Molfino, A., Lucia, S., & Rossi Fanelli, F [Filippo] (2015). Cachexia: A preventable comorbidity of cancer. A T.A.R.G.E.T. Approach. *Critical Reviews in Oncology/hematology*, *94*(2), 251–259. https://doi.org/10.1016/j.critrevonc.2014.10.014

Nedergaard, J., Bengtsson, T., & Cannon, B. (2007). Unexpected evidence for active brown adipose tissue in adult humans. *American Journal of Physiology. Endocrinology and Metabolism*, *293*(2), E444-52. https://doi.org/10.1152/ajpendo.00691.2006

Oliver, P., Picó, C., & Palou, A. (2001). Differential expression of genes for uncoupling proteins 1, 2 and 3 in brown and white adipose tissue depots during rat development. *Cellular and Molecular Life Sciences : CMLS*, *58*(3), 470–476. https://doi.org/10.1007/PL00000870

Park, A., Kim, W. K [Won Kon], & Bae, K.-H. (2014). Distinction of white, beige and brown adipocytes derived from mesenchymal stem cells. *World Journal of Stem Cells*, *6*(1), 33–42. https://doi.org/10.4252/wjsc.v6.i1.33

Päth, G., Bornstein, S. R., Gurniak, M., Chrousos, G. P., Scherbaum, W. A., & Hauner, H [H.] (2001). Human breast adipocytes express interleukin-6 (IL-6) and its receptor system: Increased IL-6 production by beta-adrenergic activation and effects of IL-6 on adipocyte function. *The Journal of Clinical Endocrinology and Metabolism*, *86*(5), 2281–2288. https://doi.org/10.1210/jcem.86.5.7494

Patsouris, D., Mandard, S., Voshol, P. J., Escher, P., Tan, N. S., Havekes, L. M., Koenig, W., März, W., Tafuri, S., Wahli, W., Müller, M., & Kersten, S. (2004). Pparalpha governs glycerol metabolism. *Journal of Clinical Investigation*, *114*(1), 94–103. https://doi.org/10.1172/JCI20468

Penna, F [Fabio], Costamagna, D., Pin, F., Camperi, A., Fanzani, A., Chiarpotto, E. M., Cavallini, G., Bonelli, G [Gabriella], Baccino, F. M [Francesco M.], & Costelli, P [Paola]

(2013). Autophagic degradation contributes to muscle wasting in cancer cachexia. *The American Journal of Pathology*, *182*(4), 1367–1378. https://doi.org/10.1016/j.ajpath.2012.12.023

Perdikari, A., Leparc, G. G., Balaz, M., Pires, N. D., Lidell, M. E., Sun, W., Fernandez-Albert, F., Müller, S., Akchiche, N., Dong, H., Balazova, L., Opitz, L., Röder, E., Klein, H., Stefanicka, P., Varga, L., Nuutila, P., Virtanen, K. A., Niemi, T., . . . Wolfrum, C. (2018). Batlas: Deconvoluting Brown Adipose Tissue. *Cell Reports*, *25*(3), 784-797.e4. https://doi.org/10.1016/j.celrep.2018.09.044

Petruzzelli, M., Schweiger, M., Schreiber, R., Campos-Olivas, R., Tsoli, M., Allen, J., Swarbrick, M., Rose-John, S., Rincon, M., Robertson, G., Zechner, R., & Wagner, E. F. (2014). A switch from white to brown fat increases energy expenditure in cancer-associated cachexia. *Cell Metabolism*, *20*(3), 433–447. https://doi.org/10.1016/j.cmet.2014.06.011

Polderman, J. A., Farhang-Razi, V., van Dieren, S., Kranke, P., DeVries, J. H., Hollmann, M. W., Preckel, B., & Hermanides, J. (2018). Adverse side effects of dexamethasone in surgical patients. *The Cochrane Database of Systematic Reviews*, *11*, CD011940. https://doi.org/10.1002/14651858.CD011940.pub3

Power, M. L., & Schulkin, J. (2008). Sex differences in fat storage, fat metabolism, and the health risks from obesity: Possible evolutionary origins. *The British Journal of Nutrition*, *99*(5), 931–940. https://doi.org/10.1017/S0007114507853347

Prado, C. M. M., Baracos, V. E., McCargar, L. J., Mourtzakis, M., Mulder, K. E., Reiman, T., Butts, C. A., Scarfe, A. G., & Sawyer, M. B. (2007). Body composition as an independent determinant of 5-fluorouracil-based chemotherapy toxicity. *Clinical Cancer Research : An Official Journal of the American Association for Cancer Research*, *13*(11), 3264–3268. https://doi.org/10.1158/1078-0432.CCR-06-3067

Prado, C. M. M., Lieffers, J. R., McCargar, L. J., Reiman, T., Sawyer, M. B., Martin, L., & Baracos, V. E. (2008). Prevalence and clinical implications of sarcopenic obesity in patients with solid tumours of the respiratory and gastrointestinal tracts: A population-based study. *The Lancet. Oncology*, *9*(7), 629–635. https://doi.org/10.1016/S1470-2045(08)70153-0

Prokopchuk, O., Steinacker, J. M., Nitsche, U., Otto, S., Bachmann, J [Jeannine], Schubert, E. C., Friess, H [Helmut], & Martignoni, M. E. (2017). Il-4 mRNA Is Downregulated in the Liver of Pancreatic Cancer Patients Suffering from Cachexia. *Nutrition and Cancer*, *69*(1), 84–91. https://doi.org/10.1080/01635581.2017.1247885

Regassa, A., Suh, M., Datar, J., Chen, C., & Kim, W. K [Woo Kyun] (2017). Fatty Acids Have Different Adipogenic Differentiation Potentials in Stromal Vascular Cells Isolated from Abdominal Fat in Laying Hens. *Lipids*, *52*(6), 513–522. https://doi.org/10.1007/s11745-017-4261-2

Robinson, M. W., Harmon, C., & O'Farrelly, C. (2016). Liver immunology and its role in inflammation and homeostasis. *Cellular & Molecular Immunology*, *13*(3), 267–276. https://doi.org/10.1038/cmi.2016.3

Roenn, J. H. von, Roth, E. L., & Craig, R. (1992). Hiv-related cachexia: Potential mechanisms and treatment. *Oncology*, *49 Suppl 2*, 50–54. https://doi.org/10.1159/000227129

Rohm, M., Schäfer, M., Laurent, V., Üstünel, B. E., Niopek, K., Algire, C., Hautzinger, O., Sijmonsma, T. P., Zota, A., Medrikova, D., Pellegata, N. S., Ryden, M., Kulyte, A., Dahlman, I., Arner, P., Petrovic, N., Cannon, B., Amri, E.-Z., Kemp, B. E., . . . Herzig, S. (2016). An AMP-activated protein kinase-stabilizing peptide ameliorates adipose tissue wasting in cancer cachexia in mice. *Nature Medicine*, *22*(10), 1120–1130. https://doi.org/10.1038/nm.4171

Rosen, E. D [Evan D.], Hsu, C.-H., Wang, X., Sakai, S., Freeman, M. W., Gonzalez, F. J., & Spiegelman, B. M [Bruce M.] (2002). C/ebpalpha induces adipogenesis through

PPARgamma: A unified pathway. *Genes & Development*, *16*(1), 22–26. https://doi.org/10.1101/gad.948702

Rosen, E. D [Evan D.], & MacDougald, O. A. (2006). Adipocyte differentiation from the inside out. *Nature Reviews. Molecular Cell Biology*, *7*(12), 885–896. https://doi.org/10.1038/nrm2066

Rosen, E. D [Evan D.], & Spiegelman, B. M [Bruce M.] (2014). What we talk about when we talk about fat. *Cell*, *156*(1-2), 20–44. https://doi.org/10.1016/j.cell.2013.12.012

Rossaint, J., & Zarbock, A. (2019). Anesthesia-induced immune modulation. *Current Opinion in Anaesthesiology*, *32*(6), 799–805. https://doi.org/10.1097/ACO.0000000000000790

Rupert, J. E., Narasimhan, A., Jengelley, D. H. A., Jiang, Y., Liu, J [Jianguo], Au, E., Silverman, L. M., Sandusky, G., Bonetto, A [Andrea], Cao, S., Lu, X., O'Connell, T. M., Liu, Y., Koniaris, L. G., & Zimmers, T. A. (2021). Tumor-derived IL-6 and trans-signaling among tumor, fat, and muscle mediate pancreatic cancer cachexia. *The Journal of Experimental Medicine*, *218*(6). https://doi.org/10.1084/jem.20190450

Russell, S. T., Hirai, K., & Tisdale, M. J [M. J.] (2002). Role of beta3-adrenergic receptors in the action of a tumour lipid mobilizing factor. *British Journal of Cancer*, *86*(3), 424–428. https://doi.org/10.1038/sj.bjc.6600086

Rydén, M., Agustsson, T., Laurencikiene, J., Britton, T., Sjölin, E., Isaksson, B., Permert, J., & Arner, P. (2008). Lipolysis--not inflammation, cell death, or lipogenesis--is involved in adipose tissue loss in cancer cachexia. *Cancer*, *113*(7), 1695–1704. https://doi.org/10.1002/cncr.23802

Saad, A., Kho, J., Almeer, G., Azzopardi, C., & Botchu, R. (2021). Lesions of the heel fat pad. *The British Journal of Radiology*, *94*(1118), 20200648. https://doi.org/10.1259/bjr.20200648

Sakuma, K., Aoi, W., & Yamaguchi, A. (2017). Molecular mechanism of sarcopenia and cachexia: Recent research advances. *Pflugers Archiv : European Journal of Physiology*, *469*(5-6), 573–591. https://doi.org/10.1007/s00424-016-1933-3

Sandri, M. (2016). Protein breakdown in cancer cachexia. *Seminars in Cell & Developmental Biology*, *54*, 11–19. https://doi.org/10.1016/j.semcdb.2015.11.002

Sato, T., Vargas, D., Miyazaki, K., Uchida, K., Ariyani, W., Miyazaki, M., Okada, J., Lizcano, F., Koibuchi, N., & Shimokawa, N. (2020). Eid1 suppresses lipid accumulation by inhibiting the expression of GPDH in 3T3-L1 preadipocytes. *Journal of Cellular Physiology*, *235*(10), 6725–6735. https://doi.org/10.1002/jcp.29567

Schoettl, T., Fischer, I. P., & Ussar, S. (2018). Heterogeneity of adipose tissue in development and metabolic function. *The Journal of Experimental Biology*, *221*(Pt Suppl 1). https://doi.org/10.1242/jeb.162958

Schultz, N. A., Christensen, I. J., Werner, J., Giese, N., Jensen, B. V., Larsen, O., Bjerregaard, J. K., Pfeiffer, P., Calatayud, D., Nielsen, S. E., Yilmaz, M. K., Holländer, N. H., Wøjdemann, M., Bojesen, S. E., Nielsen, K. R., & Johansen, J. S. (2013). Diagnostic and Prognostic Impact of Circulating YKL-40, IL-6, and CA 19.9 in Patients with Pancreatic Cancer. *PloS One*, *8*(6), e67059. https://doi.org/10.1371/journal.pone.0067059

Seale, P., Kajimura, S., Yang, W [Wenli], Chin, S., Rohas, L. M., Uldry, M., Tavernier, G., Langin, D., & Spiegelman, B. M [Bruce M.] (2007). Transcriptional control of brown fat determination by PRDM16. *Cell Metabolism*, *6*(1), 38–54. https://doi.org/10.1016/j.cmet.2007.06.001

Selva, D. M., Lecube, A., Hernández, C., Baena, J. A., Fort, J. M., & Simó, R. (2009). Lower zinc-alpha2-glycoprotein production by adipose tissue and liver in obese patients unrelated to insulin resistance. *The Journal of Clinical Endocrinology and Metabolism*, *94*(11), 4499–4507. https://doi.org/10.1210/jc.2009-0758

Sharma, M., McFarlane, C., Kambadur, R., Kukreti, H., Bonala, S., & Srinivasan, S. (2015). Myostatin: Expanding horizons. *IUBMB Life*, *67*(8), 589–600. https://doi.org/10.1002/iub.1392

Sharma, R., Zucknick, M., London, R., Kacevska, M., Liddle, C., & Clarke, S. J. (2008). Systemic inflammatory response predicts prognosis in patients with advanced-stage colorectal cancer. *Clinical Colorectal Cancer*, *7*(5), 331–337. https://doi.org/10.3816/CCC.2008.n.044

Siegrist-Kaiser, C. A., Pauli, V., Juge-Aubry, C. E., Boss, O., Pernin, A., Chin, W. W., Cusin, I., Rohner-Jeanrenaud, F., Burger, A. G., Zapf, J., & Meier, C. A. (1997). Direct effects of leptin on brown and white adipose tissue. *Journal of Clinical Investigation*, *100*(11), 2858–2864. https://doi.org/10.1172/JCI119834

Sirniö, P., Väyrynen, J. P., Klintrup, K., Mäkelä, J., Karhu, T., Herzig, K.-H., Minkkinen, I., Mäkinen, M. J., Karttunen, T. J., & Tuomisto, A. (2019). Alterations in serum amino-acid profile in the progression of colorectal cancer: Associations with systemic inflammation, tumour stage and patient survival. *British Journal of Cancer*, *120*(2), 238–246. https://doi.org/10.1038/s41416-018-0357-6

Smith, I. J., Aversa, Z., Alamdari, N., Petkova, V., & Hasselgren, P.-O. (2010). Sepsis downregulates myostatin mRNA levels without altering myostatin protein levels in skeletal muscle. *Journal of Cellular Biochemistry*, *111*(4), 1059–1073. https://doi.org/10.1002/jcb.22796

Socha, M. W., Malinowski, B., Puk, O., Wartęga, M., Bernard, P., Nowaczyk, M., Wolski, B., & Wiciński, M. (2021). C-reactive protein as a diagnostic and prognostic factor of endometrial cancer. *Critical Reviews in Oncology/hematology*, *164*, 103419. https://doi.org/10.1016/j.critrevonc.2021.103419

Sohn, J. H., Lee, Y. K., Han, J. S., Jeon, Y. G., Kim, J. in, Choe, S. S., Kim, S. J., Yoo, H. J., & Kim, J. B. (2018). Perilipin 1 (Plin1) deficiency promotes inflammatory responses in lean adipose tissue through lipid dysregulation. *The Journal of Biological Chemistry*, *293*(36), 13974–13988. https://doi.org/10.1074/jbc.RA118.003541

Song, J., Clark, A., Wade, C. E., & Wolf, S. E. (2021). Skeletal muscle wasting after a severe burn is a consequence of cachexia and sarcopenia. *JPEN. Journal of Parenteral and Enteral Nutrition.* Advance online publication. https://doi.org/10.1002/jpen.2238

Song, Z., Xiaoli, A. M., & Yang, F [Fajun] (2018). Regulation and Metabolic Significance of De Novo Lipogenesis in Adipose Tissues. *Nutrients*, *10*(10). https://doi.org/10.3390/nu10101383

Sottile, V., & Seuwen, K. (2001). A high-capacity screen for adipogenic differentiation. *Analytical Biochemistry*, *293*(1), 124–128. https://doi.org/10.1006/abio.2001.5121

Sun, D., Ding, Z., Shen, L., Yang, F [Fan], Han, J., & Wu, G. (2021). Mir-410-3P inhibits adipocyte differentiation by targeting IRS-1 in cancer-associated cachexia patients. *Lipids in Health and Disease*, *20*(1), 115. https://doi.org/10.1186/s12944-021-01530-9

Sun, Y.-S., Ye, Z.-Y., Qian, Z.-Y., Xu, X.-D., & Hu, J.-F. (2012). Expression of TRAF6 and ubiquitin mRNA in skeletal muscle of gastric cancer patients. *Journal of Experimental & Clinical Cancer Research : CR*, *31*(1), 81. https://doi.org/10.1186/1756-9966-31-81

Sung, H., Ferlay, J., Siegel, R. L., Laversanne, M., Soerjomataram, I., Jemal, A., & Bray, F. (2021). Global Cancer Statistics 2020: Globocan Estimates of Incidence and Mortality Worldwide for 36 Cancers in 185 Countries. *CA: A Cancer Journal for Clinicians*, *71*(3), 209–249. https://doi.org/10.3322/caac.21660.

Suzuki, H., Asakawa, A., Amitani, H., Nakamura, N., & Inui, A. (2013). Cancer cachexia--pathophysiology and management. *Journal of Gastroenterology*, *48*(5), 574–594. https://doi.org/10.1007/s00535-013-0787-0

Tada, T., Ohkubo, I., Niwa, M., Sasaki, M., Tateyama, H., & Eimoto, T. (1991). Immunohistochemical localization of Zn-alpha 2-glycoprotein in normal human tissues.

The Journal of Histochemistry and Cytochemistry : Official Journal of the Histochemistry Society, *39*(9), 1221–1226. https://doi.org/10.1177/39.9.1918940

Talar-Wojnarowska, R., Wozniak, M., Borkowska, A., Olakowski, M., & Malecka-Panas, E. (2020). Clinical significance of activin A and myostatin in patients with pancreatic adenocarcinoma and progressive weight loss. *Journal of Physiology and Pharmacology : An Official Journal of the Polish Physiological Society*, *71*(1). https://doi.org/10.26402/jpp.2020.1.10

Tamucci, K. A., Namwanje, M., Fan, L., & Qiang, L. (2017). The dark side of browning. *Protein & Cell.* Advance online publication. https://doi.org/10.1007/s13238-017-0434-2

Tang, Q. Q., & Lane, M. D. (2012). Adipogenesis: From stem cell to adipocyte. *Annual Review of Biochemistry*, *81*, 715–736. https://doi.org/10.1146/annurev-biochem-052110-115718

Thomas, E. L., Saeed, N., Hajnal, J. V., Brynes, A., Goldstone, A. P., Frost, G., & Bell, J. D. (1998). Magnetic resonance imaging of total body fat. *Journal of Applied Physiology (Bethesda, Md. : 1985)*, *85*(5), 1778–1785. https://doi.org/10.1152/jappl.1998.85.5.1778

Tournadre, A., Pereira, B., Dutheil, F., Giraud, C., Courteix, D., Sapin, V., Frayssac, T., Mathieu, S., Malochet-Guinamand, S., & Soubrier, M. (2017). Changes in body composition and metabolic profile during interleukin 6 inhibition in rheumatoid arthritis. *Journal of Cachexia, Sarcopenia and Muscle*, *8*(4), 639–646. https://doi.org/10.1002/jcsm.12189

Trefts, E., Gannon, M., & Wasserman, D. H. (2017). The liver. *Current Biology : CB*, *27*(21), R1147-R1151. https://doi.org/10.1016/j.cub.2017.09.019

TREW, J. A., & BEGG, R. W. (1959). In vitro incorporation of acetate-1-C14 into adipose tissue from normal and tumor-bearing rats. *Cancer Research*, *19*, 1014–1019.

Tsuchiya, A., Nagaya, H., Kanno, T., & Nishizaki, T. (2014). Oleic acid stimulates glucose uptake into adipocytes by enhancing insulin receptor signaling. *Journal of Pharmacological Sciences*, *126*(4), 337–343. https://doi.org/10.1254/jphs.14182FP

Vainer, N., Dehlendorff, C., & Johansen, J. S. (2018). Systematic literature review of IL-6 as a biomarker or treatment target in patients with gastric, bile duct, pancreatic and colorectal cancer. *Oncotarget*, *9*(51), 29820–29841. https://doi.org/10.18632/oncotarget.25661

van der Vusse, G. J. (2009). Albumin as fatty acid transporter. *Drug Metabolism and Pharmacokinetics*, *24*(4), 300–307. https://doi.org/10.2133/dmpk.24.300

Virtanen, K. A., Lidell, M. E., Orava, J., Heglind, M., Westergren, R., Niemi, T., Taittonen, M., Laine, J., Savisto, N.-J., Enerbäck, S., & Nuutila, P. (2009). Functional brown adipose tissue in healthy adults. *The New England Journal of Medicine*, *360*(15), 1518–1525. https://doi.org/10.1056/NEJMoa0808949

Wan, E. S., Cho, M. H., Boutaoui, N., Klanderman, B. J., Sylvia, J. S., Ziniti, J. P., Won, S., Lange, C., Pillai, S. G., Anderson, W. H., Kong, X., Lomas, D. A., Bakke, P. S., Gulsvik, A., Regan, E. A., Murphy, J. R., Make, B. J., Crapo, J. D., Wouters, E. F., . . . DeMeo, D. L. (2011). Genome-wide association analysis of body mass in chronic obstructive pulmonary disease. *American Journal of Respiratory Cell and Molecular Biology*, *45*(2), 304–310. https://doi.org/10.1165/rcmb.2010-0294OC

Wang, S.-W., & Sun, Y.-M. (2014). The IL-6/JAK/STAT3 pathway: Potential therapeutic strategies in treating colorectal cancer (Review). *International Journal of Oncology*, *44*(4), 1032–1040. https://doi.org/10.3892/ijo.2014.2259

Watt, D. G., Horgan, P. G., & McMillan, D. C [Donald C.] (2015). Routine clinical markers of the magnitude of the systemic inflammatory response after elective operation: A systematic review. *Surgery*, *157*(2), 362–380. https://doi.org/10.1016/j.surg.2014.09.009

Whelan, J., & Fritsche, K. (2013). Linoleic acid. *Advances in Nutrition (Bethesda, Md.)*, *4*(3), 311–312. https://doi.org/10.3945/an.113.003772

Wolf, J., Rose-John, S., & Garbers, C. (2014). Interleukin-6 and its receptors: A highly regulated and dynamic system. *Cytokine*, *70*(1), 11–20. https://doi.org/10.1016/j.cyto.2014.05.024

Wu, Z., Rosen, E. D [E. D.], Brun, R., Hauser, S., Adelmant, G., Troy, A. E., McKeon, C., Darlington, G. J., & Spiegelman, B. M [B. M.] (1999). Cross-regulation of C/EBP alpha and PPAR gamma controls the transcriptional pathway of adipogenesis and insulin sensitivity. *Molecular Cell*, *3*(2), 151–158. https://doi.org/10.1016/s1097-2765(00)80306-8

Wyke, S. M., Russell, S. T., & Tisdale, M. J [M. J.] (2004). Induction of proteasome expression in skeletal muscle is attenuated by inhibitors of NF-kappaB activation. *British Journal of Cancer*, *91*(9), 1742–1750. https://doi.org/10.1038/sj.bjc.6602165

Yang, W [Wei], Huang, J., Wu, H., Wang, Y., Du, Z., Ling, Y., Wang, W., Wu, Q., & Gao, W. (2020). Molecular mechanisms of cancer cachexia-induced muscle atrophy (Review). *Molecular Medicine Reports*, *22*(6), 4967–4980. https://doi.org/10.3892/mmr.2020.11608

Yanting, C., Yang, Q. Y., Ma, G. L., Du, M., Harrison, J. H., & Block, E. (2018). Dose- and type-dependent effects of long-chain fatty acids on adipogenesis and lipogenesis of bovine adipocytes. *Journal of Dairy Science*, *101*(2), 1601–1615. https://doi.org/10.3168/jds.2017-13312

Yu, Y.-L., Fan, C.-W., Tseng, W.-K., Chang, P.-H., Kuo, H.-C., Pan, Y.-P., & Yeh, K.-Y. (2021). Correlation Between the Glasgow Prognostic Score and the Serum Cytokine Profile in Taiwanese Patients with Colorectal Cancer. *The International Journal of Biological Markers*, *36*(2), 40–49. https://doi.org/10.1177/17246008211022769

Zhou, X [Xiaolan], Wang, J. L., Lu, J., Song, Y., Kwak, K. S., Jiao, Q., Rosenfeld, R., Chen, Q., Boone, T., Simonet, W. S., Lacey, D. L., Goldberg, A. L., & Han, H. Q. (2010). Reversal of cancer cachexia and muscle wasting by ActRIIB antagonism leads to prolonged survival. *Cell*, *142*(4), 531–543. https://doi.org/10.1016/j.cell.2010.07.011

Acknowledgements

Ein besonderer Dank gilt meinem Doktorvater Prof. Hans Hauner, der mir die Möglichkeit gegeben hat, ein vollkommen neues Projekt maßgeblich mitzugestalten. Herzlichen Dank für das mir entgegengebrachte Vertrauen, Ihre Leitung und Unterstützung. Ebenso danke ich meiner Mentorin Prof. Melina Claussnitzer, deren fachliche Expertise stets eine Bereicherung für mich war, sowie allen Mitgliedern meiner Prüfungskommission.

Ohne das Team der Chirurgischen Klinik und Poliklinik des Klinikums rechts der Isar wäre die Kachexie-Studie ebenfalls nicht möglich gewesen. Die Zusammenarbeit mit Prof. Marc Martignoni, Dr. Olga Prokopchuk und Prof. Klaus-Peter Janssen war lehrreich, spannend und voller neuer Erfahrungen.

Ich danke meinen ehemaligen Kollegen des Lehrstuhls für Ernährungsmedizin für die Geduld während der vielen Stunden Fett-Prep, für die Gespräche bei unseren Seerunden und für die wertvollen Ratschläge in so manch schwierigem Moment. Besonders danke ich dir Sylvi, damals wie heute setzt du Himmel und Hölle für „deine“ Doktoranden in Bewegung und dir Manu, ohne deine Expertise und Geduld wären meine Laborfähigkeiten nicht die, die es heute sind.

Langes Pendeln kann eine Quälerei sein, nicht jedoch in meinem Fall: meine Zug-Truppe Sandra, Janine und Tanja hat mir jeden Morgen ein Lächeln aufs Gesicht und so manches Mal einen Kaffee in meine Hand gezaubert. Kathi, danke für deine berufliche wie private Unterstützung, du hast wahrlich Berliner-Flair in mein Münchner Leben gebracht.

Ein ganz besonderer Dank gilt vor allem dir Tanja: ohne deine Unterstützung im Kachexie-Projekt wäre ich verloren gewesen. Du bist ein Macher und hast die Studie vorangetrieben, wie ich allein es niemals gekonnt hätte. Danke für dieses Teamwork!

Last but not least gilt mein Dank meiner Familie, meinen langjährigen Freunden und allerliebsten Kroatien-Biologen. Danke, dass ihr mich über die Jahre so ausdauernd unterstützt habt, ich weiß, es war nicht immer leicht mit mir. Ohne euren Rückhalt hätte ich die Hochs und Tiefs nicht gemeistert.